Politecnico di Torino

Civil Engineering
2022/2023
Degree session March 2023

PARAMETRIC STUDY FOR WALL-TO-WALL CONNECTION IN MIXED STEEL CONCRETE STRUCTURES

Professor:
Rosario Ceravolo

Student:
Simone De Troia

Ai miei genitori e a
mia sorella Chiara

Author

Simone De Troia

Double degree student in:

Structures and Infrastructures
Politecnico di Torino

Civil Engineering and Urban Management
KTH Royal Institute of Technology

Place for Project

Montreuil, France
Egis Industries

Professors

Rosario Ceravolo
Turin, Italy
Politecnico di Torino

Raid Karoumi
Stockholm, Sweden
KTH Royal Institute of Technology

Supervisors

Silvano Erlicher
Miquel Huguet Aguilera
Michele Massarella
Montreuil, France
EGIS Industries

ACKNOWLEDGEMENTS

Questo spazio lo dedico per ringraziare le persone che in questi anni di università mi hanno aiutato a crescere personalmente e professionalmete.

Prima di tutti, un sentito grazie al Politecnico di Torino, l'università che mi ha accolto in questo lungo percorso formativo dalla triennale fino ad oggi, e che mi ha formato e mi ha visto diventare uomo e professionista. Grazie al mio relatore del Politecnico il prof. Rosario Ceravolo perché ha saputo trasmettere in me l'entusiasmo e la voglia di conoscenza nelle sue materie, delineando la mia futura strada professionale. Grazie perché mi ha offerto l'opportunità di questo progetto di tesi che mi ha ulteriormente formato ed ha rappresentato un punto fondamentale nella mia carriera universitaria.

Grazie al KTH, l'università in cui sono stato ospite nel mio ultimo anno di magistrale, che mi ha dato la possibilità di estendere il mio bagaglio culturale in un beckground internazionale. Grazie al mio relatore del KTH prof. Raid Karoumi e ai suoi preziosi consigli nell'avanzamento del progetto di tesi.

Grazie ad EGIS, e all' ing. Silvano Erlicher, per la spledinda opportunità di lavorare su questo interessante e innoviativo progetto di tesi. Grazie ai miei supervisor, lo chef de projet Miquel Huguet Aguilera e l'ing. Michele Massarella, che con la loro professionalità ed esperienza mi hanno guidato, supportato e indirizzato in ogni istante nello sviluppo del progetto di tesi.

Grazie di cuore a mia madre e mio padre perché hanno sempre sostenuto i miei sogni, credendo in me e incoraggiandomi in ogni mia scelta, senza farmi mai sentire solo. Grazie a mia sorella Chiara, da sempre un punto fermo nella mia vita e una spalla su cui contare.

Grazie ai miei amici di corso, Maurizio e Gabriel, da semplici colleghi sono diventati grandi amici per la vita, con cui ho imparato in questi anni a condividere gioie e difficoltà, universitarie ma soprattutto personali.

Grazie ai miei amici di sempre Aurelio, Agnese e Gloria, che nonostante la distanza sanno essere sempre al mio fianco nei momenti più belli ma soprattutto in quelli più brutti.

Grazie ai miei amici "di giù" Augusto, Alessandro, Luigi, Fosca, Alessia, Eliana, Gianni, Cristina, Simona per tutti i sorrisi e le risate che mi avete regalato.

Grazie ai miei coinquilini di Erasmus Theo e Javi, due fratelli acquisiti che mi hanno dato la forza di affrontare un’esperienza davvero importante nella mia vita, che ha rappresentato un punto di svolta, e che sarebbe stata completamente diversa senza voi.

Grazie ai miei amici di “Tazzoni” Federica, Dario e Gianluca per le camomille e le chiacchierate notturne, e per i viaggetti in giro per il mondo.

Grazie a tutti i miei amici di Erasmus con cui ho condiviso una delle esperienze più forti e più belle della mia vita: Lucia, Anna, Ludo, Fra, Ila, Ayman.

Ed infine grazie ad Ethel, new entry nella mia vita ma che in poco tempo è riuscita ad occupare un posto importante per me. Grazie per il supporto di questi mesi nell’esperenza parigina, sei riuscita a darmi la forza e l’entusiasmo giusto per affrontare i miei momenti di tristezza e solitudine.

ABSTRACT

The objective of this thesis work is to study the connection between two Steel Concrete Structures (SCS) wall modules using embedded connection bars. The SCSs under investigation consist of two steel faceplates held together by tie bars, concrete is cast inside, and stress transmission between the concrete and the steel plates is provided by shear connectors as headed studs.

The working principle is similar to that of Reinforced Concrete (RC), where the faceplates provide the tensile strength, replacing the rebars in RC, and the concrete the compressive strength. One of the main differences, which makes the use of SCS advantageous, is that the concrete is confined and thus improves its compressive performance by 4-5 times compared to normal RC. Further, the confinement due to the plates ensures insulation of the concrete from external agents, improving its durability. The use of prefabricated modules to be placed on site and the concrete cast inside reduces the working time and costs. For all these reasons, and especially for its higher performance compared to RC, this construction strategy is perfectly suited to the needs of large constructions such as nuclear reactors.

However, one of the main disadvantages is the lack of codes, there are only two international codes JEAG 4618 (Architectural Institute of Japan, 2005) and ANSI/AISC N690-18 (American Institute of Steel Construction, 2018), a disadvantage that AFCEN is trying to solve by creating a European nuclear code to be included in the RCC-CW. AFCEN instructed EDF that in turn entrusted EGIS to compile a PTAN report as a technical justification for the chapters related to SCS in the nuclear application. The topic of this thesis is one of the PTAN technical specifications to be solved and is related to a second main drawback of the SCS system arising from the way the modules are connected. Currently, the most commonly used connection systems are welding and bolting, while the alternative proposed in this thesis project is the use of embedded connection bars. The use of welding to connect modules increases the working time and costs, creating potential problems, especially for thicker faceplates, when internal welding is not possible and can only be performed from the outside.

The analysed solution consists of using longitudinal bars positioned between two modules to ensure the connection, leaving a gap of 2 cm or more between the faceplates of two adjacent modules and solving the problems of single-sided welding and reducing the execution time. The analysis of this connection strategy is carried out in a parametric

study in which 29 different configurations are tested in bending and 26 in tension to obtain general rules for the design. In almost all the models the failure occurs in the studs with reductions in the connection strength compared to the ultimate SCS wall capacity from 22% to 60% in bending and from 74% to 88% in tension, respectively for M48 and M30 as bar diameters models.

The conclusion of the analysis showed that the design of the shear-headed stud capacity is poor, due to the combined effect of shear and tension reducing the pure shear capacity by 63%. In fact, more studs are needed than estimated to reach the ultimate capacity of the bars or plates, which should be the two preferred failure modes of the connection.

ACRONYMS

AFCEN Association Française pour les règles de Conception de construction et de surveillance en exploitation des matériels des chaudières Electro Nucléaires

EDF Électricité de France

EDF-DT EDF Direction Technique

PTAN Technical Status on the Design and Construction of Steel Concrete Structures

RCC-CW Rules for design and construction of PWR nuclear civil works

PWR Pressurized water reactor

SCS Steel Concrete Structure

RC Reinforced Concrete

SCIENCE Steel Concrete for Industrial, Energy and Nuclear Efficiency

SCHEDULE Steel Concrete High-Efficiency Demonstration eUropean colLaborative Experience

FE Finite Element

SUMMARY

Chapter 1

Introduction

Companies involved in the nuclear industry from the nuclear or conventional energy sectors make up the global association known as "Association Française pour les règles de Conception de construction et de surveillance en exploitation des matériels des chaudières Electro Nucléaires" (AFCEN)[1]. The main goals of AFCEN are to preserve up-to-date codes that offer precise and practical guidelines for the design, construction, and in-service inspection of components used in commercial or experimental nuclear power plants, as well as to guarantee accredited and easily accessible training programs that allow code users to reach a high level of competence, knowledge, and practical skill. AFCEN has instructed the Direction Technique of EDF[2] (EDF-DT) to compile a report called" Technical Status on the Design and Construction of Steel Concrete Structures" (PTAN), as well as the design chapters and construction chapters that ought to be included in the revision of the RCC-CW[3] code scheduled for 2023. The PTAN report [1] will serve as the technical justification for the specific chapters that will be included in the RCC-CW, concerning the design of nuclear reactors by means of Steel Concrete Structure (SCS). Some of the essential activities outlined in the Technical Specification have been assigned to EGIS[4] by EDF-DT as "technical support". One of the technical specifications to be solved is the subject of this thesis and specifically the design of the SCS wall-to-wall connection using embedded connection bars.

[1] *French Association for the Design, Construction and Monitoring of Electro-Nuclear Plant Equipment*

[2] *French energy delivery and production company, with the government owning a majority of its share*

[3] *Rules for design and construction of PWR nuclear civil works*

[4] *Premier international consulting, engineering, and operational business*

1.1 Background

A Steel Concrete Structure (SCS) is a composite structure between the outer steel faceplates and the concrete cast inside. The basic idea is the same as with reinforced concrete (RC), where concrete provides compressive strength, and instead of rebars like in RC, faceplates offer tensile strength. Concrete is poured inside prefabricated steel modules that are put on the work site in order to cut down the costs and working time. The concrete is confined from the faceplates, which increases its compressive performance by 4-5 times compared to regular RC and is one of the primary distinctions that make using SCS favourable. The faceplates' confinement guarantees that the concrete is protected from external conditions, enhancing its durability.
This construction technique is ideal for the requirements of major structures such as nuclear reactors because of all of the above factors, and notably because of its superior performance over RC [2].

Different types of SCS solutions can be classified according to the link between the two faceplates and the stress transmission between steel and concrete. Mainly three different SCS types can be listed: direct link, semi-link and indirect link [2].

- Direct link: using transverse bars welded or bolted at the ends onto the faceplates, with the main advantage that there are no problems of pullout failure of the steel components from the concrete (see Figure 1).

Figure 1 – Direct link type [2]

- Semi-link: using a J-hook or U-connector welded onto each plate. This solution is easier to implement during manufacture because each plate can be produced and then assembled together, but results in reduced faceplate connection performance compared to the direct connection, which can lead to the possibility of pullout failure for the steel components but still maintaining a certain tensile strength in the connectors (see Figure 2).

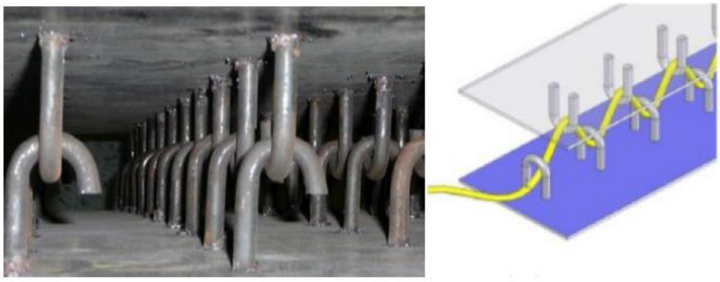

Figure 2 – Semi-link type [2]

- Indirect link: using headed studs welded onto each plate. Once again advantageous in the assembly between studs and plate, but with problems of the pullout failure of the steel components from the concrete and the problem on-site to keep the plates at the set distance for pouring the concrete inside. Definitively, this solution is optimal in shear stress transmission between concrete and steel, but with a limited tensional capacity that rather reduces the capacity of the stud itself with respect to the semi-link solution (see Figure 3).

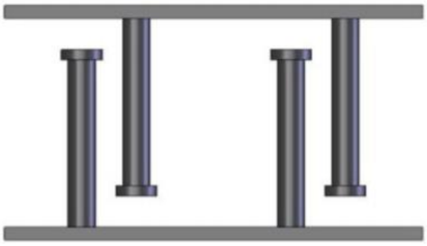

Figure 3 – Direct-link type [2]

Figure 4 shows the different types of connectors with each type of failure, in particular for the indirect link and the semi-link is represented by the minimum between fracture, pullout, breakout, and punching shear failures.

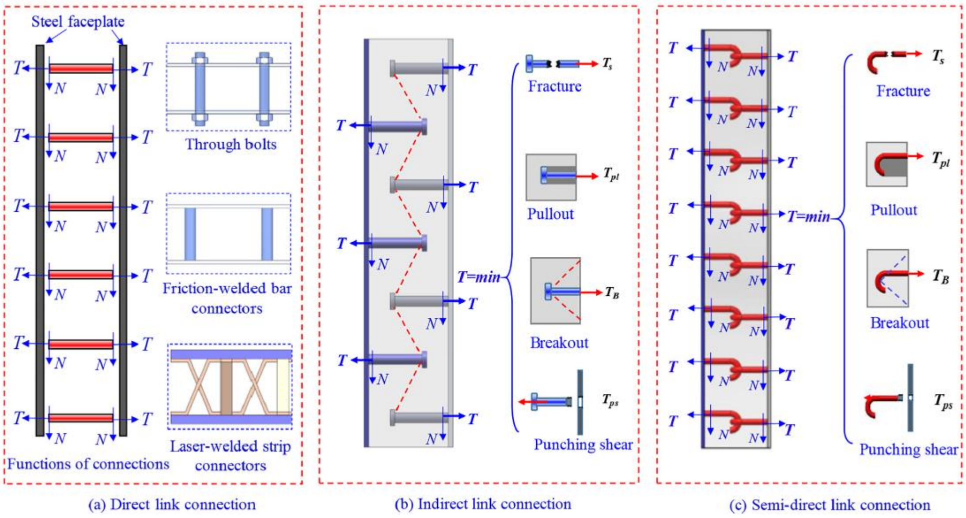

Figure 4 – Different connector types [3]

While many articles can be found in the literature describing the strength of the listed SCS types and also other solutions not mentioned, such as the case of the improved direct link by means of enhanced C-channels [3], the same cannot be said for the connection solutions between the different SCS modules. This represents the main obstacle to the use of this construction technique, i.e. the lack of studies on all design aspects, which translates into a lack of design codes. In fact, only two international codes are available: JEAG 4618 (Architectural Institute of Japan, 2005) and ANSI/AISC N690-18 (American Institute of Steel Construction, 2018).

As stated in the American code, the main solutions for the connection between two SC modules can be either welded or bolted [4]. These solutions create continuity in the connection without the need to evaluate the reduction in strength of the connection relative to the SC wall but these can be designed simply by following the standards of EN 1993-1-8 [5].

The welding consists of a total or partial penetration and it can be performed only from the outside since access inside the modules is not possible. This, especially for thicker faceplates, creates a stability problem in the connection.

The bolt can be performed with a cover plate with pre-drilled or in-site drilled holes, to increase the working tolerance in the relative positions between the modules.

Anyway, in both cases, welded and bolted solutions, the tolerances to be respected are millimetric. These high accuracies increase working time and thus costs, not to mention the highly specialised workers to perform the welding [1].

1.2 Problem and purpose

EDF uses an SCS that mixes direct and indirect links, combining the advantages and disadvantages of these types of links described in the previous section. These are the same as those used in the US code that uses tie bars as direct links and studs as indirect links [4].

The SCS system under consideration consists then of two steel faceplates held together at a fixed distance, in large square patterns, by tie bars, and in the squares, there is a higher density of headed studs. The concrete is cast inside and the transmission of stresses between the concrete and the steel plates is ensured by the headed studs.

This solution reduces the number of direct connections (tie bars), which are useful for preventing the pullout failure of steel objects from the concrete, for maintaining the module thickness during concrete pouring and are responsible for the confinement of the

concrete by holding the tensile force. However, at the same time, shear transmission can simply be realised by indirect connections (headed studs), since tie bars do not lead to any improvement in shear transmission compared to studs, rather, a large density of direct connections may reduce the capacity of the SCS [3].
The design guidance of this type of SCS, excluding the connection between modules, in a format consistent with the Eurocodes can be found in the SCI-P414 document [6], part of the SCIENCE (Steel Concrete for Industrial, Energy and Nuclear Efficiency) project [7], which consists of a series of tests and design guidelines of the SCS in which EDF and EGIS are partners.

The main solutions for connecting SCS wall modules are conventionally welded or bolted connections [4]. Unfortunately, these solutions require small tolerances in work operations, resulting in increased costs and execution time. Another problem concerns welding stability issues. In fact, most of the time welding can only be done from the outer side of the plates, and when thick plates are used this can create problems with the stability of the connection that does not guarantee continuity of strength. EDF has developed and patented a solution in the framework of the SCIENCE European research project, which uses embedded connection bars, placed inside the modules for high tolerances. In-plane position tolerances can easily reach 2 or more centimetres. This leads to improved execution time by ensuring high performance in the connection.

EDF entrusted EGID, with the realisation of the PTAN document [1], for the design analysis of this SCS connection with embedded connection bars, and this thesis project is the initial point of this design, focusing specifically on the connection between two SC walls, examining the bending and axial strength of the connection for a wide range of connection configurations.

1.3 Methodology and limitations of the analysis

Parametric analysis can be performed to study the design of the SC wall connection with embedded connection bars. The different configurations can be realised as a value variation, for each parameter considered, with respect to the reference case defined by EDF in chapter 7 of the document PTAN [1]. The parameter values considered are related to geometry and material properties. Specifically, the parameters are:

- Geometrical parameters:
  - the diameters of studs and embedded connection bars;

    - the thickness of the faceplates,
    - the longitudinal and transversal spacing of tie bars, studs and connection bars
- Material parameters:
    - the variation of the faceplate and connection bars' steel grade.

The numerical model can be realised on the basis of the WP5 experimental test developed within the SCIENCE project [7], which consists of a series of tests, including the ones to understand the thermo-mechanical behaviour of the SCS and the bending strength of the SC wall connection using embedded connection bars (WP5 test). Once the numerical model matches the experimental results, it can be simplified to obtain a parametric model to be run for different combination values.

The limitation of this analysis is that only one available experiment is used to calibrate the numerical analysis; this implements the internal validity of the analysis, but more experimental data should be used as control points to extend the validity of the analysis as external. However, further tests are planned as part of the SCHEDULE (Steel Concrete High-Efficiency Demonstration eUropean colLaborative Experience) project, which consists of the calculation and construction of DUS (Diesel for Ultimate Safeguard) as a Pilot Building in SCS using embedded connection bars and welding connections [8]. Once completed, further bending and axial tests can be carried out and then compared with the parametric results to extend the validity of the analysis.

Chapter 2

Methodology

This chapter presents the hypotheses and the methodology of the analysis for the parametric studies for the wall-to-wall connections based on the main hypotheses presented in chapter 7 of the document PTAN [1]. The objective of this study is to determine the bending and axial stiffnesses and resistances of the connection system of wall modules using embedded connection bars with a parametric study that aims at assessing the behaviour of a large range of wall module connections.

2.1 The connection solution

In this study, the system of connection between the SC wall modules by embedded connection bars positioned within the modules is considered. This solution allows higher tolerances than the conventional welded or bolted connections, which can be up to 2 cm or more in the in-plane direction of the modules.

Figure 5 presents the geometry of the connection and the passage of internal forces through all the different components. Tensile forces of the faceplate are transmitted to the embedded connection bars through the studs, which have a smaller spacing and higher density in the connection area. Tie bars, welded or bolted onto the plates, ensure the relative position of the plates, eliminating pulling-out failure of the plates from concrete and ensuring, by holding the tensile stress, that the plates perform the confinement. The concrete is highly compressed near the head of the embedded bars, with a compression that can be more than 150 MPa in a C30/37 concrete, which can withstand due to the improved performance provided by the confinement.

There are two desired modes of ductile failure: *the steel plate failure* or *the embedded connection bars failure*.

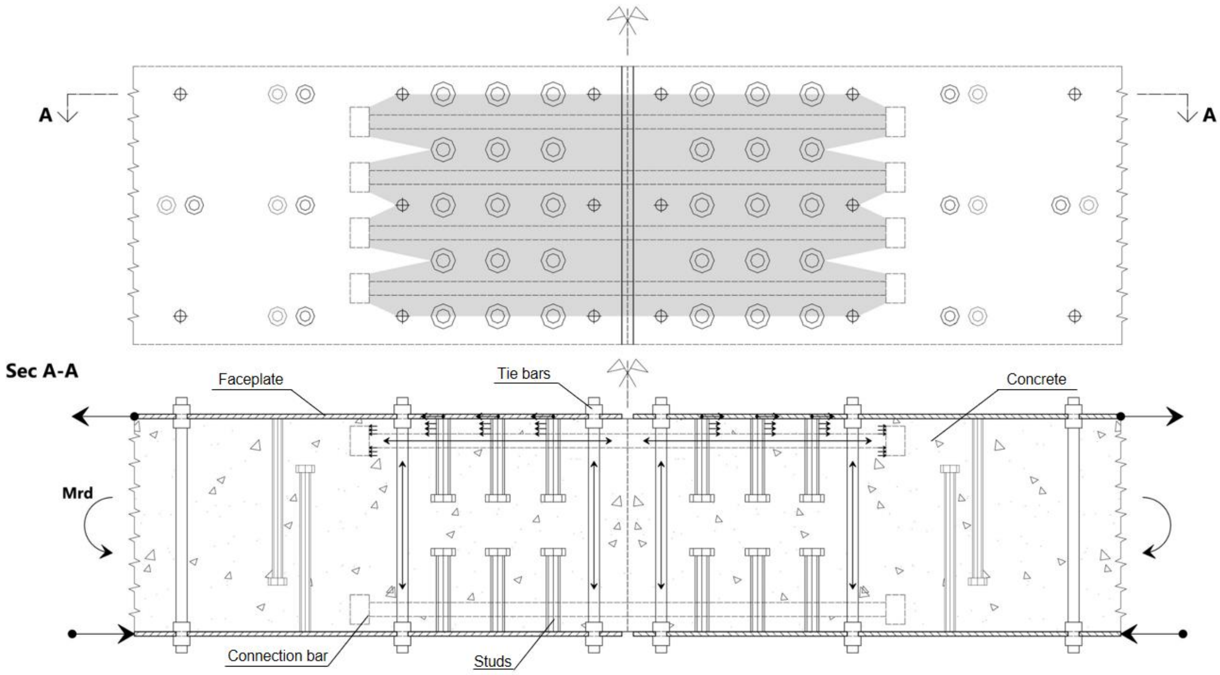

Figure 5 - Considered geometry for SCS wall modules connection by embedded connection bars

2.2 Material mechanical properties

The considered mechanical properties of concrete and steel materials are described in the following sections.

2.2.1 Concrete behaviour

The mechanical properties of concrete are not variable for the parametric analysis and the retained values for these parameters are:

Table 1 – Concrete material properties

Element	Description	Parameter	Units	Type	Values
Concrete C30/37	Density	ρ	kg/m^3	Constant	2200
	Compressive yielding strength	f_c	MPa	Constant	30
	Maximum aggregate size	d_{max}	mm	Constant	16

2.2.2 Steel behaviour

Regarding density, elastic and post-elastic stiffness and Poisson's ratio the parameters have the same value for all the steel elements in the model. The only parameter that changes among steel elements is the yielding strength, and therefore consequently the ultimate strength, and specifically, faceplates and tie-bars have the same strength value, while are different for studs and embedded connection bars.

Faceplates and Tie-bars

For faceplates and tie-bars the steel grades used are S235 and S355. The elastic and uniaxial nonlinear behaviour depends on the parameters in Table 2. The yielding and ultimate strengths refer to Table 3.1 of EN 1993-1-1[9]. The values of the reference case are marked in bold.

Table 2 - Faceplates and tie-bars mechanical properties

Element	Description	Parameter	Units	Type	Values
Steel for faceplates and tie-bars	Density	ρ_s	kg/m^3	Constant	7850
	Young's modulus	E_s	GPa	Constant	210
	Yielding strength	f_{sy}	MPa	Variable (2)	235; 355
	Ultimate strength	f_{su}	MPa	Variable (2)	360; 510
	Post-elastic modulus	E_p	GPa	Constant	1,30
	Poisson ratio	ν_s	-	Constant	0,3

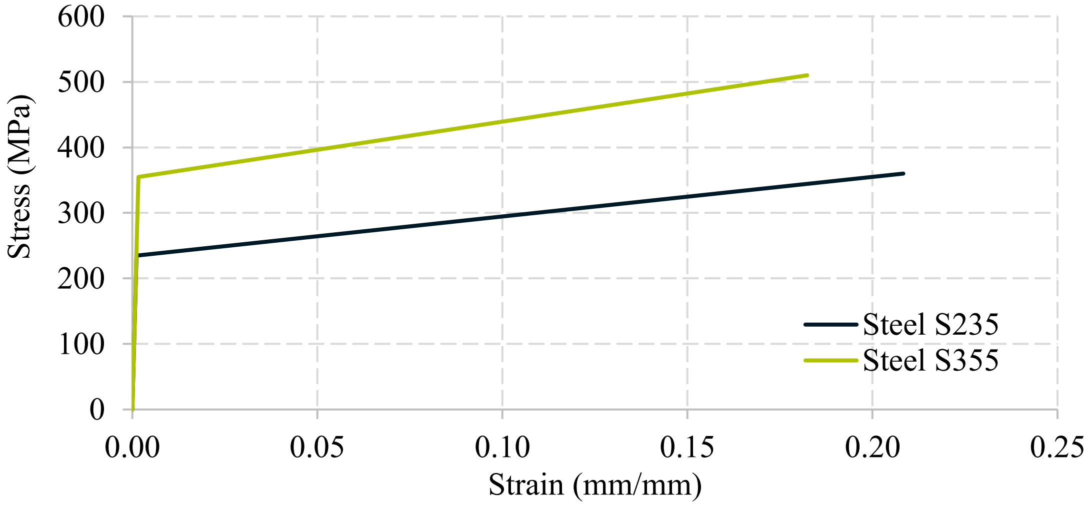

Figure 6 - Considered uniaxial mechanical behaviour for S235 and S355 steel (faceplates and tie-bars)

Studs

For the studs the steel grade used is S235. The yielding and ultimate strength refer to Table 3.1 of EN 1993-1-1[9]. The elastic and uniaxial nonlinear behaviour depends on the following parameters.

Table 3 – S235 steel studs' mechanical properties

Element	Description	Parameter	Units	Type	Values
Steel for studs	Density	ρ_s	kg/m^3	Constant	7850
	Young's modulus	E_s	GPa	Constant	210
	Yielding strength	f_{sy}	MPa	Constant	235
	Ultimate strength	f_{su}	MPa	Constant	360
	Post-elastic modulus	E_p	GPa	Constant	1,30
	Poisson ratio	ν_s	-	Constant	0,3

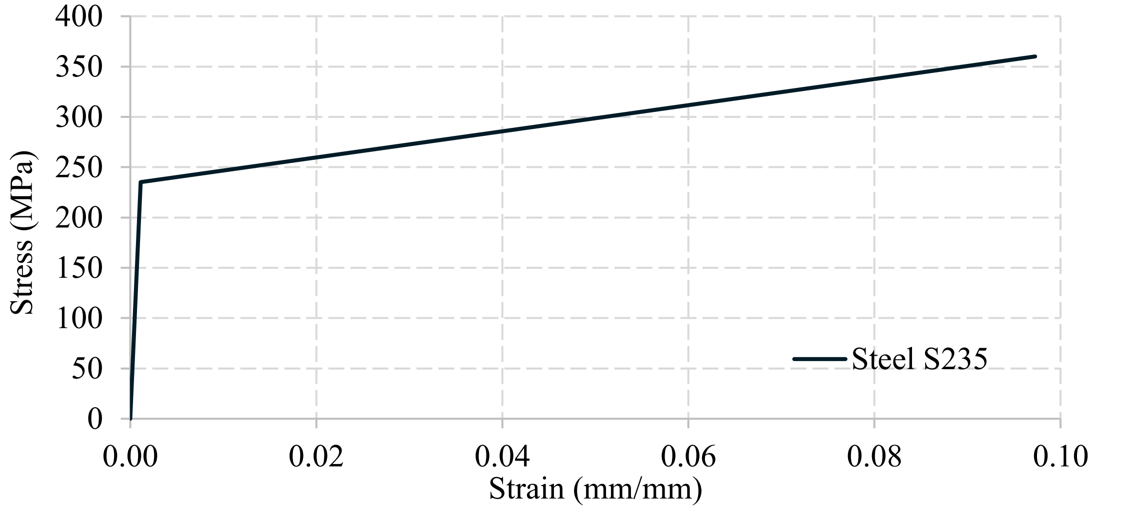

Figure 7 - Considered uniaxial mechanical behaviour for S235 steel (studs)

Embedded connection bars:

For the connection bars the steel grades used are 8.8 and 10.9 with yielding strengths respectively of 640 and 900 MPa and ultimate strength of 800 and 1000 MPa, as reported in Table 3.1 of EN 1993-1-8 [5]. The elastic and uniaxial nonlinear behaviour depends on the following parameters. The values of the reference case are marked in bold.

Table 4 - Embedded connection bars' mechanical properties

Element	Description	Parameter	Units	Type	Values
Steel for embedded connection bar	Density	ρ_s	kg/m^3	Constant	7850
	Young's modulus	E_s	GPa	Constant	210
	Yielding strength	f_{sy}	MPa	Variable (2)	**640**; 900
	Ultimate strength	f_{su}	MPa	Variable (2)	**800**; 1000
	Post-elastic modulus	E_p	GPa	Constant	1,30
	Poisson ratio	ν_s	-	Constant	0,3

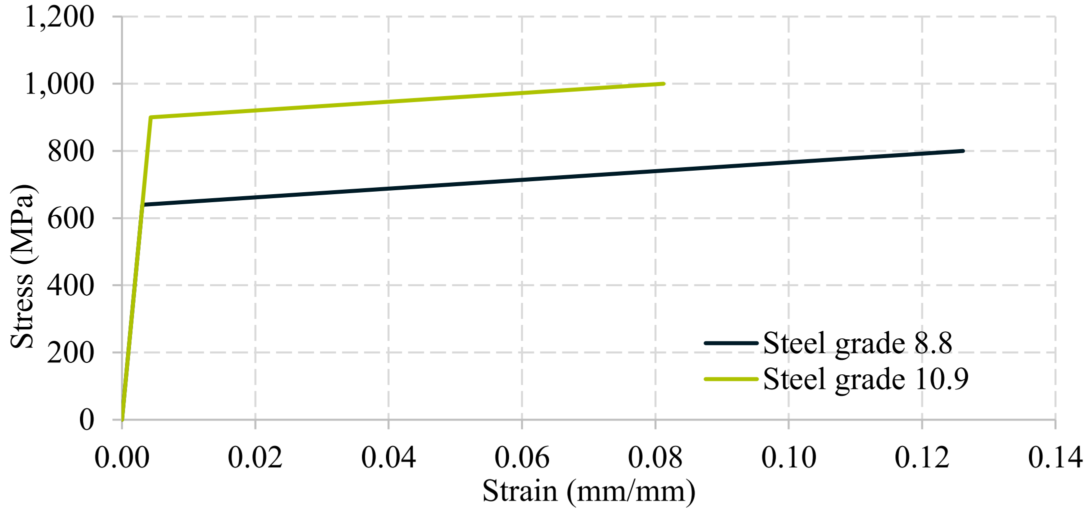

Figure 8 – Uniaxial mechanical behaviour for 8.8 and 10.9 steel grades (embedded connection bars)

2.3 Geometric parameters

The parametric analysis for the wall-to-wall connection solutions considers variable values for some geometric parameters of the connection components. The retained set of geometric parameter values is presented in the following section.

Table 5 presents the constant and variable geometric parametric values for the five elements of this solution: concrete wall, faceplates, tie bars, studs, and embedded connection bars. The values of the reference case are marked in bold.

Table 5 – Geometrical parameters

Element	Description	Parameter	Units	Type	Values
Wall	thickness	H_c	mm	Variable (3)	300, 400, **500**
Faceplates	thickness	t_p	mm	Variable (5)	6, **8**, 10, 12, 14
Tie-bars	diameter	d_t	mm	Constant	20
	x, y-spacing	s_{tx}, s_{ty}	mm	Variable (3)	**400,** 500, 600
Studs	diameter	d_s	mm	Variable (3)	19, **22**,25
	x-spacing	s_{sx}	mm	Variable (4)	75, **100**, 125, 150
	y- spacing	s_{sy}	mm	Variable (5)	125, **133**, 166, 200, 250
	length	h_s	mm	Variable (4)	100, **150**, 200, 250
Embedded connection bars	diameter	d_b	mm	Variable (4)	M30, M36, M42, **M48**
	y-spacing	*s_{by}	mm	Variable (5)	125, **133**, 166, 200, 250
	length	l_b	mm	Variable	≤1000

*Same spacing as stud

The resulting geometry is presented in Figure 9 where the geometry for the steel and concrete components of the model is shown, while Figure 10 and Figure 11 show the geometrical parameters referred to the model.

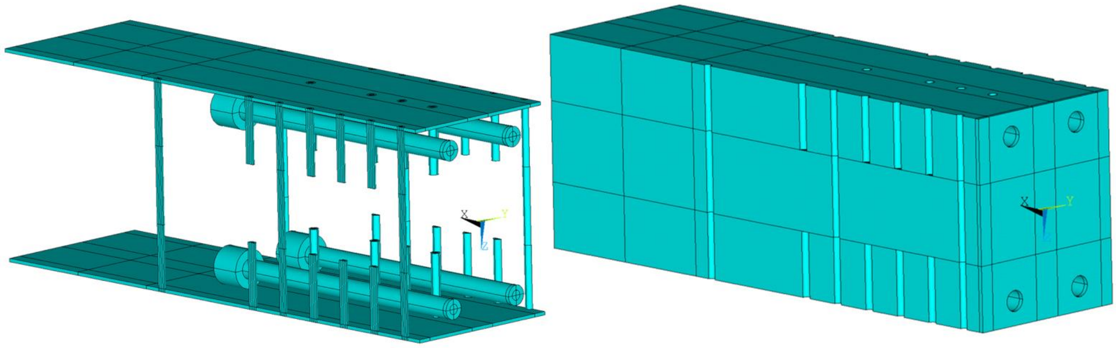

(a) (b)

Figure 9 – Geometry of the model. (a) Steel components (b) Concrete component

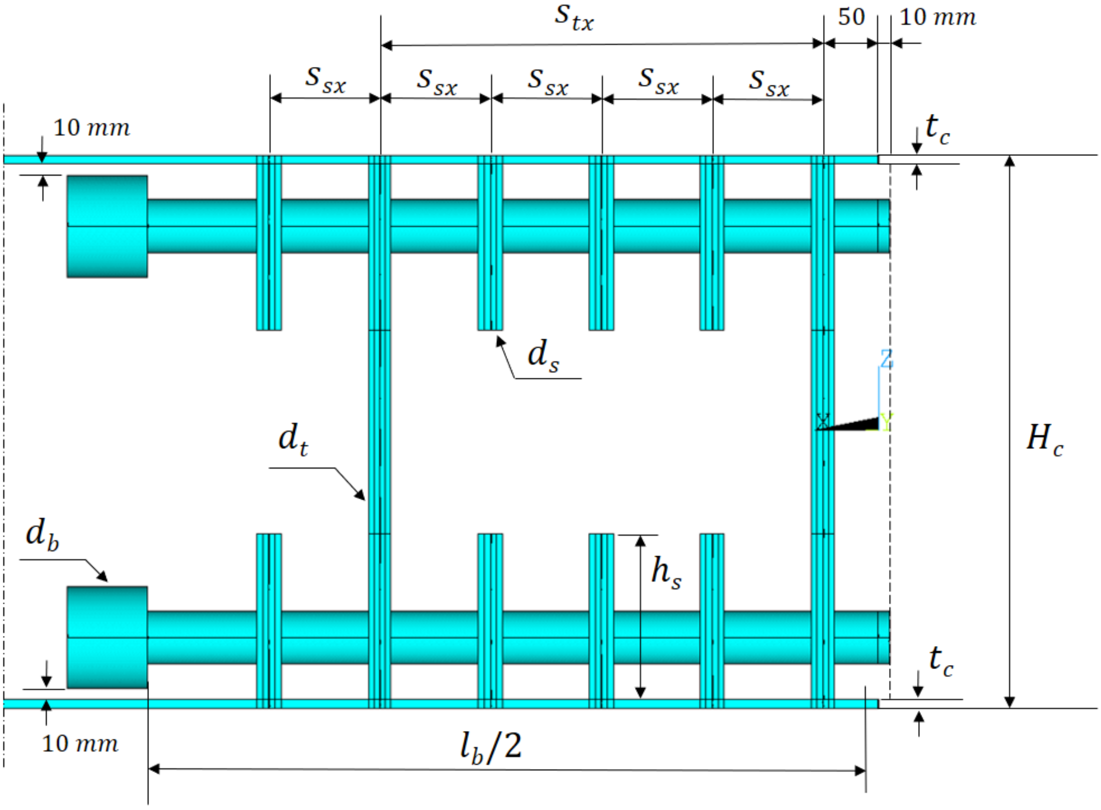

Figure 10 – Geometrical parameters referred to the model’s geometry

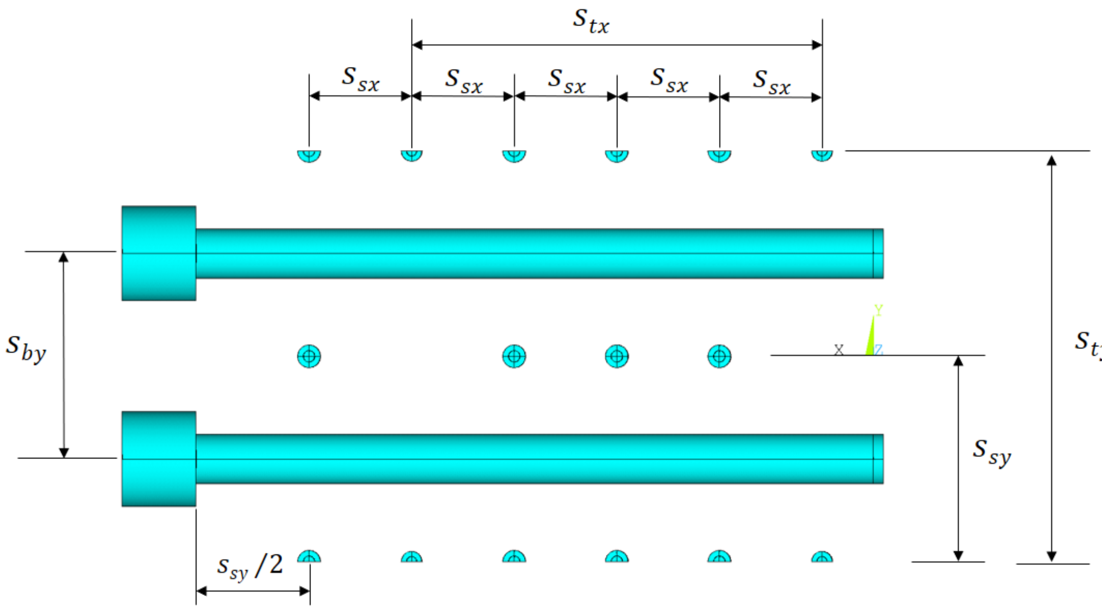

Figure 11 - Geometrical parameters referred to the model’s geometry

Given a large number of geometrical parameters and values, some simplifications and assumptions can be made:

- Only square shapes for the tie spacing, consequently vertical (s_{ty}) and horizontal (s_{tx}) spacing are equal and it can be referred to them with s_t;
- The connection bars' vertical spacing (s_{by}) is considered the same as that of the studs (s_{sy}).
- Connection bars’ diameter (d_b) and length (l_b) are variable in accordance with specific geometric rules presented in 2.4.2, where the values can be calculated as a function of the other geometric parameters.
- The distance between the connection bar heads and the faceplate is constant and equal to 10 mm.
- The distance between the end of the faceplates and the first row of studs or tie bars is constant and equal to 50 mm.
- The gap between the two SC modules is constant and equal to 20 mm.

2.4 Parametric studies for connection solutions

In total, 11 variable parameters were counted: two materials and nine geometrical properties, which are presented in Table 6 with all their respective variable values.

Table 6 - All variable parameters values

Parameter	Units	Values				
$f_{sy,plate}$	MPa	235	355			
$f_{sy,bar}$	MPa	640	900			
H_c	mm	300	400	500		
t_p	mm	6	8	10	12	14
s_t	mm	400	500	600		
d_s	mm	19	22	25		
s_{sx}	mm	75	100	125	150	
s_{sy}	mm	125	133	166	200	250
h_s	mm	100	150	200	250	
d_b	mm	M30	M36	M42	M48	
l_b	mm	≤ 1000				

For the different values to coexist in a single combination, certain geometric rules, presented in the document SCI-P414 [6] and resumed in the following formulas, must be observed, where each formula represents a different design concept.

- **Faceplate** thickness conditions:

  The following two formulae represent respectively: the ductility condition of the SCS and the failure condition first in the studs and then in the plates.

$$\frac{t_p}{h_c} \in [0.0075; 0.033]$$

$$\frac{d_s}{t_p} \leq 2.5$$

- **Studs** and **tie-bars** spacing conditions:

  Since the global square pattern of the tie bars and the within designation of the studs, these formulas ensure the net amount of studs in the tie spacing.

$$\frac{s_t}{s_{sx}} = integer$$

$$\frac{s_t}{s_{sy}} = integer$$

- **Stud** diameters and spacing conditions:

  The criteria represented by the ratio of spacing to stud diameter ensure sufficient concrete around the studs to make them work properly.

$$\frac{s_{sx}}{d_s} \geq 5$$
$$\frac{s_{sy}}{d_s} \geq 4$$

- **Stud** and **Faceplate** diameters and spacing conditions:

  The spacing between the studs is limited by the thickness of the plate to avoid compression buckling of the plate between two studs.

$$\frac{s_s}{t_p} \leq 37 \text{ (S235)}$$

Neglecting the length of the embedded connecting bars (l_b), which will be calculated later as a function of the other parameters, the total number of parameters can be reduced to 10. Combining all the different values taken by each of them, 172800 different combinations can be obtained. This is a huge number of combinations to be developed by parametric analysis. Therefore, a selection of combinations is necessary. A *one-to-one variation of the parameters from the reference case* selection is applied, changing only one parameter for each combination from the reference case to observe the effect of each.

2.4.1 One-to-one variation of parameters from the reference case

This method of obtaining parameter combinations consists of taking the reference case and for each parameter performing combinations by changing one-to-one all possible values that the parameters can take. In this way, the contribution of each parameter can be highlighted in terms of performance, but at the same time, the sensitivity increases only around the reference case. If all the parameters in one combination change from the reference case, the conclusion might be different.

Table 7 contains all the combinations needed from the reference case to perform the one-to-one parameter variation selection. The first combination is the reference case, marked in bold, while the different colours represent the different parameters varied in the combinations by holding the others unchanged. Sometimes also other values change, especially for the spacing combinations, this is to enable from a geometric point of view the physical realization of the combination.

Table 7 - Parameter combination values with a one-to-one parameters' variation selection

Comb N.	$f_{sy,p}$ (MPa)	$f_{sy,b}$ (MPa)	H_c (mm)	t_p (mm)	s_t (mm)	s_{sx} (mm)	s_{sy} (mm)	d_s (mm)	h_s (mm)	d_b (mm)	l_b (mm)
1	355	640	500	8	400	100	200	22	150	M48	1320
2	235	640	500	8	400	100	200	22	150	M48	1320
3	355	900	500	8	400	100	200	22	150	M48	1520
4	355	640	300	8	400	100	200	22	200	M47	1320
5	355	640	300	8	400	100	200	22	150	M48	1320
6	355	640	400	8	400	100	200	22	150	M48	1320
7	355	640	500	6	400	100	200	22	150	M48	1320
8	355	640	500	10	400	100	200	22	150	M48	1320
9	355	640	500	12	400	100	200	22	150	M48	1320
10	355	640	500	14	400	100	200	22	150	M48	1320
11	355	640	500	8	500	100	125	22	150	M42	845
12	355	640	500	8	500	125	125	22	150	M42	1245
13	355	640	500	8	600	75	200	22	150	M48	920
14	355	640	500	8	600	100	200	22	150	M48	1120
15	355	640	500	8	600	120	200	22	150	M48	1520
16	355	640	500	8	600	150	200	22	150	M48	1820
17	355	640	500	8	400	100	133	22	150	M42	1053
18	355	640	500	8	400	100	200	22	150	M42	1120
19	355	640	500	8	500	100	125	22	150	M48	1245
20	355	640	500	8	500	100	166	22	150	M48	1286
21	355	640	500	8	500	100	250	22	150	M48	1370
22	355	640	500	8	400	100	200	19	150	M48	1920
23	355	640	500	8	400	100	200	25	150	M48	1120
24	355	640	500	8	400	100	200	22	100	M48	1320
25	355	640	500	8	400	100	200	22	200	M48	1320
26	355	640	500	8	400	100	200	22	250	M48	1320
27	355	640	400	8	400	100	200	22	250	M48	1320
28	355	640	500	8	400	100	200	22	150	M30	720
29	355	640	500	8	400	100	200	22	150	M36	1120

2.4.2 Connection bar lengths and diameters computation

In the parametric analysis, the length and diameter of the connection bars depend on the other values in the combination, unless it is for combinations 28 and 29 where the diameter becomes the only reference value to vary and it is no anymore a dependent variable. The computation of these two parameters is explained below.

Embedded connection bars' diameter

The diameter is the maximum allowed, between the standard values of M30, M36, M42, and M48, defined in Figure 12, to pass the head between two studs with a margin of 10 mm from each. This means that the value is a function of the vertical distance between the studs, therefore the vertical studs' spacing (s_{sy}), and the studs' diameter (d_s). Figure 13 shows the geometry of the described problem, and Table 8 collects the values of the combinations, such as the vertical available distance (d_h), the maximum head diameters that fit according to the described rules (d_{b2}) and consequently, the connection bar diameter (d_{b1}).

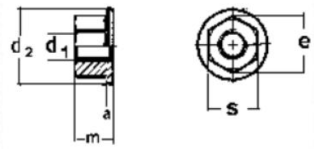

d_1	$d_{2\,(h13)}$	s	m $_{(js15)}$	a	e $_{min}$
M 6	14	10	9	3	11.05
M 8	18	13	12	3.5	14.38
M 10[1)]	22	16(17)	15	4	17.77(18.90)
M 12[1)]	25	18(19)	18	4	20.03(21.10)
M 14[1)]	28	21(22)	21	4	23.35(24.49)
M 16	31	24	24	5	26.75
M 18	34	27	27	5	29.56
M 20	37	30	30	6	32.95
M 22[1)]	40	34(32)	33	6	37.29(35.03)
M 24	45	36	36	6	39.55
M 27	50	41	40	7	45.20
M 30	58	46	45	8	50.85
M 36	68	55	54	10	60.79
M 42	80	65	63	12	71.30
M 48	92	75	72	14	82.60

Figure 12 – Head and connection bar standard dimensions [1]

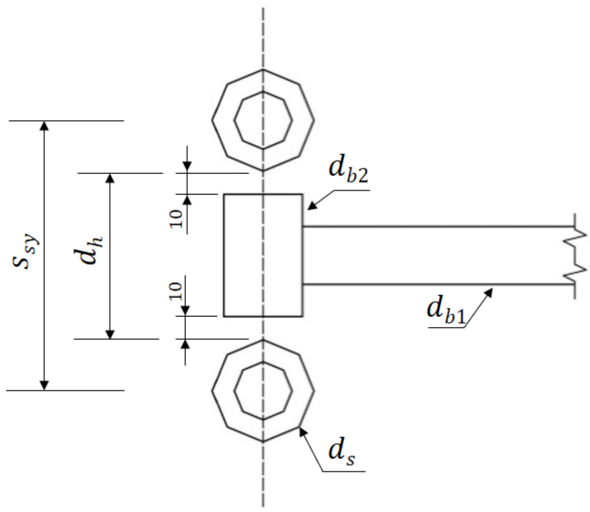

Figure 13 - Geometrical criteria for the connection bars diameter estimation

Table 8 – Embedded connection bars' diameters

Comb N.	*d_h (mm)	d_{b1} (mm)	d_{b2} (mm)
1	158	M48	92
2	158	M48	92
3	158	M48	92
4	158	M48	92
5	158	M48	92
6	158	M48	92
7	158	M48	92
8	158	M48	92
9	158	M48	92
10	158	M48	92
11	83	M42	80
12	83	M42	80
13	158	M48	92
14	158	M48	92
15	158	M48	92
16	158	M48	92
17	91	M42	80
18	158	M42	80
19	83	M48	92
20	124	M48	92
21	208	M48	92
22	161	M48	92
23	155	M48	92
24	158	M48	92
25	158	M48	92
26	158	M48	92
27	158	M48	92
28	-	M30	58
29	-	M36	68

*$(d_h = s_{sy} - d_s - 20)$

For each combination, the maximum available distance (d_h) can be calculated as the difference between the vertical studs' spacing, reduced by the stud ray on each side and a further reduction due to the margin between the connection bars' heads and the studs. Once d_h has been calculated, the maximum allowable diameter is chosen from the standard values of Figure 12 selecting the allowable d_{b2} and the the actual diameter d_{b1}.

Embedded connection bars' length

The total length of the connection bars depends on the number of studs used and as described earlier in the stress operating mechanism for this connection system, stresses reach the connection bars through the studs. The amount of studs to be used is therefore a function of the ultimate strength of the connection bars since the maximum stress reached by the bar must be divided among the studs according to their ultimate shear strength. The design ultimate tensile strength of the connection bar is a function of the bar area and ultimate tensile strength, as shown in the formula below, according to Table 3.2 in EN 1993-1-8[5].

$$N_{u,Rd} = \frac{0.9 A_{net} f_{u,b}}{\gamma_v}$$

Where the A_{net} is the reduced cross-section and the safety factor $\gamma_v = 1.25$.

The studs' design ultimate shear strength according to paragraph 6.6.3 of EN 1994-1-1 [11] is a function of the following formulas:

$$P_{Rd,s} = \frac{0.8 f_{u,s} \pi {d_s}^2}{4\gamma_v}$$

$$P_{Rd,c} = \frac{0.29 d_s^2 \sqrt{f_{ck} E_{cm}}}{\gamma_v}$$

Where the first represents the steel strength of the studs, while the second refers to the concrete strength criteria. The ultimate strength is for all the cases 360 MPa since studs have always steel S235, also concrete does not change type (C30/37) with f_{ck}= 30 MPa and Young's mean modulus calculated according to Table 3.1 of EN 1992-1-1 [14]:

$$E_{cm} = 22\left(\frac{f_{ck} + 8}{10}\right)^{0.3}$$

Table 9 represents the shear tensile strength per stud diameter, while Table 10 shows the tensile strength referred to different connection bar diameters and for the two different grades 8.8 ($N_{Rd,8.8}$) and 10.9 ($N_{Rd,10.9}$), and according to the stud diameters' strength the number of studs needed per connection bars' diameter and steel grade is presented in Table 11.

Table 9 - Studs ultimate shear strength

d_s (mm)	A (mm²)	$P_{Rd,s}$ (kN)	$P_{Rd,c}$ (kN)	Min value (kN)
19	284	82	83	82
22	380	109	111	109
25	491	141	144	141

Table 10 - Connection bar ultimate tensile strength and number of studs needed to cover the strength

Connection bar diameter	d_b (mm)	A (mm²)	A_{net} (mm²)	$N_{Rd,8.8}$ (kN)	$N_{Rd,10.9}$ (MN)
M30	30	707	561	323	404
M36	36	1020	817	471	588
M42	42	1385	1120	645	806
M48	48	1810	1470	847	1058

Table 11 - Number of studs per connection bar diameter and grade at different studs' diameter

d_s (mm)	19	22	25	19	22	25
Conn. bar grade / Conn. bar diameter	Grade 8.8			Grade 10.9		
M30	4	3	3	5	4	3
M36	6	5	4	8	6	5
M42	8	6	5	10	8	6
M48	11	8	6	13	10	8

The final length of the connection bar is estimated for each previous combination based on the diameter of the connection bars, the steel grade, and then the number of studs needed to transmit the ultimate bar's strength and its spacing. The total number is estimated to be divided into two symmetrical rows, as shown in Figure 14.

Three different configurations can be found, where in the first the head of the connection bars is located within a tie bar spacing, the second where the head is located immediately after the tie bars with one or more tie spacing, or finally, one or more tie spacing with additional studs after the last tie bars line.

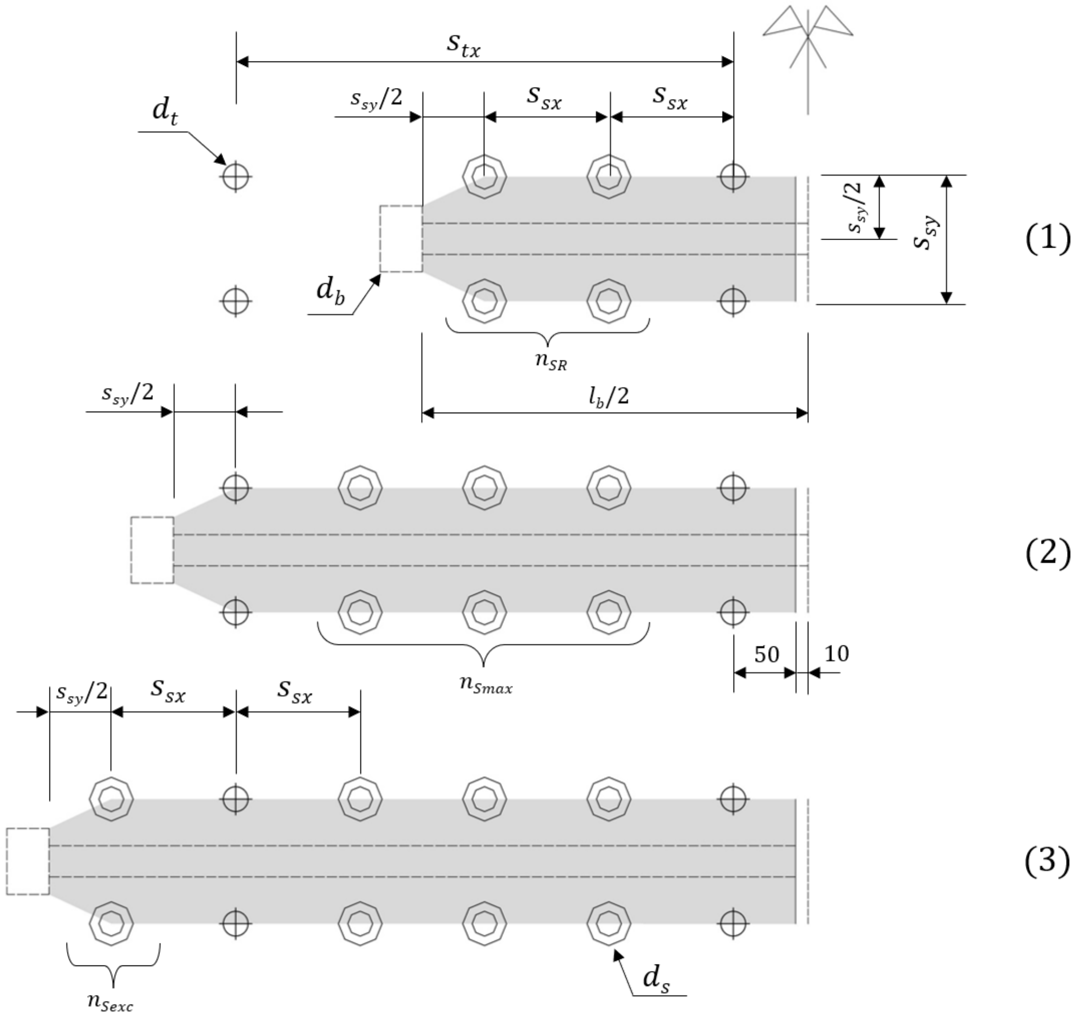

Figure 14 – Configurations of connection bars

Table 12 collects the estimation of the length per each previous combination according to the following considerations for the final length:

- To the final length, 60 mm is added, which corresponds to 50 mm as the minimum distance between the end of the faceplates and the first row of tie bars, and 10 mm as the half-distance gap between the two SC wall modules and where the symmetry of the connection begins.
- The head of the connection bars must be after or before a row of tie bars or studs, so the final distance is also a function of the tie spacing.
- To have an angle of almost 45° for stress transmission between the head of the connection bars and the first row of tie bars or studs, a distance equal to half the vertical stud spacing between the latter two is considered.

Table 12 - Estimation of the connection bar lengths

Comb N.	d_b (mm)	$f_{sy,b}$ (MPa)	d_s (mm)	$^{(1)}n_s$	$^{(2)}n_{s,max}$	$^{(3)}n_t$	l_b (mm)
1	M48	640	22	8	3	2	1320
2	M48	640	22	8	3	2	1320
3	M48	900	22	10	3	2	1520
4	M48	640	22	8	3	2	1320
5	M48	640	22	8	3	2	1320
6	M48	640	22	8	3	2	1320
7	M48	640	22	8	3	2	1320
8	M48	640	22	8	3	2	1320
9	M48	640	22	8	3	2	1320
10	M48	640	22	8	3	2	1320
11	M42	640	22	6	4	1	845
12	M42	640	22	6	3	2	1245
13	M48	640	22	8	7	1	920
14	M48	640	22	8	5	1	1120
15	M48	640	22	8	4	2	1520
16	M48	640	22	8	3	2	1820
17	M42	640	22	6	3	2	1053
18	M42	640	22	6	3	2	1120
19	M48	640	22	8	4	2	1245
20	M48	640	22	8	4	2	1286
21	M48	640	22	8	4	2	1370
22	M48	640	19	11	3	3	1920
23	M48	640	25	6	3	2	1120
24	M48	640	22	8	3	2	1320
25	M48	640	22	8	3	2	1320
26	M48	640	22	8	3	2	1320
27	M48	640	22	8	3	2	1320
28	M30	640	22	3	3	1	720
29	M36	640	22	5	3	2	1120

(1) Number of studs for a given connection bar diameter, steel grade and stud diameter
(2) Maximum number of studs allowed per tie spacing $s_t/s_{sx} - 1$
(3) Number of tie bar spacing needed to fit the studs and the connection heads

2.5 Boundary conditions and load hypothesis

In this section are presented the boundary conditions and the load hypothesis for both bending and axial analysis.

2.5.1 Bending analysis

This analysis aims to evaluate the bending stiffness, the elastic limit and the ultimate bending moment of the connection.

Model assumptions

For the bending analysis, the will is to apply a pure bending moment, constantly, along the connection. This can be done by reproducing a four-point beam test, which consists of two outermost points where the force is applied and two intermediate points represented by the supports, as shown in Figure 15. The bending is linear increasing between the point where the force is applied and the support, while is constant between the two supports.

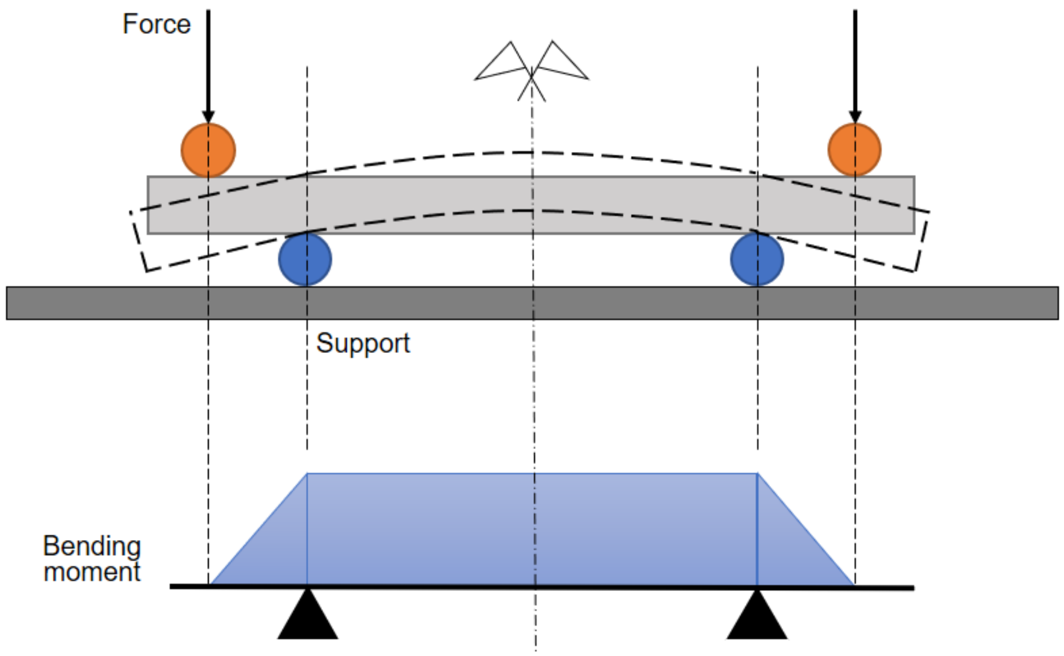

Figure 15 – Four-points beam test

For symmetrical conditions, only half of the beam can be modelled, but also at the width of the beam can be applied symmetrical conditions since solutions can be obtained per linear meter, so only a strip corresponding to the tie spacing can be modelled.

The parametric model is a simplification of the Specimen E model presented later in Chapter 3 as FE model validation from experimental results. The objective of the parametric analysis is to analyse the behaviour of the connection, especially in the non-linear field, and to avoid the non-linear effect in the part of the beam where the bending moment increases up to the constant values a stiffener can be applied to replace the rest of the beam. It corresponds to an elastic material 100 times stiffer than steel, which does not deform, but with the sole purpose of applying the moment to the connection.

Figure 16 shows the reference case model as a representation of the parametric models intended to reproduce the four-point beam experiment to evaluate a constant moment for all cases, with the symmetry simplifications mentioned and the stiffener for the load applications. In the following sections, Boundary conditions and Load hypotheses are evaluated in detail.

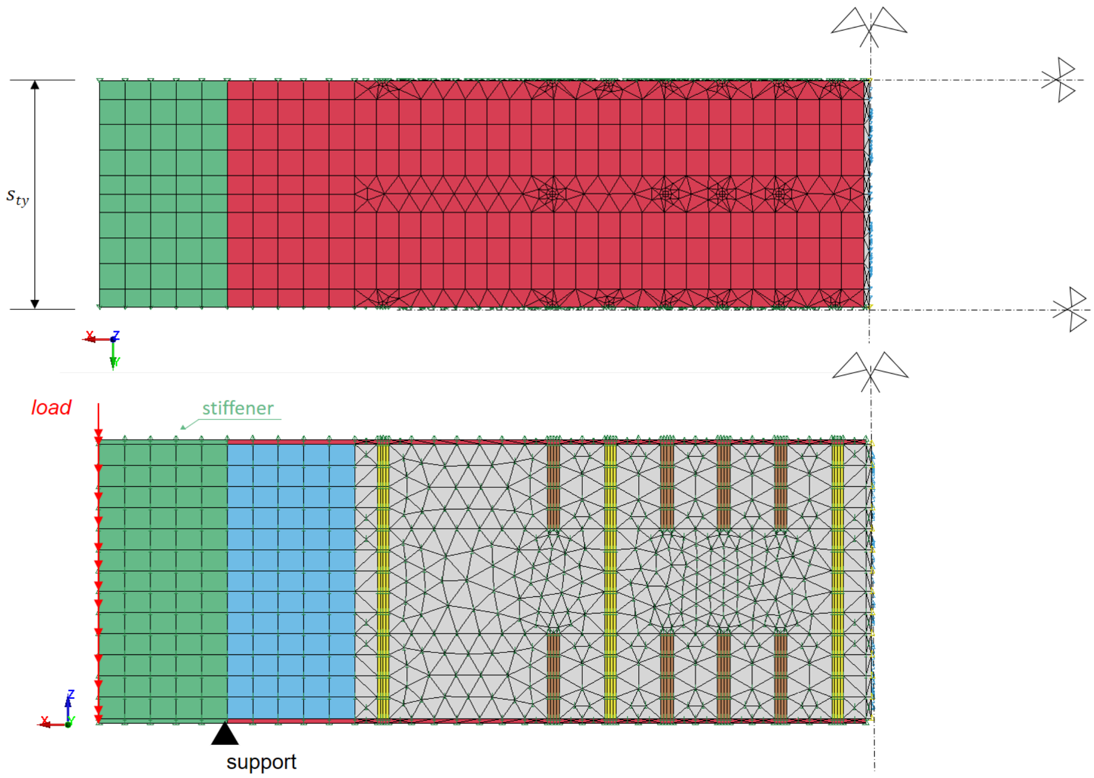

Figure 16 – Parametrical model

Boundary conditions

Figure 17 and Figure 18 show the boundary conditions of the model:

- According to Figure 17, the right and left faces of the model are restrained in the y-direction, which represents a symmetry condition by repeating the module along the y-axis (*planes xz*).
- According to Figure 18, the right face of the model is restrained in the x-direction, which represents a symmetry condition in the longitudinal direction in correspondence with the beam midspan (*plane yz*).
- Vertical movement is restrained (z-direction) for one line of nodes in correspondence with the support.
- Unilateral contact conditions between concrete and steel (embedded connection bars, tie bars, studs, and faceplates) elements in the connection zone are applied.

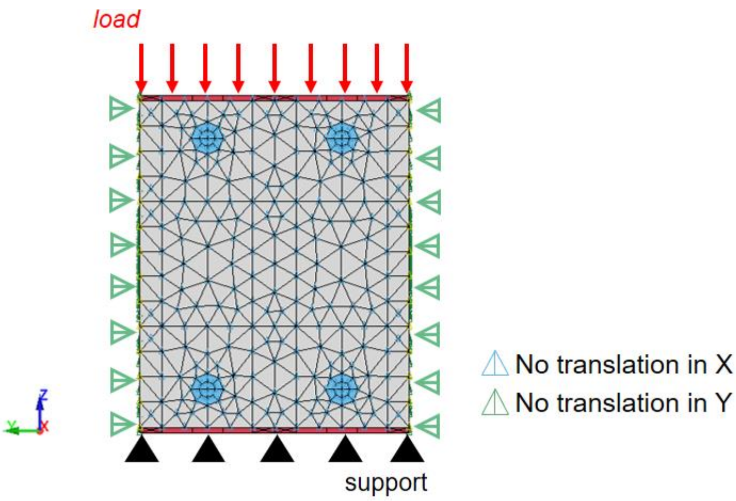

Figure 17 - Boundary conditions of the model (bending analysis)

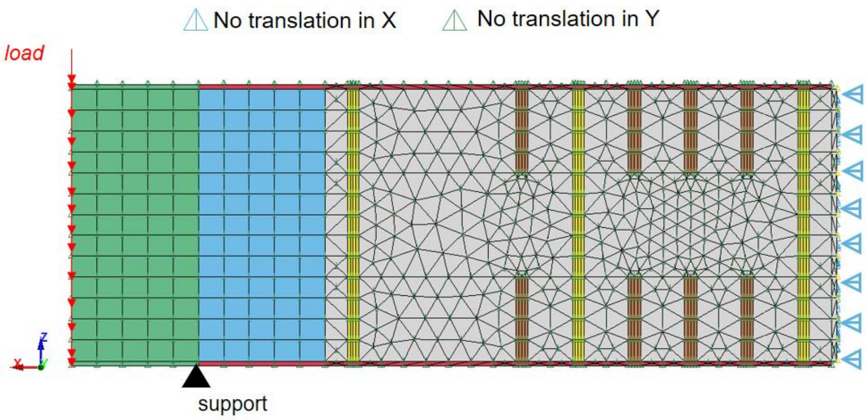

Figure 18 - Boundary conditions of the model (bending analysis)

Load hypotheses

The applied load is a vertical force with a monotonic increment in an interval of 0.25 s, and the maximum applied force depends on the bending capacity of the connection bars, neglecting the contribution of the concrete. This means that the maximum bending moment that the bars can withstand depends on their ultimate tensile strength (N_{Rd}) and internal lever arms (d), as shown in Figure 19. The formulation of the maximum applicable bending moment is:

$$M_{Rd} = N_{Rd} d$$

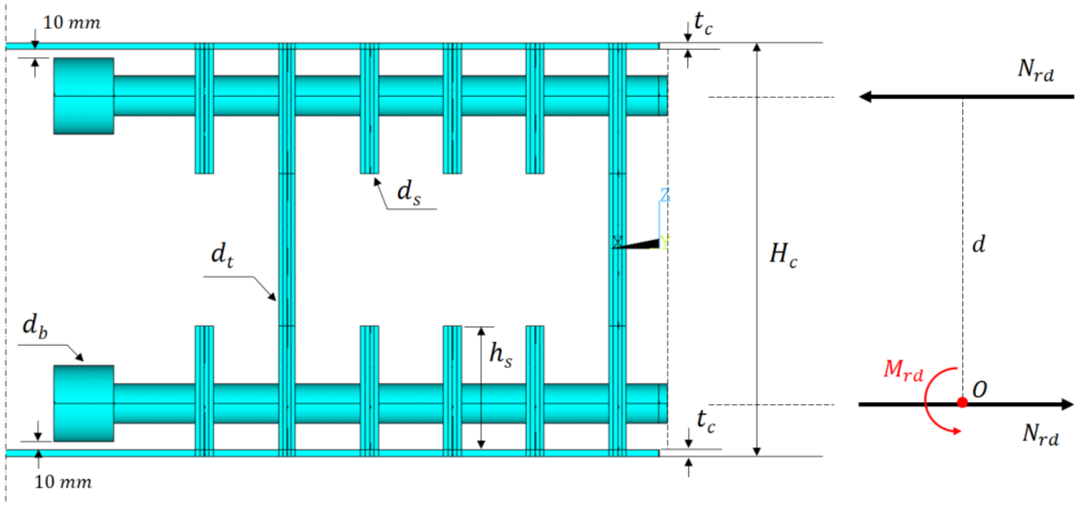

Figure 19 –Ultimate bending moment application

This resistance moment, in turn, is divided by the lever arm of the stiffener, which is constant for all cases and corresponds to 225 mm, and this becomes the value of the total applied force. To avoid localized deformation, the force is applied in a distributed way over the surface of the stiffener. Figure 20 shows the application of the load to the model.

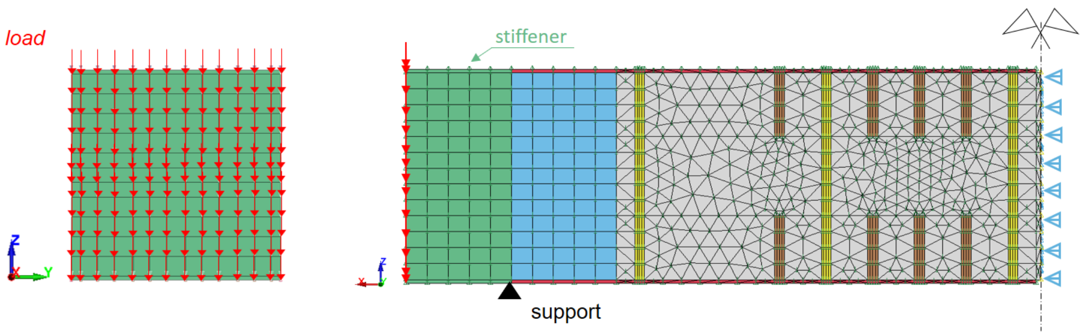

Figure 20 - Load application on the FE model (bending analysis)

The application of a monotonic load will be sufficient to understand how the connection will behave in terms of stiffness and ultimate capacity since another load application, such as cyclic loading, has been tested and the results show convergence with monotonic loading. More details on the application of cyclic loading are presented in Appendix 1.

2.5.2 Tensile axial analysis

This analysis aims to evaluate the axial stiffness and the ultimate axial force of the connection in tension.

Model assumptions

For the axial analysis, the aim is to apply pure tension stresses to the beam.

The same model used in the bending analysis can be used with some modifications:

- Elimination of the vertical constraints (*z-direction*), which were intended to simulate the supports for the four-point beam test for the application of a constant bending moment to the connection.
- Rotation of the applied force horizontally (*x-direction*) to pull the cross-section and reproduce a tensile test.

This time, unlike in the case of bending where, due to the loading conditions, one part of the beam cross-section is in compression and the other in tension, in the axial test the entire cross-section is in tension, so an additional symmetry condition can be identified in the *plane xz* modelling of only half of the entire wall thickness (H_c) as can be seen in Figure 21, with a consequent reduction in the calculation time.

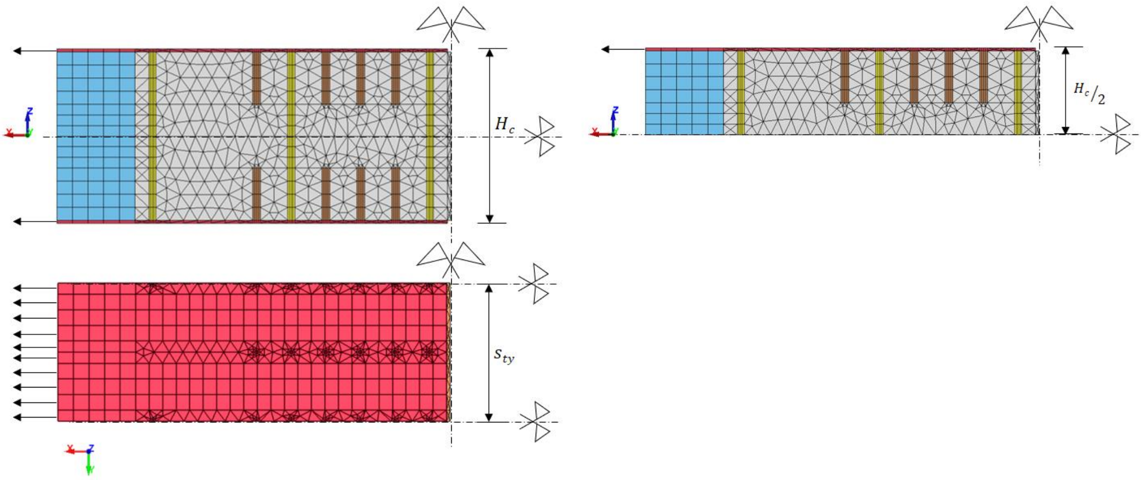

Figure 21 – Symmetrical conditions for the axial problem

Boundary conditions

Figure 22 shows the boundary conditions of the model, these are almost entirely similar to those of the bending problem, already present in 2.5.1, except for the condition of symmetry with respect to wall thickness that can be represented by constraining the face corresponding to the cut at the centre of the wall in the z-direction (*plane xy*)

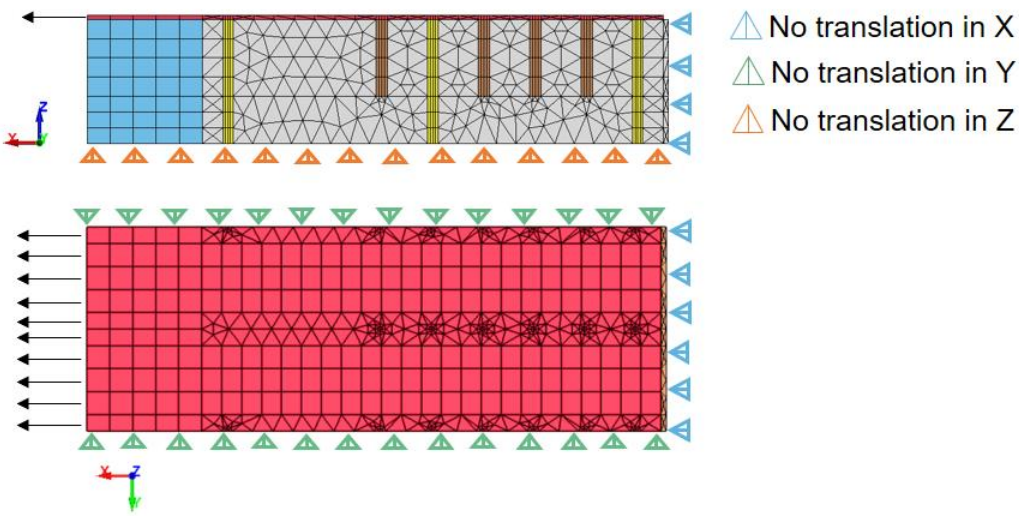

Figure 22 - Boundary conditions of the model (axial analysis)

Load hypothesis

The applied load is a horizontal pressure with a monotonic increment in an interval of 0.25 s and the maximum applied (σ_{max}) depends on the axial capacity of the connection bars (N_{rd}), neglecting the contribution of the concrete, according to the following formula:

$$\sigma_{max} = \frac{\sum_i N_{rd,i}}{A_{plate}}$$

Where the A_{plate} represents the total faceplate areas and the pressure is only applied to the plates to avoid local deformations of the concrete. The use of a stiffener, as done for the bending model; was considered unnecessary, as the applied pressure generates tension in the plate without local deformations or buckling.

Chapter 3

FE model for the numerical calculations

The FE modelling strategy consists of using Ansys [10] to develop the mesh and then the FE software LS-DYNA [11] to perform an explicit pseudo-static nonlinear analysis. The objective is to evaluate elastic and plastic stiffness, ultimate capacities and failure modes.

The main difference between the two models, axial and bending, is the application of force, but the axial model is a cut of the bending model. For this reason, all the observations that will be made for the bending model in terms of meshing, non-linear phenomena and model validation will be the same for the axial model.

The FE bending model mesh for the *reference case* is presented in section 3.1 and the nonlinear phenomena taken into account in the model are presented in section 3.2

The resulting model is:

- validated in Chapter 4 by comparison against experimental results;
- used to calculate the parametric analysis for the bending in section 5.1;
- used to calculate the parametric analysis for the tension in section 0.

3.1 FE model mesh

This section aims to essentially highlight the choices made in obtaining the mesh and based on these, describe the mesh obtained.

3.1.1 FE meshing choices

The main choices for creating the FE mesh from the geometries are presented below by the component elements of the connection, respectively as studs and tie bars, connection bars, concrete and faceplates.

Studs and tie bars

The mesh of studs and tie bars is made from solid tetrahedral elements, to represent the nonlinear behaviour in the connection zone. The geometry is simplified to reduce the complexity of the concrete mesh around these elements, so the stud heads are not modelled as the complex geometry of the tie bars. In fact, these latter are usually screwed next to the connection with the possible presence of a nut and washer, instead, a simple cylinder attached to the plate is modelled for simplicity. For both, studs and tie bars contained in the *planes xz* of symmetry, half cross-sections of the model are considered and modelled, due to the symmetry conditions.

Embedded connection bars

The embedded connection bars mesh with solid tetrahedral elements, for a better understanding of the non-linear behaviour and have a simplified geometry to simplify the concrete mesh around these elements. The simplification consists of the connection bars' head shape simply defined by a cylinder without the addition of any other nuts or washers.

Concrete

For the concrete, the mesh around the connection bars, tie bars, and studs consists of solid tetrahedral elements. Further away from these areas are more regular hexahedral elements. The mesh is finer in the connection area and coarser in the rest of the model. An automatic surface-to-surface contact is introduced in the connection area that simulates the real adhesion between concrete and steel. To reduce computational times of calculations, contact between concrete and steel elements is defined only in the connection zone. Given the simplified geometry of the stud heads, to reproduce the effects of anchoring, the merged nodes between the concrete and the stud edge surface are considered, where the stud heads were supposed to be.

Faceplates

Since faceplates are the outermost objects that envelop the rest of the model, they adapt their mesh to the previous ones, presenting hexahedral and tetrahedral shapes, more or less fine, with the studs and tie bars sections as element shapes on the plate.
The main hypothesis is that, at least in the part away from the studs or tie bars, the plates are only in tension or compression. For this reason, in this part of the plate hexahedral elements can be used with only one element per thickness (1-element hexahedral mesh in Figure 23)

Local deformations of the plates with bending effects are mainly localised around the studs or tie bars. These parts are a connection between the hexahedral mesh of the plates with the tetrahedral mesh for the concrete surrounding the tie bars and studs. To connect these two different mesh shapes, only tetrahedral elements can be used, ending on average with more than one element in the thickness. This is ideal for a greater understanding of the bending effects of these areas (2-elements tetrahedral mesh in Figure 23).
This hypothesis is confirmed by a test performed on the bending reference case and presented in Appendix 2, where two hexahedral elements are considered in the thickness and consequently, even more in the tetrahedral parts. The results of the test led to the same values confirming the goodness of the hypothesis made.

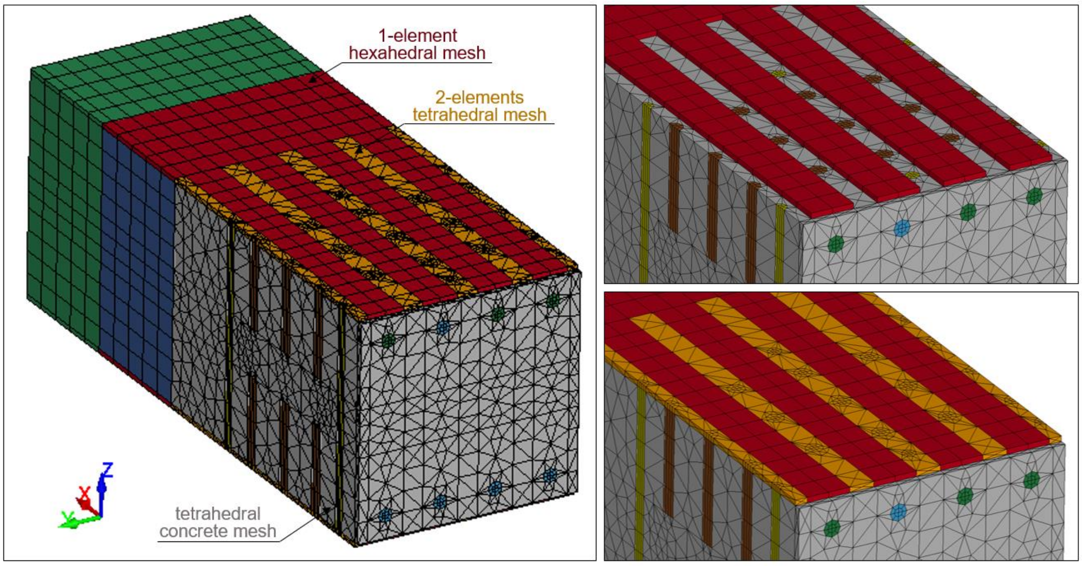

Figure 23 – Differences in faceplate mesh shape (hexahedral-red and tetrahedral-yellow)

Figure 24 resumes the main geometric simplifications in the design of connection bars, tie bars and studs.

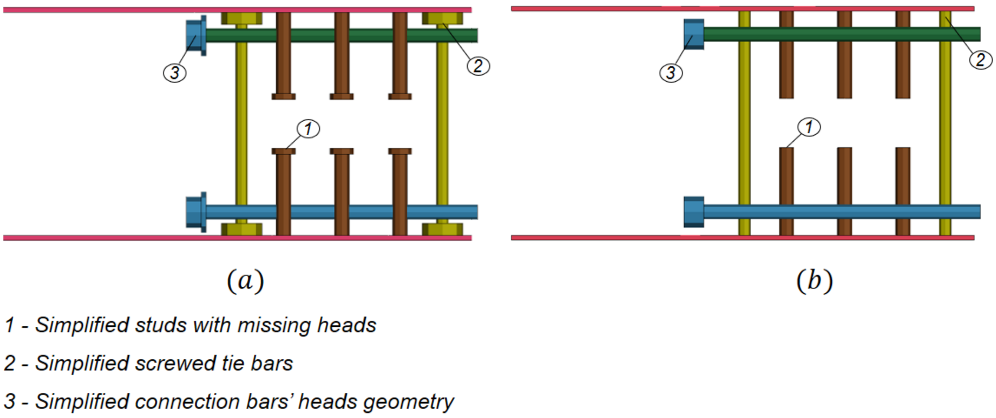

Figure 24 - Modelling simplification (a) Model with large design details (b) Simplified model

3.1.2 Obtained FE mesh

Following the modelling choices described in the previous section, the FE meshing is performed with Ansys [10] FE software for both analyses, bending and axial for each combination.

The FE parametric model consists of only one type of solid element for concrete, faceplates, studs, tie bars and embedded connection bars. Specifically, in Ansys, the solid element used is 3D SOLID164 with 3 displacements as degrees of freedom at each node and with a possible mesh shape of 8 nodes for the hexahedral formulation and 4-5 nodes for the tetrahedral one (see Figure 25).

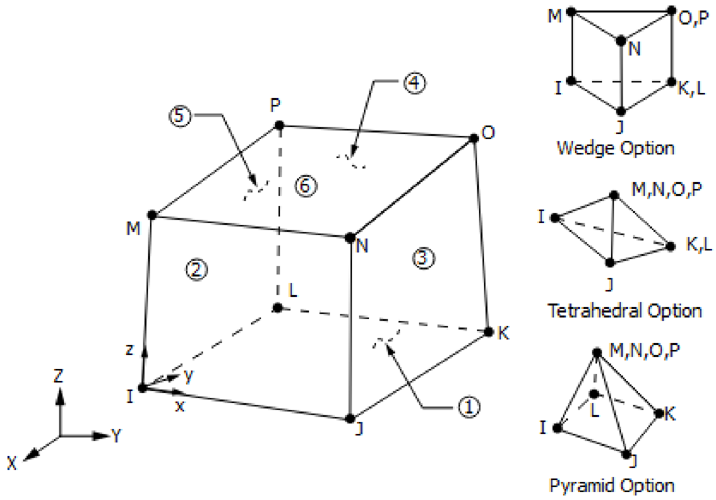

Figure 25 - SOLID 164 Ansys element [10]

A constant stress-reduced integration is used, corresponding to a single integration point at the centre of both hexahedral and tetrahedral elements. This is in order to reduce shear-locking effects leading to stiffer behaviour as in the case of full integration, and also for the reduction of calculation time.

The mesh size is on average 37.5 mm in the connection zone, where the mesh needs to be finer, while it increases to 50 mm for the far elements, where the mesh can be greater. All cylindrical elements, such as connection bars, tie bars and studs, have longitudinal elements of the same length as the connection zone size, while the circumferences are always divided into 8 parts. Figure 26 and Figure 27 show some details of the mesh of the bending reference case.

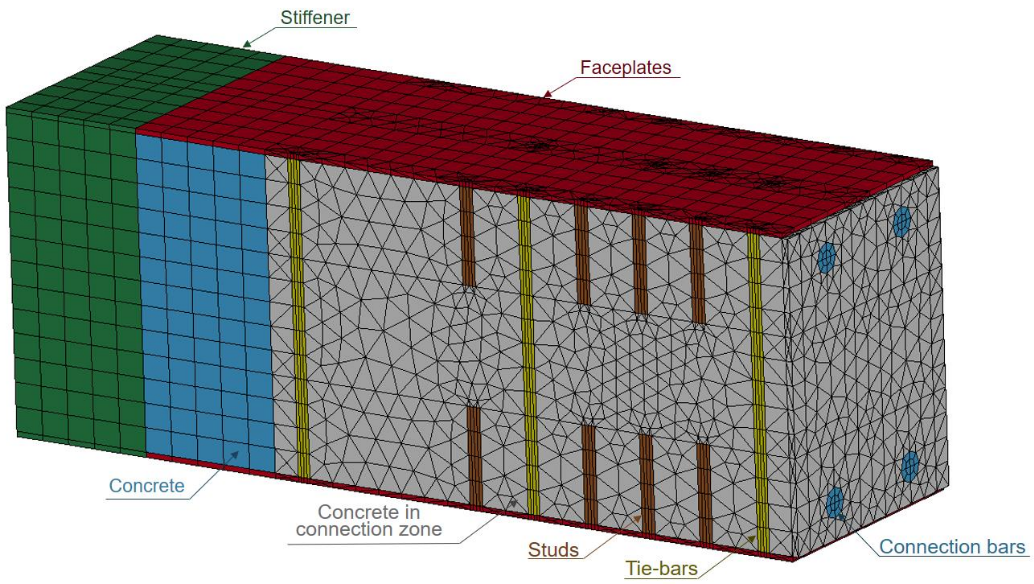

Figure 26 – Meshed reference case model

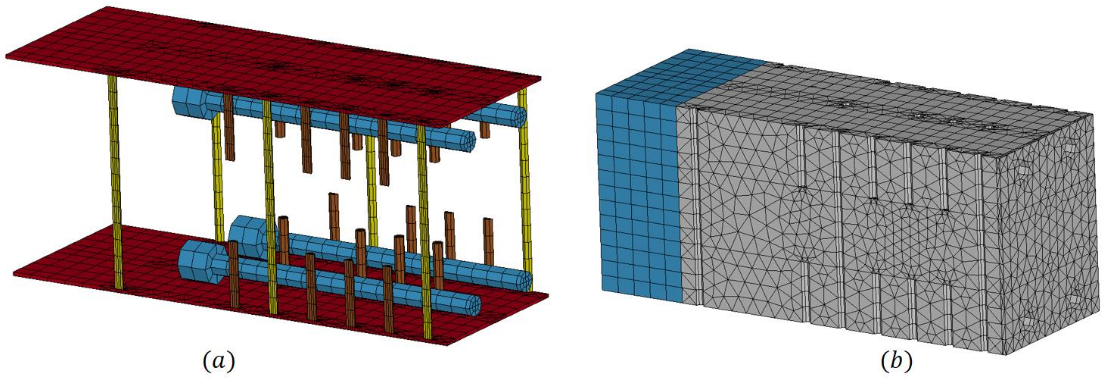

Figure 27 – (a) Details of steel objects mesh (b) Details of concrete mesh

Following are the intervals of variation of the number of elements per analysis: bending and axial.

- For the bending analysis, the total number of elements varies from a minimum of 46397 for model 28 to a maximum of 131339 for model 16. The first is the model with M30 as connection bar diameter, which is the shortest model since a reduced number of studs is required to transmit the ultimate strength; the second is the model with the largest spacing values, respectively 600 mm for tie bars and studs spacing as 150 mm for longitudinal and 200 mm for vertical. The average calculation time for running the model is 12 hours.
- For axial analysis, the total number of elements varies between a minimum and a maximum identified in the same previous models for bending, and are respectively 27236 and 71026, with an average calculation time for running the model of 5 hours.

Integration type considerations

A *reduced integration* is used in the parametric analysis. The choice stems from the possibility of too-stiff solutions given by shear locking, especially in the case of not optimal aspect ratios as in the case of certain elements in the model. A further reason stems from a limitation in the use of LS-DYNA as the explicit solver, as no full integration tetrahedral elements are defined for the explicit analysis.

On the other hand, a potential problem that reduced integration can address are *spurious deformations* and in particular the zero-energy mode as hourglass deformation, where the numerical adsorption of energy leads to a non-physical deformation mode. During the model run, this deformation can be controlled and the limit recommended in the LS-DYNA manual [12] is 0.11 as the overall ratio of hourglass energy to internal energy.

Figure 28 shows the evolution over time of the ratio between hourglass energy and internal energy for the reference case of bending. As can be seen, the overall values, addressed as the *Total*, are in the recommended range and it follows the trend of concrete, which appears to be the object that governs the global ratio behaviour of the model. Looking at the individual components, some peaks can be seen, especially in the tie bars and studs, but these recover after a while.

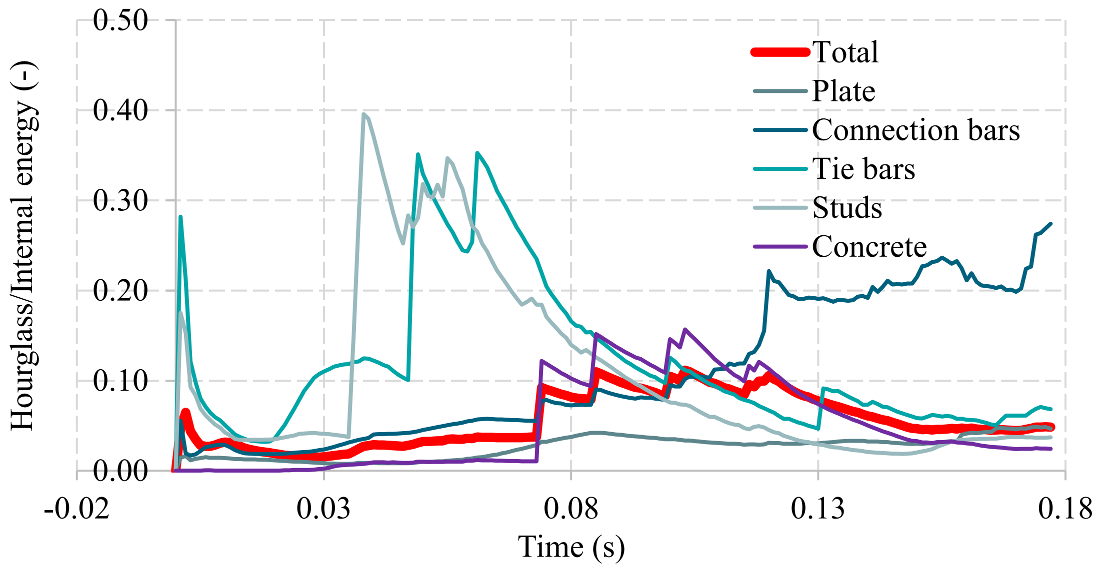

Figure 28 – Ratio of hourglass energy to internal energy for the bending reference case

Figure 29 shows the deformation of the bending reference case at 0.05s in correspondence with one of the peaks in the hourglass to internal energy ratio for the tie bars. The deformations present a scale factor of 10 times in the x-direction, and a typical hourglass deformation in the tie bars can be observed.

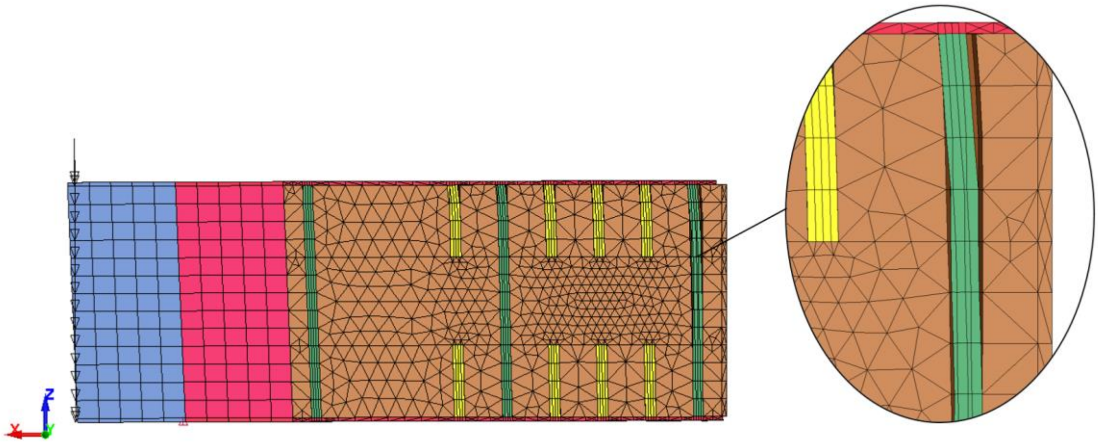

Figure 29 – Bending reference case deformation at 0.05s with hourglass tie bars deformation (10 times the scaling factor for x-deformation)

The conclusion is that, with the exception of singular values that recover overtime during the calculation, the ranges are under control and make the use of reduced integration a good option for the mesh assumption.

Mesh size and time-step considerations

In the explicit analysis, the calculation time depends on the time-step, as it will improve or reduce the number of steps in the calculation, and this in turn depends on many factors, but mainly on the material, element size and shape, in one word the aspect ratio. The smallest value of the time step recorded in the model among all the elements will define the global time step. In fact, the time step can be calculated as the ratio of the *characteristic length* (L_c) to the *adiabatic sound speed* (c), i.e., the sound speed in a material.

- The *characteristic length* can be obtained, for an 8-node solid element, from the ratio of the element volume (V_e) to the maximum element area of the element itself (A_{max}). This means that the calculation time depends on the quality of the mesh. The best element shape is the regular tetrahedron and hexahedron, where the best ratio can be found. A deformation from a regular volume leads to a maximisation of the area of the element, which leads to a reduction in the time step.

  Following, it is reported the critical time-step expression that can be found in the Ls-DYNA Manual [12].

$$\Delta t_e = \frac{L_c}{c} = \frac{V_e}{A_{max} c}$$

In this analysis, different mesh sizes were tested and the optimal values came out to be 37.5 and 50 mm, respectively for the parts with higher and lower element densification, leading to an average time-step of $1.13 \cdot 10^{-7}$. The model was tested in a range between 30 to 70 mm and it was observed that the results were not mesh-dependent, at least for this range. The conclusion on mesh size is related to the optimum in terms of calculation time.

- The *adiabatic sound speed* expression is proportional to the square root of the ratio of the material's stiffness to its density, as shown in the following formula [12]:

$$c = \sqrt{\frac{E(1-\nu)}{(1+\nu)(1-2\nu)\rho}}$$

The choice to use a material 100 times stiffer than steel for the stiffener to apply the bending load in the bending parametric model, was a good compromise between the need to have a stiffer element for load transmission, to limit the non-linear behaviour influences, and the need not to influence the time step. In fact, higher values of Young's modulus (E) would lead to higher values for the sound speed and, consequently, to lower time-step values.

3.2 Considered nonlinear phenomena

The FE model represents the nonlinear behaviour of the wall-to-wall connection by considering two different nonlinear phenomena in LS-DYNA calculations:

- The material nonlinear behaviour of elements by using nonlinear constitutive models;
- The contact condition at the concrete-steel interface by using a unilateral contact condition.

3.2.1 Concrete nonlinear behaviour

The constitutive law chosen in this study for Concrete is CSCM (Concrete Smooth surface Cap Model) implemented in LS-DYNA [12]. The model describes the nonlinear behaviour of concrete in both compression and tension until the failure. The model formulation takes into account two nonlinear phenomena:

- Post-elastic concrete behaviour, which replicates the stresses of inelastic concrete;
- Damage to concrete, simulating the decline in stiffness of concrete due to both compressive and tensile behaviours. The internal variable for this occurrence is the

scalar damage variable, which runs from d=0 (undamaged material) to d=0.99 (highly damaged material).

Figure 30 shows the general shape of the concrete model yield surface in two dimensions:

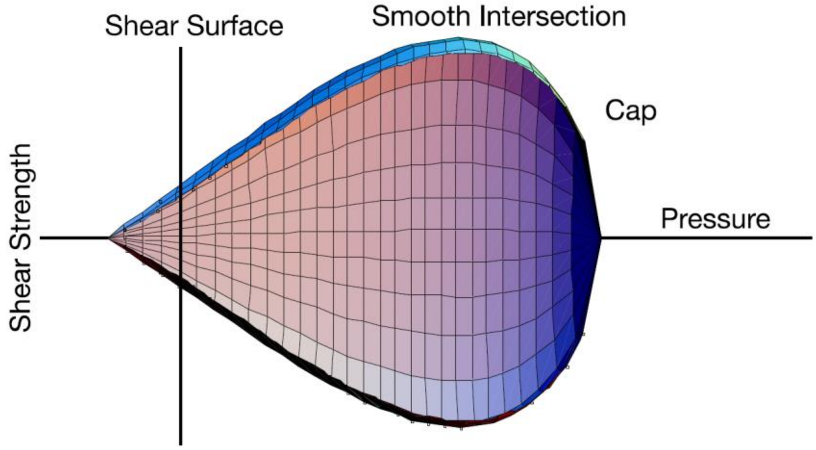

Figure 30 - General shape of concrete model yield surface in two dimensions [13]

The option of LS-DYNA for eroding highly-damaged concrete elements is activated. More in detail, it has been chosen that a concrete element is eroded if the damage variable reaches and concrete strain is higher than 5%. The choice of 5% is only determined by the purpose of a clearer visualization of the crack pattern. In fact, as can be seen in Appendix 3, the use of erode setting in a monotonic load does not affect the results contrary to a cyclic load application The CSCM model depends on a considerable set of parameters, but they can be estimated automatically by LS-DYNA from the three “basic” parameters: density, compressive strength, and maximum aggregate size. With these retained parameters for concrete of class C30/37, a uniaxial compression test gives the following stress-strain curve:

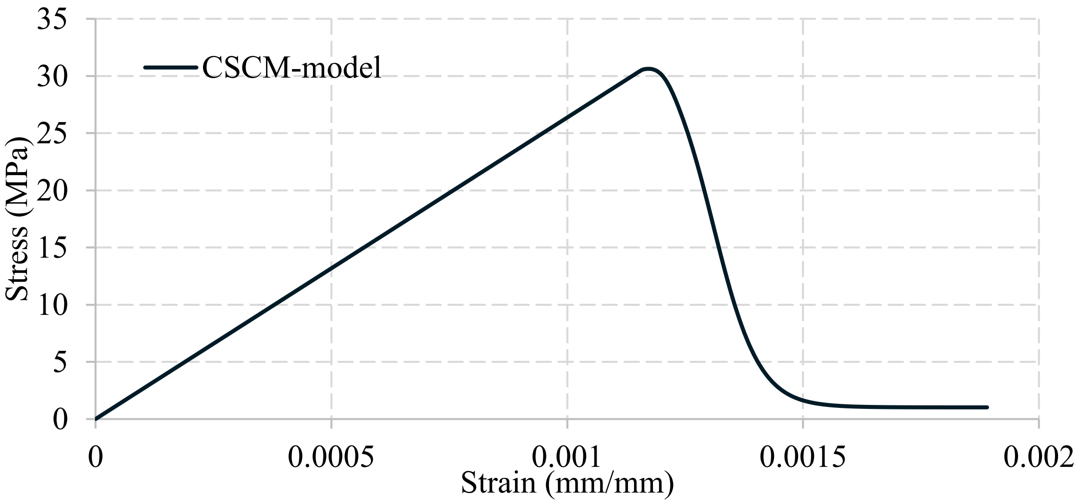

Figure 31 - Stress-strain curve for a uniaxial compression test with CSCM model

The model takes into account the increase of compressive strength for confined concrete. Two different tests were carried out on an 8 nodes unitary cubic element made of concrete C30/37:

- Compressive test with increasing confinement pressure;
- Compressive and tensile test with oedometric boundary conditions.

Compressive test with increasing confinement pressure

The test consists of taking 8 nodes unitary cubic element and constraining the base in the vertical direction as simple supports. Increasing confinement pressure, from 0 to 30 MPa, with the application to all cubic surfaces, and then the application of the compressive pressure on the top surface until the failure. Figure 32 shows the uniaxial vertical compression and the confinement configurations. The test aims to reproduce the confinement effect given by the faceplates.

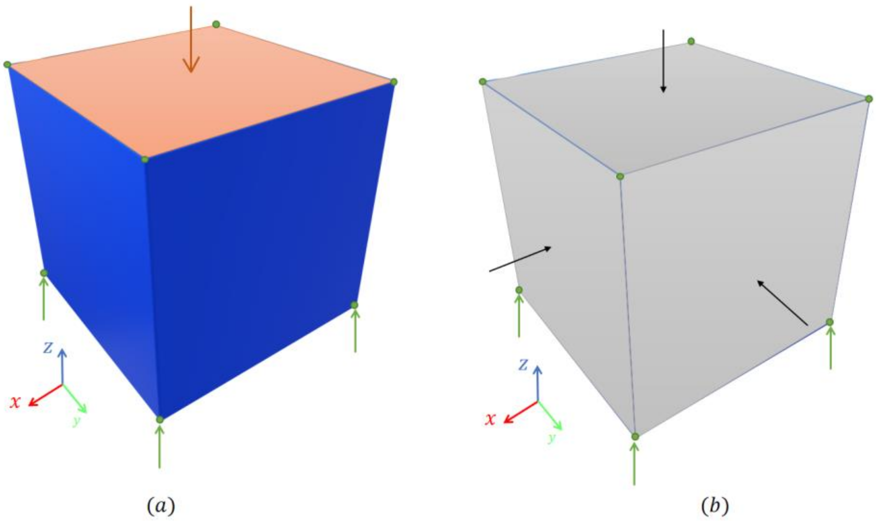

Figure 32 – (a) Compressive pressure application (b) Confinement pressure application

Figure 33 shows the stress-strain results, and it can be seen that concrete of 30 MPa as a characteristic strength by increasing the confining pressure increases, in turn, its ultimate capacity.

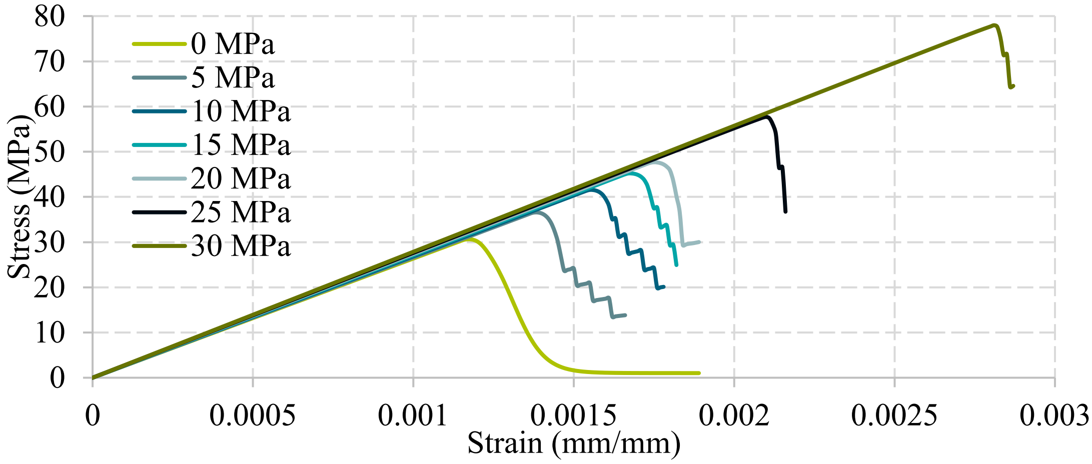

Figure 33 - Stress-strain curve for a uniaxial compression test with increasing confinement pressure from 0 to 30 MPa with CSCM model

Compressive and tensile test with oedometric boundary conditions.

This second test is performed on the same 8 nodes unitary cubic element, but this time oedometric conditions are applied, as shown in Figure 34. Therefore, vertical and two directions horizontal movements are constrained at the base, while only the two horizontal movements are constrained at the upper nodes, allowing vertical movements but no horizontals. This test aims to reproduce the effect of SC wall continuity over simple modelled strips. In opposition to the ordinary oedometric test, where only compression is applied, this time both compression and tensile are applied.

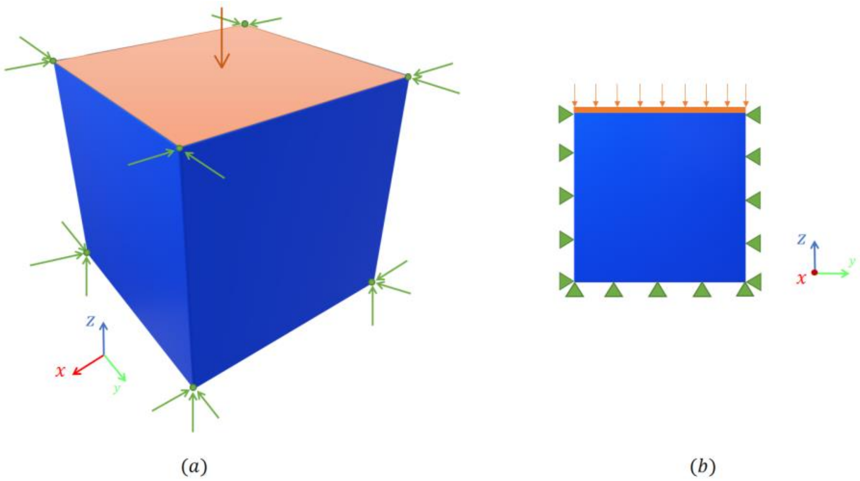

Figure 34 – (a) Compressive and tensile pressure application (b) Oedometric boundary conditions

Once again, an improvement in the ultimate capacity for compression is noted, as shown in Figure 35. While no improvement is noted for the tensile strength. In fact, the maximum value achieved is 2.90 MPa corresponding to the average tensile strength for concrete class C30/37[14].

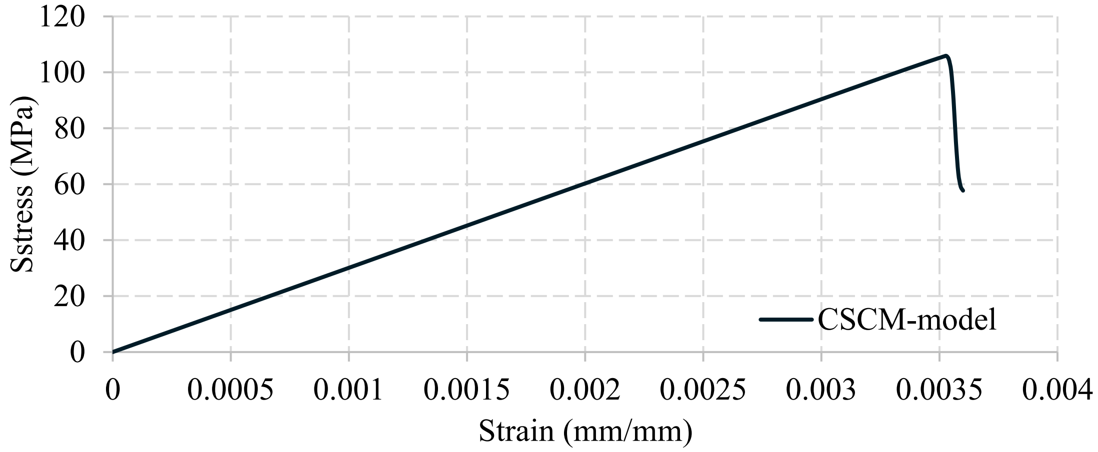

Figure 35 - Stress-strain curve for a uniaxial compression test with oedometric boundary conditions with CSCM model

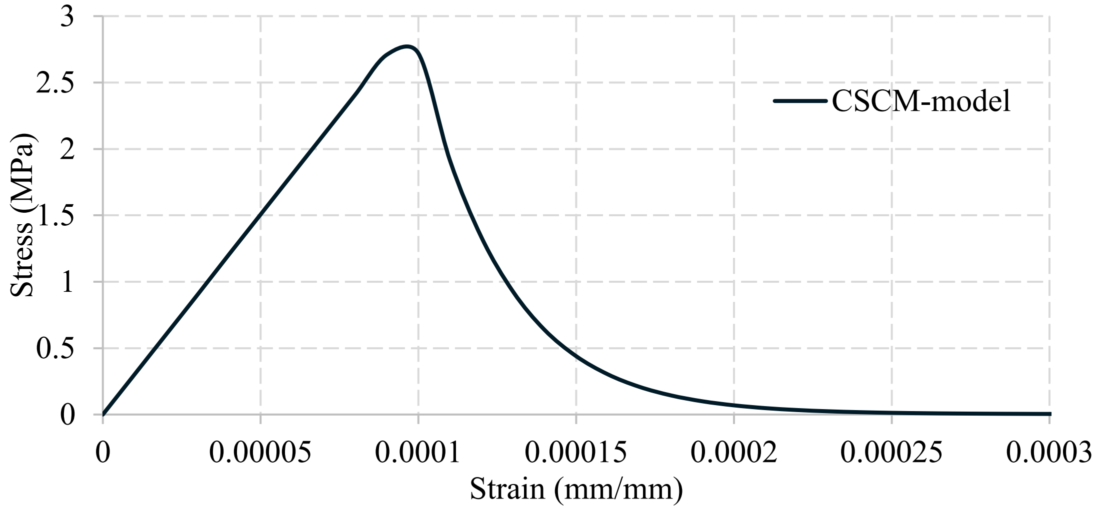

Figure 36 - Stress-strain curve for a uniaxial tensile test with oedometric boundary conditions with CSCM model

3.2.2 Steel nonlinear behaviour

Steel elements are modelled with an elastic-plastic behaviour with linear kinematic hardening. In LS-DYNA, the constitutive model representing this behaviour is MAT_PLASTIC_KINEMATIC [11]. The low is defined as a double continuous line, where the first slope is defined by the elastic stiffness, the second by the post-elastic stiffness, and the limit between these two is the yield stress. Additional parameters to be provided for calculation are steel density and Poisson's coefficient.

Eventually, the LS-DYNA erode option can also be activated for steel. Based on the bi-linear low, it is possible to calculate the strains corresponding to the ultimate stress for each steel grade and add them into the settings. The steel element that reaches this stain

value disappears and no longer contributes to the resistance. In particular, only the axial analysis is developed with the eroding options activated for a better understanding of the failure modes. Indeed, with an infinite plastic branch, it is more difficult to make the distinction between local failure, for a specific element, and global one.
In Appendix 3, the reference case is tested for bending with the steel-erode options activated and it can be seen that the failure appears in both cases simultaneously.

Figure 37 shows the MAT_PLASTIC_KINEMATIC model, under a uniaxial tensile test on an 8-node unitary cubic element of steel grade S235, with and without the erode option. Basically, the difference is a drop in resistance at the ultimate stress.

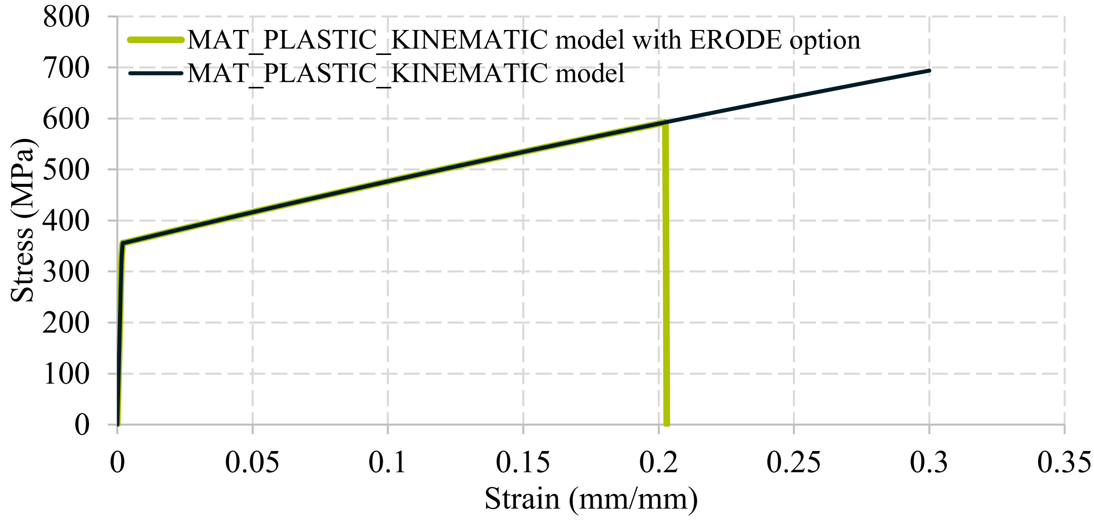

Figure 37 - Stress-strain curve for a uniaxial tensile test with Linear kinematic hardening law

3.2.3 Unilateral contact condition for concrete-steel interface

As presented in the boundary conditions section described in 2.5.1 for bending and 2.5.2 for axial, a contact condition is applied at the interface between the concrete and steel elements in the connection zone. Except for the end surfaces of the studs in contact with the concrete, wherein the actual design there are heads that provide the anchorage. In order to reproduce the effect of the anchors, a merged condition is realised between these nodes, so in actual fact, the stud is doubly clamped at the base with the faceplate and at the head with the concrete.

In LS-DYNA the AUTOMATIC SURFACE-TO-SURFACE contact allows the introduction of master elements (steel elements) that move and slave elements (concrete

elements) that deform due to the movement of the former. Only deformation is present, with no penetration. This provides a more realistic contact and a better estimation of the friction between these elements. This condition provides a free-sliding effect along the connection bars, as they are not ribbed or with improved adhesion.
The use of this automatic estimation for the contact conditions turned out to be the best solution with respect also to another alternative tested in which a layer of weak material is used around the connection bars and at the contact between the faceplates and the concrete to simulate the sliding effect between these elements.

Figure 38 shows the detail of the contact condition in the connection zone and the clamped head conditions for the studs.

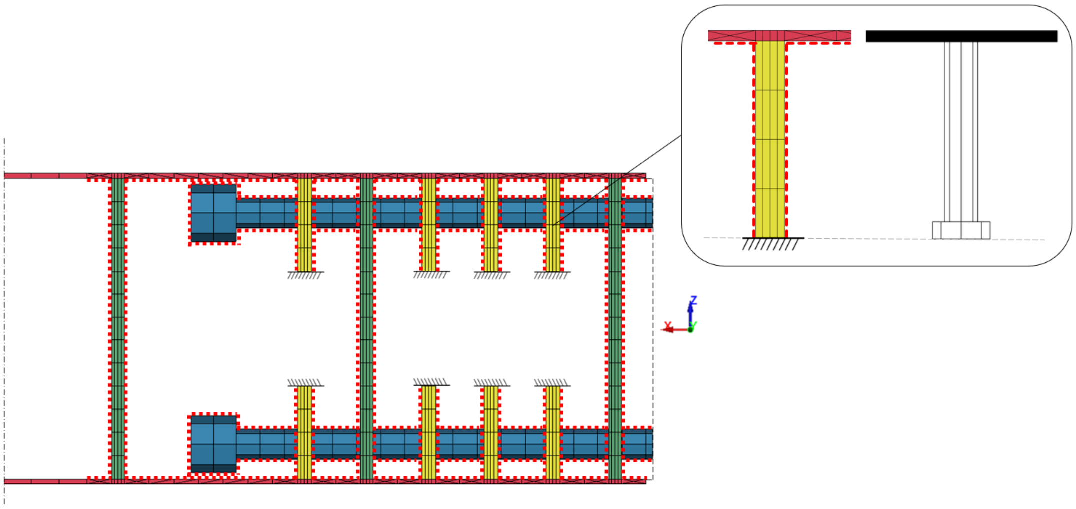

Figure 38 – Detail of the contact conditions in the connection zone

Chapter 4

FE model validation

In this chapter, the FE model presented in Chapter 3 is validated by comparison to the available experimental results.

4.1 FE model validation from experimental results

The available experimental results are those of the test performed for the experimental part of WP5 in the SCIENCE project [15]. For this study, the geometry and properties of the SPECIMEN E are used as a reference for the numerical calculation.

The validation consists of two different steps:

- Creation of Specimen E numerical model based on the geometry of the WP5 bending test and definitions of numerical assumptions to match numerical and experimental results;
- Simplification of the Specimen E numerical model to obtain the parametric model presented in Chapter 3.

4.1.1 Numerical modelling based on the geometry and properties of the SPECIMEN E

The experimental test of WP5 in the SCIENCE project, referring to the SPECIMEN E, is described in this section.

The test consists of a 4,8 m span beam specimen configured for a four-point bending test with simple supports at both ends and 1MN capacity actuators located at 0,3 m and 4,7 m from the end of the specimen (see Figure 88). An imposed vertical load is assured by two hydraulic jacks with a load application of 2mm/min. The test is performed up to the maximum extension of the actuator which is 200mm. Figure 39 shows the global mechanical set-up with the instrumentations and Figure 40 shows Specimen E at the end of the test.

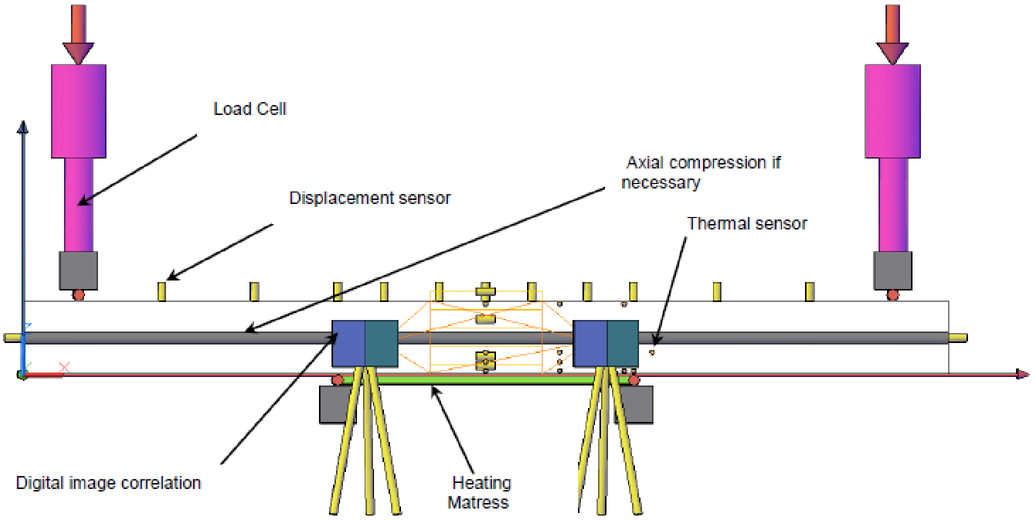

Figure 39 - Global Mechanical Set-up including the instrumentations [15]

Figure 40 - Specimen E at the end of the test [15]

Boundary conditions and load hypotheses

Since the parametric model is modelled based on the four-point beam test, which turns out to be a simplification of the experimental model, the same observations made for the parametric model, in terms of mesh choices and non-linear phenomena presented for the parametrical model in Chapter 3, can be fully extended to the Specimen E model. The main difference between the two models is the modelling of the beam away from the connection zone and the application of the load. Further observations, specific to the Specimen E model, are given in the following sections.

Figure 41 shows the geometry of Specimen E with its components, and the beam strip that can be modelled is highlighted in light grey. In addition, Figure 42 shows the geometry detailed of the modelled part and Figure 43 the actual model geometry.

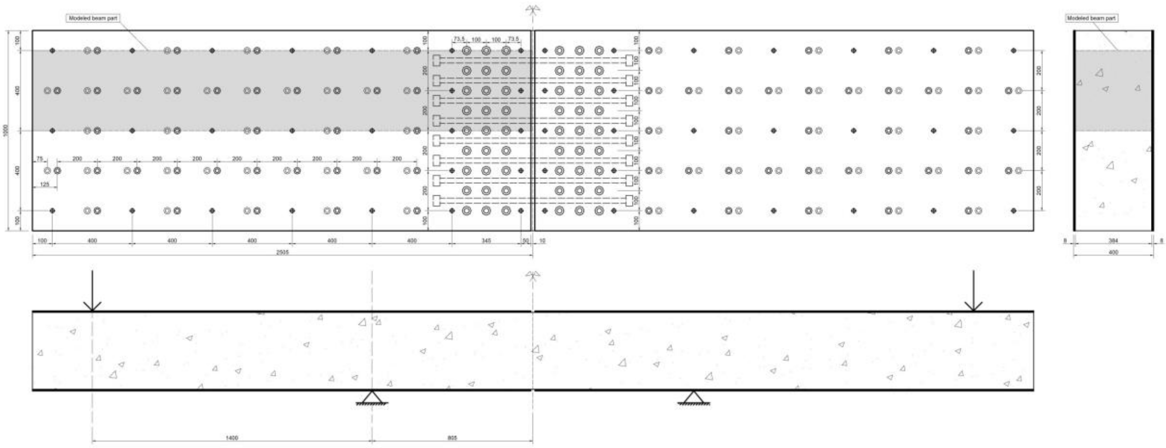

Figure 41 - Geometry of Specimen E

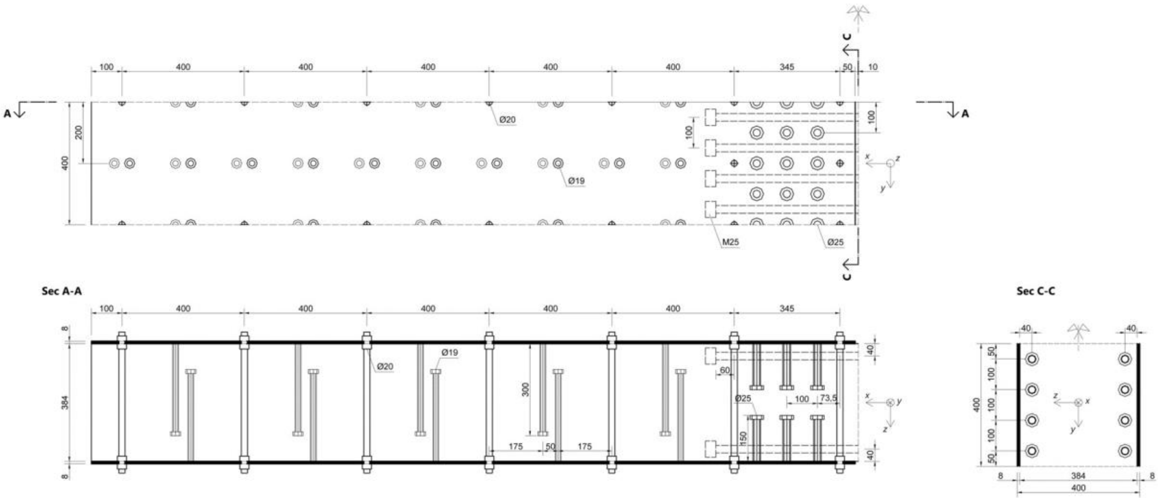

Figure 42 - Detail of the geometry of the modelled beam part

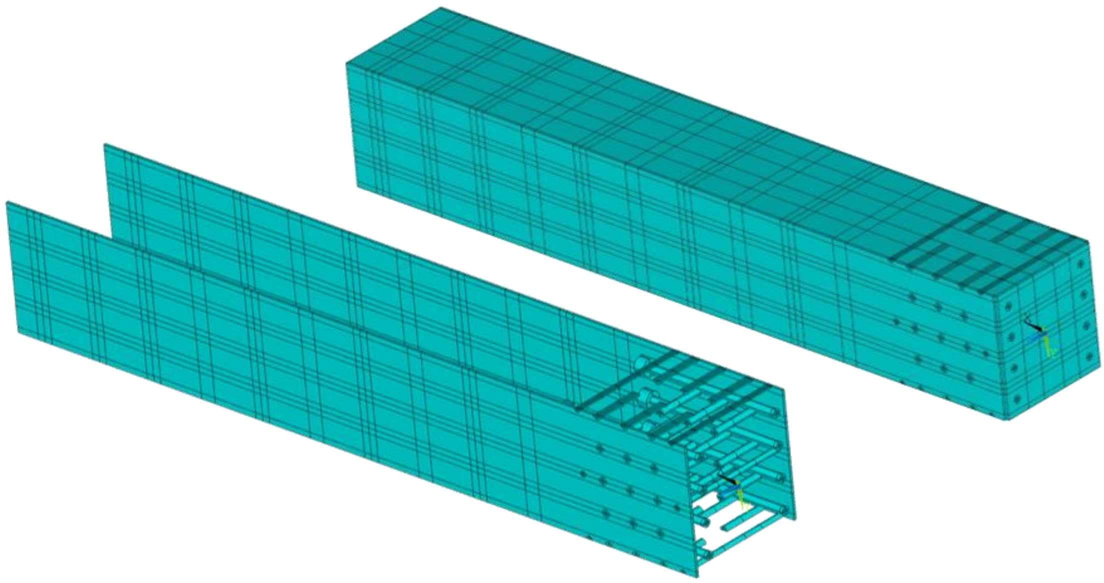

Figure 43 - Model geometry

- Boundaries conditions

  There is a symmetry in the midspan in the longitudinal direction of the beam and in the transverse direction a series repetition of the strip as for the parametric model.

- Load application

  The main modelling difference between the two models, parametric and Specimen E, is that in the parametric model only the part to the right of the support (see Figure 44), corresponding to the connection zone, can be modelled, whereas for Specimen E the entire model must be modelled without longitudinal geometrical simplifications. In the former case, the focus is more on the connection zone only, and everything to the left is only a modelling strategy for a matter of load application; in the latter, the aim is to reproduce the experimental test as closely as possible.

  For the load application of Specimen E, the entire beam is modelled without the use of any stiffener, but rather with a configuration closer to the actual test load application, using a monotonic incremental force at the jack position. To reduce the concentration of stresses at the load application position, resulting in local deformations, the nodal force is distributed between three lines of nodes and along the beam width nodes.

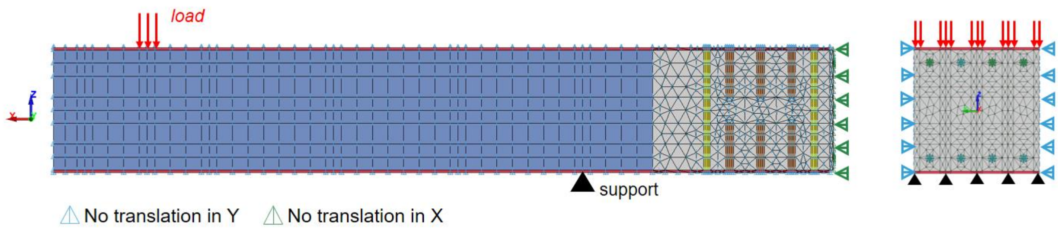

Figure 44 – Specimen E model

FE meshing choices

The main choices for creating the FE mesh from the geometries are the same for the parametrical model already presented in 3.1.1, further choices to be made in addition to those already presented can be found below:

- Studs and tie bars:

  For the studs and tie bars mashing solid elements are used in the "connection zone," adjacent to the embedded connection bars, while beam elements are modelled in the rest of the model. The use of the beam element is done to simplify the mesh, while the volumetric elements are used in order to represent the nonlinear behaviour in the connection zone.

Half cross-sections of studs and tie bars contained in the *planes xz* of symmetry of the model are considered, due to the symmetry conditions. A geometric half cross-section is defined for volumetric elements, and an equivalent cross-section is defined for beam elements, consisting of a reduced modelled circular cross-section area equal to half the actual cross-section.

- Embedded connection bars

  The connection bars in the compression part of the beam have a steel grade of 8.8 while in the tensile part, 3 out of 4 bars have a steel grade of 10.9 and one is 8.8.

- Faceplates:

  Studs and tie bars are considered welded to the faceplate for both volumetric and beam elements. This condition is simply expressed by the presence of common nodes between these two elements.

Obtained FE mesh

Following the previous choices, the FE meshing is performed with Ansys [10] FE software. The FE model is composed of two different types of finite elements:

- Solid elements for concrete, faceplate, studs, tie-bars, and embedded connection bars: 3D SOLID164 model which has 3 displacements as degrees of freedom at each of the 8 nodes of the hexahedral and tetrahedral mesh support element (see Figure 25):
- Beam elements for studs and tie-bars outside the connection zone: 3D BEAM161 model which has 3 displacements as degrees of freedom at each of the 2 nodes of the mesh support element (see Figure 45):

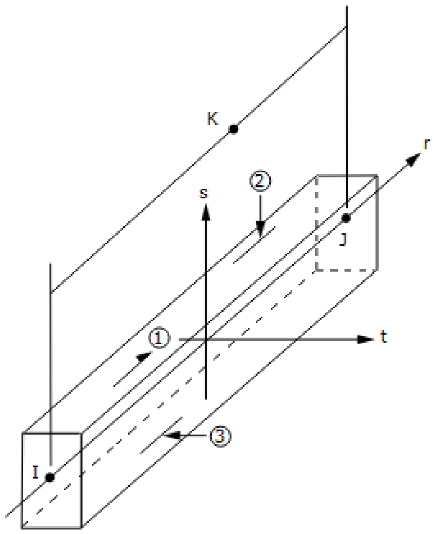

Figure 45 - BEAM 161 Ansys element [10]

Table 13 shows the number of finite elements (total and per component) for the model mesh. On average, the mesh in the reference case is 45 mm for elements in the connection zone and 70 mm for elements outside the connection zone.

Table 13 - Number of finite elements for the model mesh

Component	Solid elements	Beam elements	TOT
Faceplates	5045	-	5045
Concrete	30273	-	30273
Connection bars	1472	-	1472
Tie-bars	480	-	480
Tie-bars beam	-	80	80
Studs	1152	-	1152
Studs beam	-	240	240
Total			38742

Some global views of the FE mesh are presented in Figure 46, Figure 47 and Figure 48.

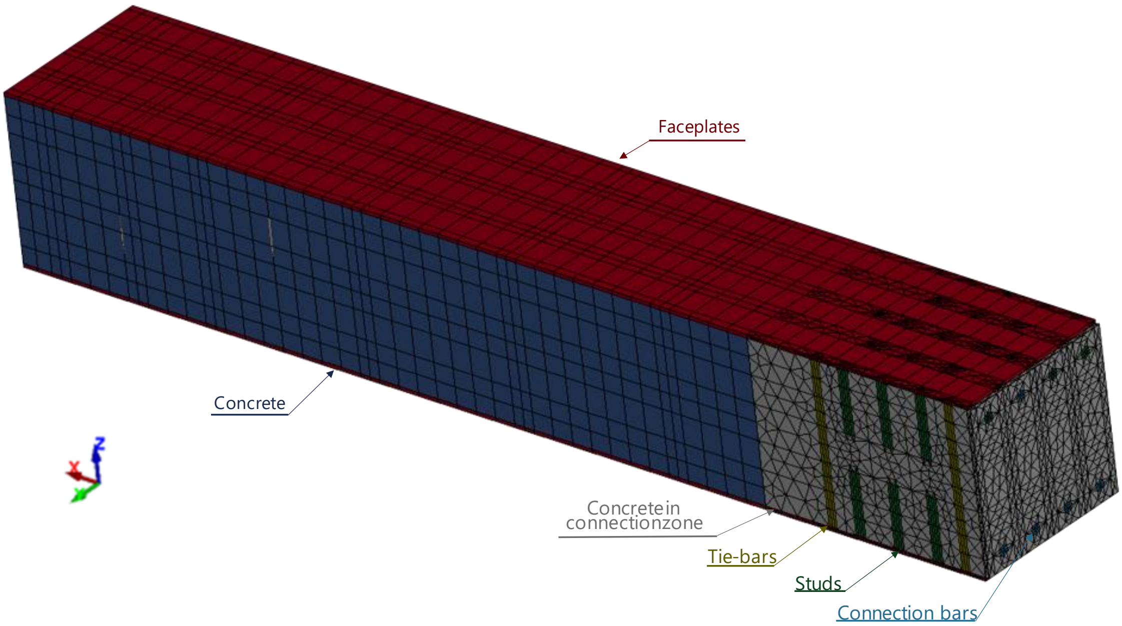

Figure 46 – Specimen E model

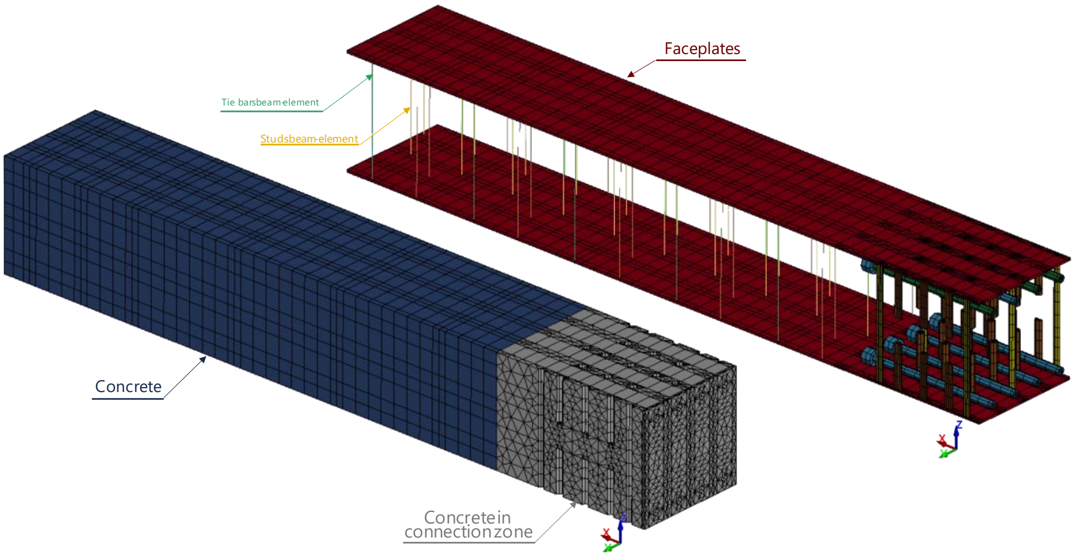

Figure 47 - FE model with concrete and steel objects detailed

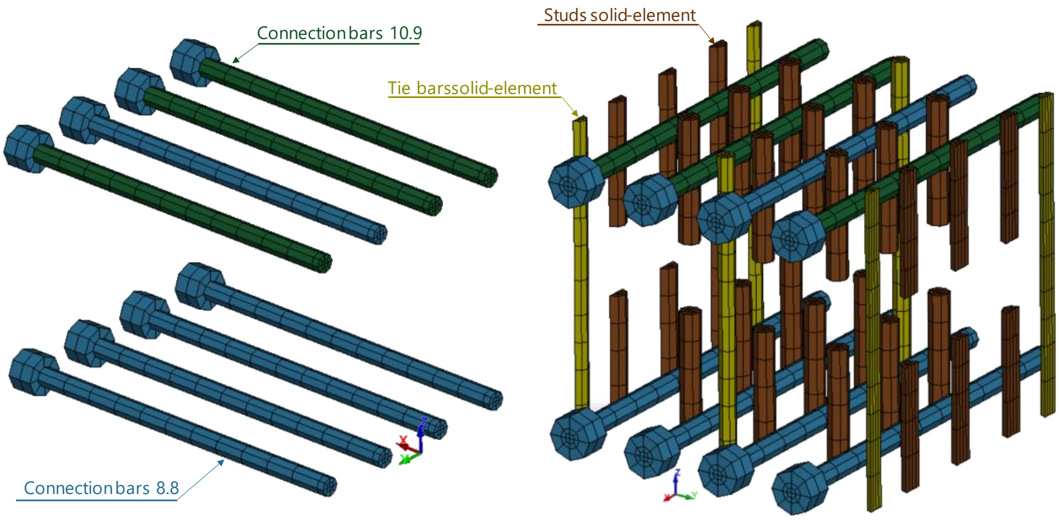

Figure 48 – Solid mesh of connection bars, tie bars, and studs details

Material and geometric property values

From Table 14 to Table 18, all material and geometric properties are shown for each component: concrete, faceplates, tie bars, studs and embedded connection bars. The material properties referring to yield and ultimate stress are given by experimental results, reported in Appendix 4, while all others refer to standard values.

Table 14 – Concrete properties

Element	Description	Parameter	Units	Values
Concrete C30/37	Density	ρ	kg/m^3	2200
	Compressive yielding strength	f_c	MPa	38
	Maximum aggregate size	d_{max}	mm	16
	Thickness	H_c	mm	400

Table 15 – Faceplates' properties

Element	Description	Parameter	Units	Values
Faceplates $S235JR + N$	Density	ρ_s	kg/m^3	7850
	Young's modulus	E_s	GPa	210
	Yielding strength	f_{sy}	MPa	299
	Failure strength	f_{su}	MPa	423
	Post-elastic modulus	E_p	GPa	1.30
	Poisson ratio	ν_s	-	0.3
	Thickness	t_p	mm	8

Table 16 - Tie bars properties

Element	Description	Parameter	Units	Values
Tie bars for beam and sold elem. $S355JR + AR$	Density	ρ_s	kg/m^3	7850
	Young's modulus	E_s	GPa	210
	Yielding strength	f_{sy}	MPa	434
	Failure strength	f_{su}	MPa	555
	Post-elastic modulus	E_p	GPa	1.30
	Poisson ratio	ν_s	-	0.3
	Diameter	d_t	mm	20
Tie for solid elem.	Horizontal spacing	s_{tx}	mm	345
	Vertical spacing	s_{ty}	mm	200
Tie for beam elem.	Horizontal spacing	s_{tx}	mm	400
	Vertical spacing	s_{ty}	mm	400

Table 17 - Suds properties

Element	Description	Parameter	Units	Values
Studs for solid and beam elem. $S235J2 + C450$	Density	ρ_s	kg/m^3	7850
	Young's modulus	E_s	GPa	210
	Post-elastic modulus	E_p	GPa	1.30
	Poisson ratio	ν_s	-	0.3
Studs for solid elem. $\phi 25$	Yielding strength	f_{sy}	MPa	402
	Failure strength	f_{su}	MPa	519
	Diameter	d_s	mm	25
	Horizontal spacing	s_{sx}	mm	100
	Vertical spacing	s_{sy}	mm	100
Studs for beam elem. $\phi 19$	Yielding strength	f_{sy}	MPa	450
	Failure strength	f_{su}	MPa	532
	Diameter	d_s	mm	19
	Horizontal spacing	s_{sx}	mm	175
	Vertical spacing	s_{sy}	mm	200

Table 18 - Connection bars properties

Element	Description	Parameter	Units	Values
Embedded connection bars 8.8 and 10.9	Density	ρ_s	kg/m^3	7850
	Young's modulus	E_s	GPa	210
	Yielding strength	f_{sy}	MPa	640, 900
	Failure strength	f_{su}	MPa	800, 1000
	Post-elastic modulus	E_p	GPa	1.30
	Poisson ratio	ν_s	-	0.3
	Diameter	d_b	mm	25
	Vertical spacing	s_{by}	mm	200

4.1.2 Simplification of the model to obtain the parametric model

As explained earlier, the parametric model is created from the idea of a four-point beam as the available experiment and it is a simplification of the Specimen E model, which is the closest representation of the experiment, but this large model has disadvantages in terms of parametric performance:

- The calculation time performance. In fact, the large model takes 26 hours compared to 10 hours for the short model.
- Non-linear effects in the beam tail. The part beyond the support and away from the connection zone must be modelled and modified according to the different combinations, thus becoming part of the parametric analysis, with the possibility of non-linear effects influencing the results.

Figure 49 shows the two models using the same geometric parameters and materials as in the experimental test. After the support, in the connection zone, nothing changes, while the main difference concerns the rest of the beam and the application of the load. As can be seen, the lever arm of the Specimen E model is much larger than the parametric one, respectively 1.4 m versus 0.225 m. For this reason, a greater force must be applied to the parametric model for the same bending moment, with the possibility of local deformations. From here is the idea of using a stiffener with an elastic material 100 times stiffer than steel, and the distribution of the load all over the edge-face.

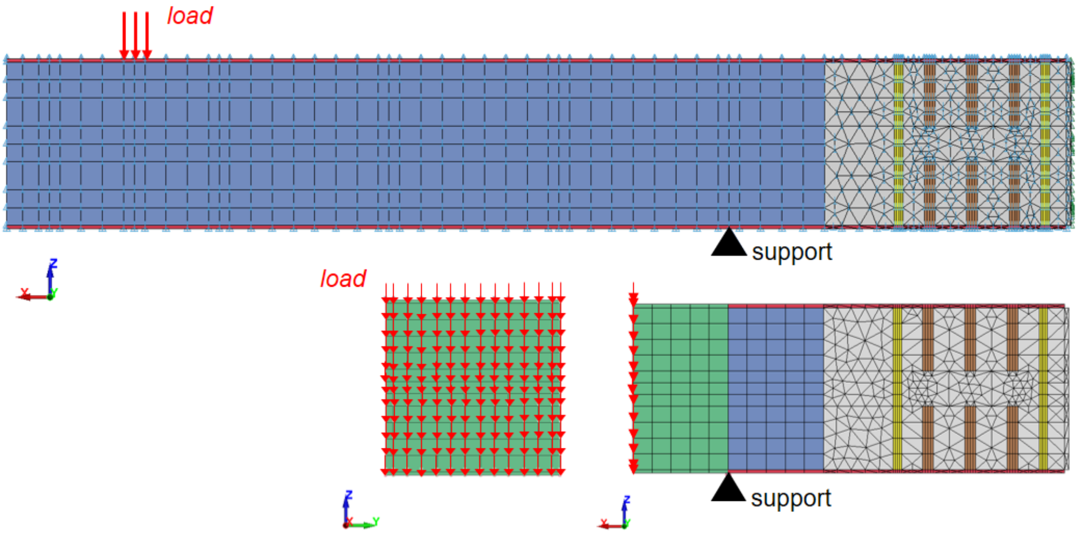

Figure 49 – Above Specimen E model, below parametrical model

4.2 Comparison between experimental and numerical results

The results of the experimental test are provided by the sensors installed on the specimen. Specifically, sensors D7, D8, D9, D10, D11, and D12 measure vertical displacement (*z-direction*) and are positioned along the length of the beam, as shown in Figure 50. Sensor D7 represents the displacement of the beam in correspondence with the midspan. The additional JD sensor measures the displacement of the jack, i.e., the displacement at the applied force.

Sensors D14, D15, D16 and D17 measure the horizontal displacement of the concrete along the entire thickness of the beam, positioned symmetrically with respect to the centre of the beam, as shown in Figure 50. The sensors run from the bottom of the beam thickness to the top and, in particular, only sensor D14 records negative values, representing compression, while all others show positive values, signifying tension.

The following sections present the comparison between the obtained results for both Parametric and Specimen E numerical models with the experimental data of the experimental part of WP5 in the SCIENCE project [15].

Since the experimental results refer to a model with a width of 1 m, the results obtained from the models, which have a base of 0.4 m, were scaled to make the comparison with the experimental data congruent.

The triple comparison is only possible with displacements D7 to D10 because, being the parametric model shortest, they are the only available vertical displacements. Of all of them, the most representative is considered to be the midspan. The D10 sensor is in correspondence with the support where there is no vertical displacement, which is why it is neglected in the comparison for a clearer display of the graphs that only include significant data.

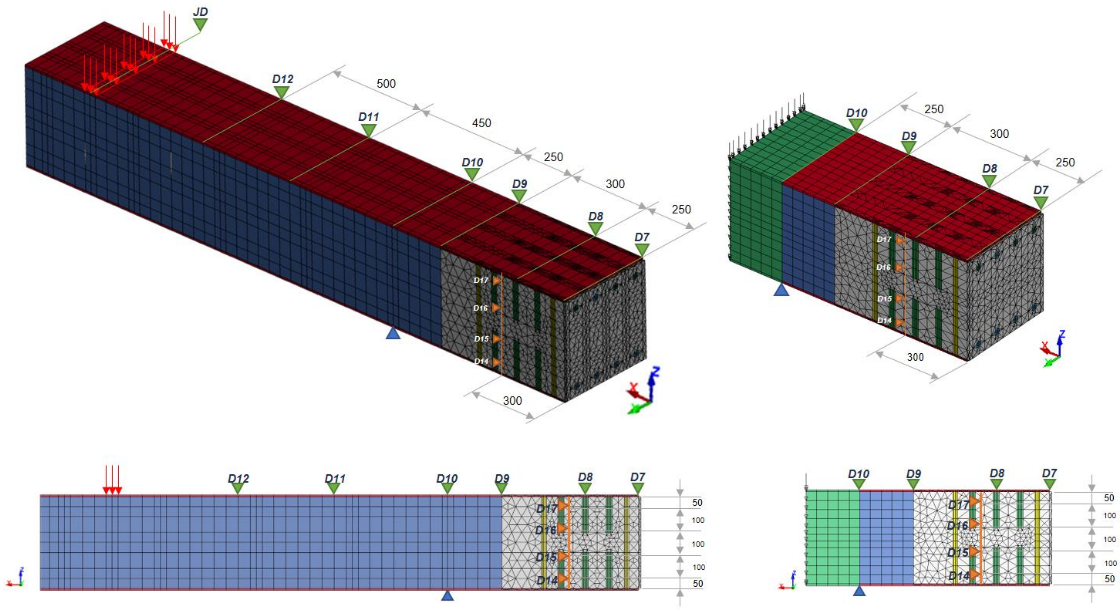

Figure 50 - Position of sensors on the models

The conclusion of these comparisons is that the two numerical results of the parametric model and the Specimen E model are similar, with even better results for the parametric model in the connection zone in terms of displacements. In fact, for the latter, all non-linear effects in the rest of the beam are removed. This leads to the conclusion that the simplification of removing the rest of the beam and using a stiffener to apply the load is consistent. However, both results tend towards the experimental ones, which leads to a further conclusion: the validation of both numerical models, but especially of the parametric one, since it is intended to be used for the parametric analysis.

4.2.1 Bending moment versus displacements comparison

Figure 51 shows the comparison of the jack displacement and the bending moment for the Specimen E model with the experimental results, while Figure 52 shows the comparison of the midspan displacement and the bending moment for both numerical models parametric and Specimen E with the experimental results.

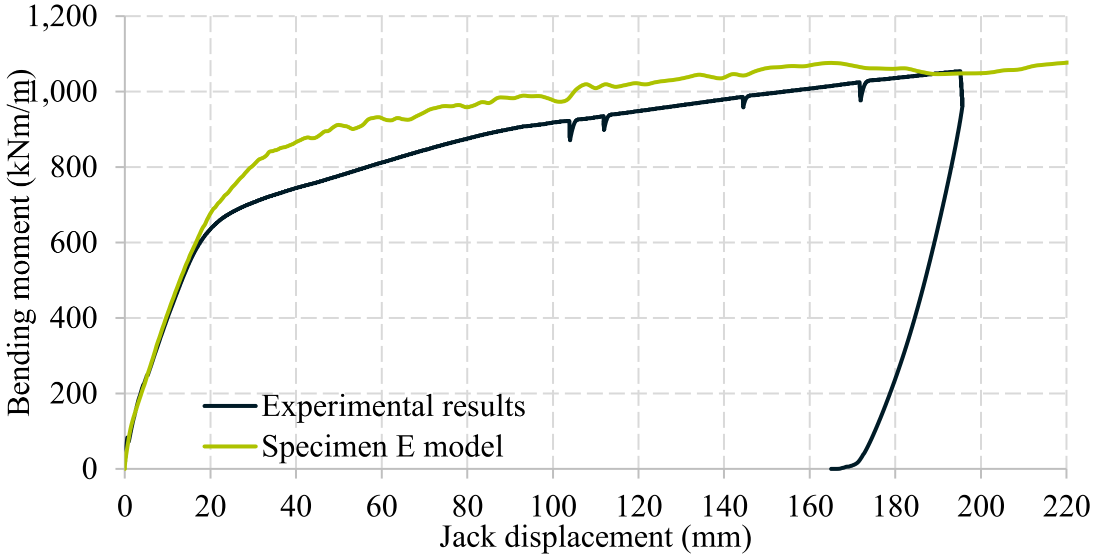

Figure 51 - Jack displacement (JD) vs bending moment – Comparison of SCIENCE experimental results with Specimen E numerical model

In this first comparison, it can be seen that the Specimen E numerical model perfectly matches the experimental results at the beginning of the curve, corresponding to the elastic phase, up to 15 mm of jack displacement. After that, when the plastic phase begins, the numerical model is stiffer than the experimental results, with a maximum difference of 17% recorded at 40 mm of jack displacement. The difference decreases more and more until it becomes zero at the end of the test for 200 mm of jack displacement and 1050 kNm of bending moment.

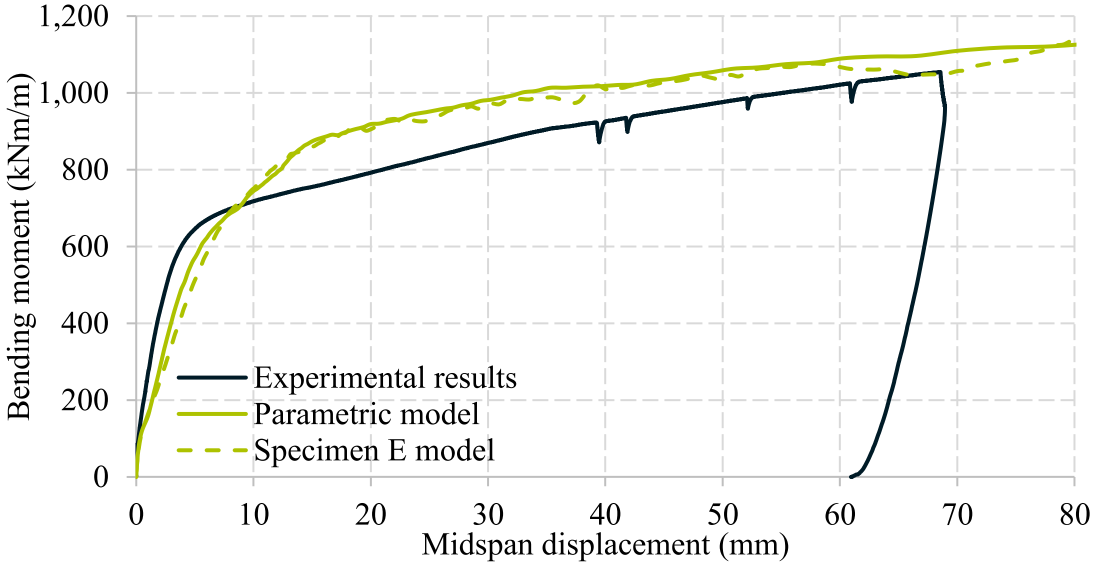

Figure 52 - Jack displacement (JD) vs bending moment – Comparison of SCIENCE experimental results with Parametric and Specimen E numerical models

Unlike the previous model, this triple comparison between the Specimen E model, the parametric model and the experimental results shows more significant differences from the start. In fact, the effective elastic phase of the concrete is up to 0.35 mm midspan displacement, where the first crack occurs in the concrete at the tensile part at the midspan of the beam. After this point, there is a reduction in strength in both the experimental and numerical values, and then the models recover their strength but with a softer bending stiffness than the initial one. However, the two numerical models are 35% softer at this stage than the experimental data.

At 600 kNm of bending moment, the beginning of the plastic phase is noted. Once again, a stiffer behaviour is recognised in the numerical models with a maximum difference with the experimental values of 16% at 18 mm of midspan displacement to become almost zero at 70 mm of midspan displacement corresponding to the end of the test.

4.2.2 Vertical displacement at sensors D7 to D12 comparison

Figure 53 shows the comparison of the jack displacement and the vertical displacements D7 to D12 for the Specimen E model with the experimental results, while Figure 54 shows the comparison of the midspan displacement and the vertical displacements D8 and D9 for both numerical models parametric and Specimen E with the experimental results.

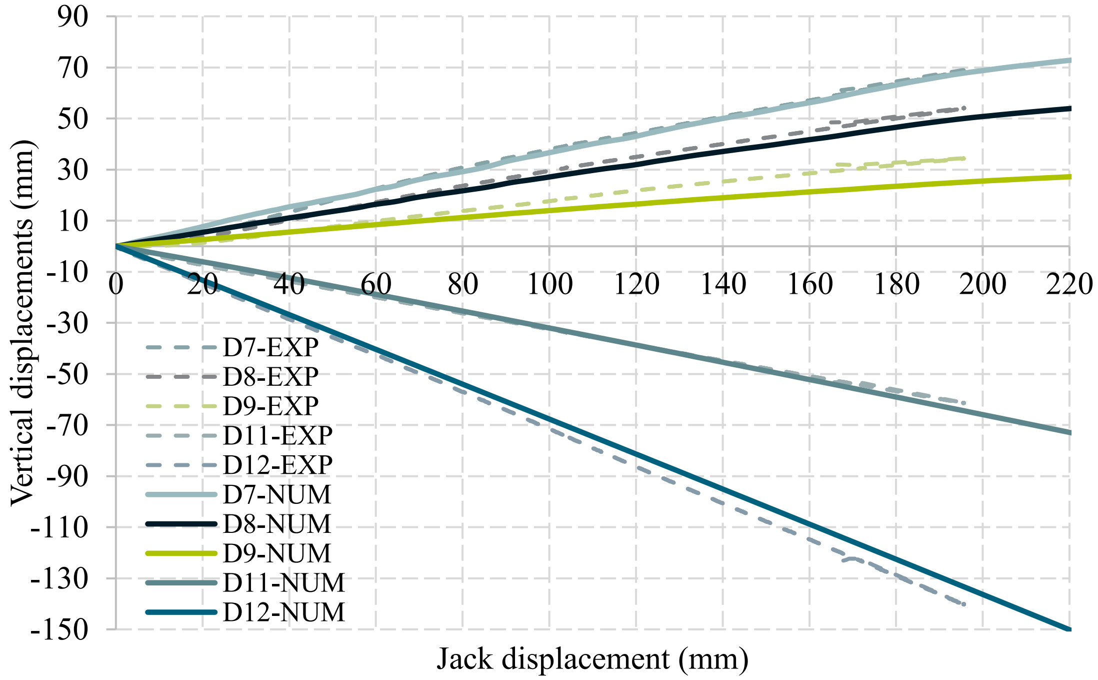

Figure 53 – Jack displacement (JD) vs Vertical displacements (D7 to D12) – Comparison of SCIENCE experimental results with Specimen E numerical model

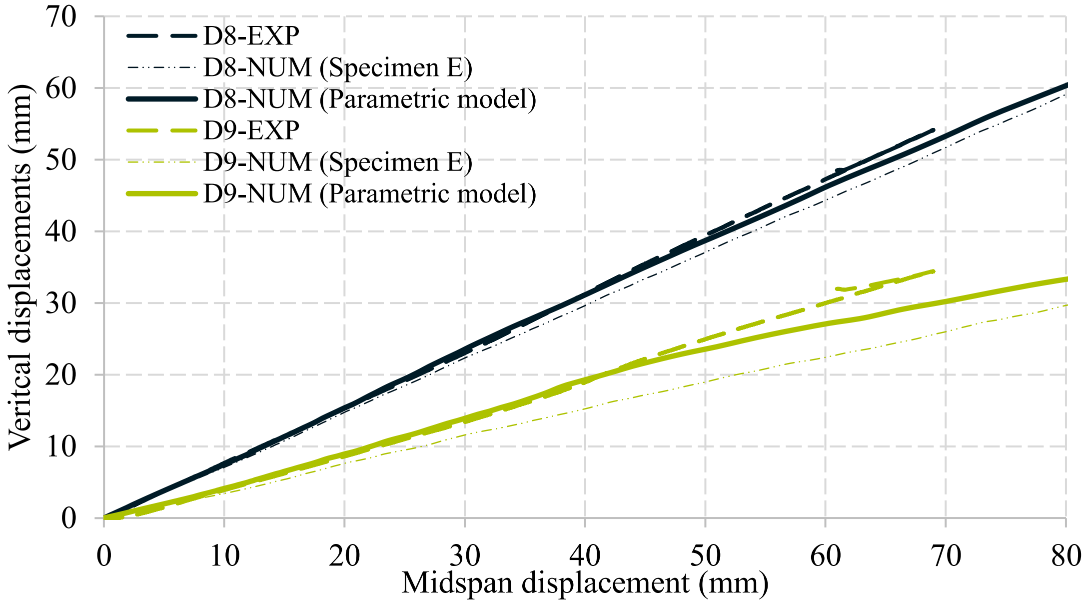

Figure 54 - Midspan displacement (D7) vs Vertical displacements (D8 and D7) – Comparison of SCIENCE experimental results with Specimen E and Parametric numerical models

In terms of vertical displacements, both numerical models correspond to the experimental values. There is a slight difference for D9, the sensor close to the support in the connection zone, with worse values for the Specimen E model probably due to the fact that this model is affected by the non-linear behaviours of the rest of the beam.

4.2.3 Horizontal displacement at sensor D14 to D17 and Curvature comparison

Figure 55 shows the comparison of the jack displacement and the horizontal displacements D14 to D17 for the Specimen E model with the experimental results, while Figure 56 shows the comparison of the midspan displacement and the horizontal displacements D14 to D17 for both numerical models parametric and Specimen E with the experimental results.

Figure 57 shows the comparison between the jack displacement and curvature of the Specimen E model and the experimental results, calculated as the ratio between the difference of the outermost horizontal displacements (D14 and D17) and their vertical distance of 300 mm, as the following formula shows:

$$\chi = \frac{D17 - D14}{300}$$

Figure 58 shows the comparison of the midspan displacement and the curvature for both numerical models parametric and Specimen E with the experimental results.

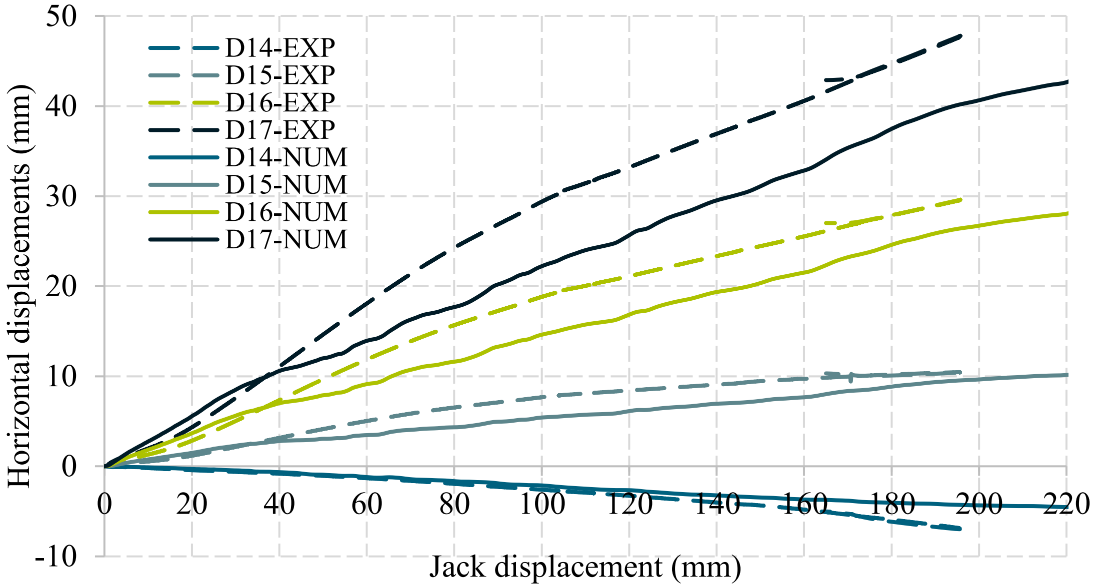

Figure 55 - Jack displacement (JD) vs Horizontal displacements (D14 to D17) – Comparison of SCIENCE experimental results with Specimen E numerical model

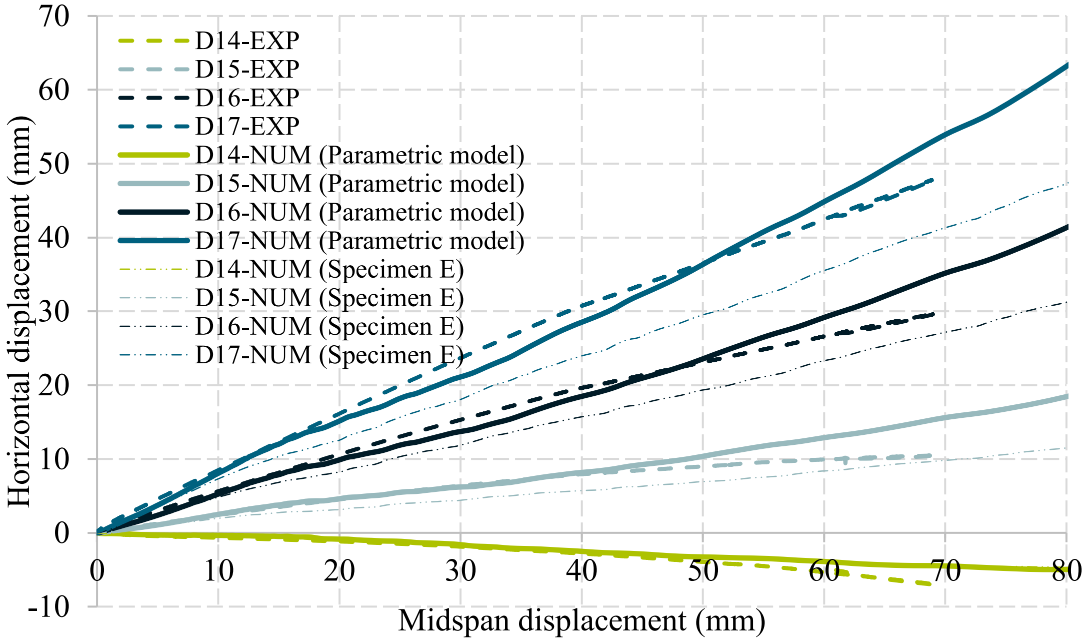

Figure 56 - Midspan displacement (D7) vs Horizontal displacements (D14 to D17) – Comparison of SCIENCE experimental results with Specimen E and Parametric numerical models

From the horizontal displacements, the effect of the non-linear numerical behaviour of the rest of the beam on the connection modelled for the Specimen E model, compared to the parametric model which does not include this part, is evident. In fact, the numerical influence of this part is due to the poor modelling conditions, i.e., of the course elements, the absence of real unilateral contact conditions and the poor interaction of the beam elements of studs and tie bars with the solid concrete elements. The comparison in Figure 55 shows that up to 40 mm of jack displacement, corresponding to the elastic phase and the beginning of the plastic phase, the experimental and numerical results are close. Whereas for higher values, worse results are observed, with a maximum difference in D17, corresponding to one of the outermost horizontal displacements, which from 80 mm of jack displacement maintains a 25% gap difference.

The situation is different for the parametric model, where the horizontal displacement values are close to the experimental ones with a maximum difference of 15% measured in D17 at 70 mm midspan displacement.

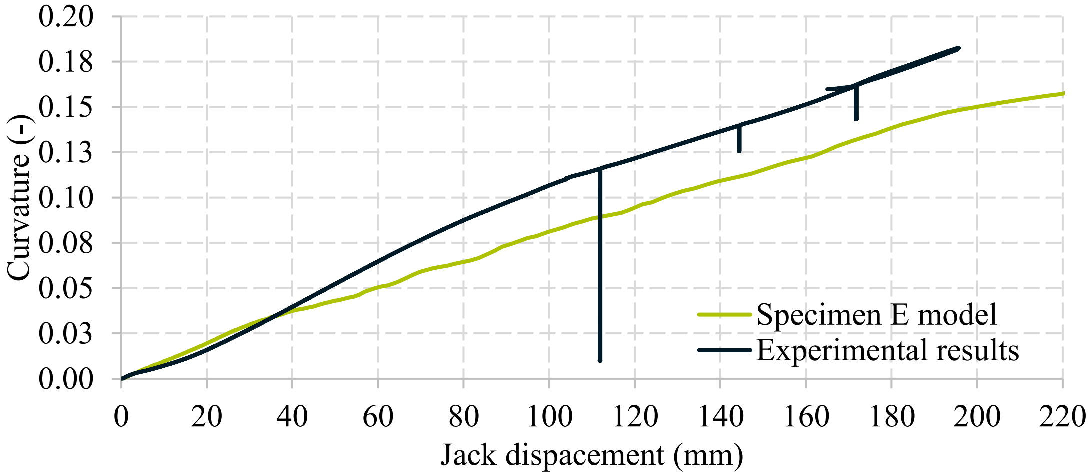

Figure 57 - Jack displacement (JD) vs Curvature – Comparison of SCIENCE experimental results with Specimen E numerical model

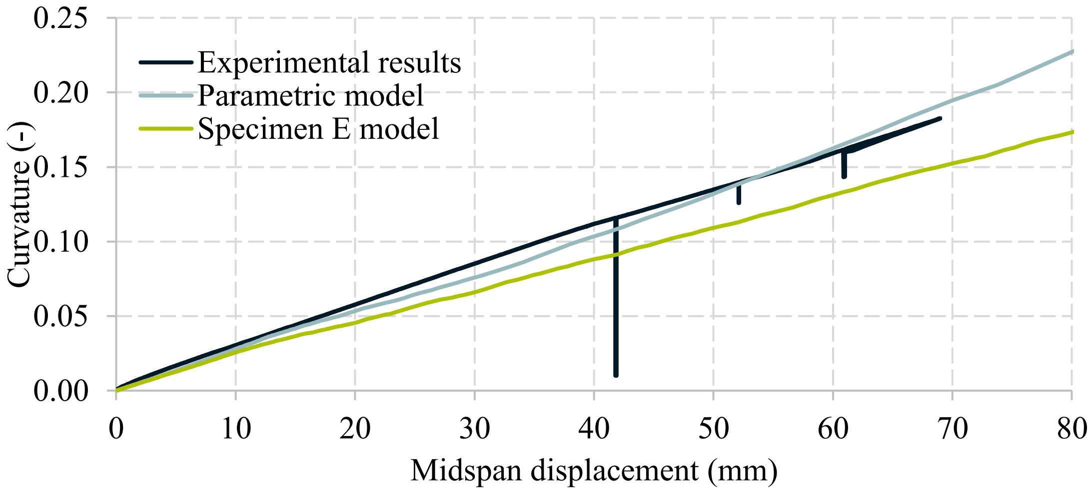

Figure 58 – Midspan displacement (D7) vs Curvature – Comparison of SCIENCE experimental results with Specimen E numerical model

Since the curvature is a function of the horizontal displacements, the same conclusions can be drawn. Once again, an increased difference is observed in the numerical results of Specimen E with the comparison of the jack displacements in Figure 58 after the elastic phase and the beginning of the plastic phase, with a maximum difference of 19% at 200 mm. On the other hand, a complete correspondence between the experimental results and those of the parametric model is observed.

4.2.4 Graphical comparison between the Specimen E and Parametric numerical models

In this section, a graphical comparison of stress distribution, elastic or plastic strain or damage variables is presented between the two numerical models for each component: faceplates, embedded connection bars, studs and tie bars, and concrete.

Faceplates

Figure 59 presents the comparison of the axial stress (x-stress) and the effective plastic strain at 70 mm midspan displacement, corresponding to the end of the experimental test, for the faceplates of the two models, Specimen E and the parametric model. For both, the ultimate values are 423 MPa as ultimate stress and according to the bilinear law with hardening, the associated ultimate strain is 9.68% as defined in section 3.2.2.

Due to the bending of the beam, the upper plate is in tension, while the lower plate is in compression. As can be seen in the image comparison, there is a concentration of stresses in the plates at the connection bar heads, particularly with the plate in tension, where failure is reached. This is due to the way the connection bars are deformed. In fact, during bending, as can be seen in Figure 60, the heads deform by moving upwards, but since they are surrounded by concrete, this in turn pushes the plate, generating an increase in stress and consequently leading to a failure of the plate.

Since the plates are the weakest object in the experimental test, this local failure becomes the global failure of the connection.

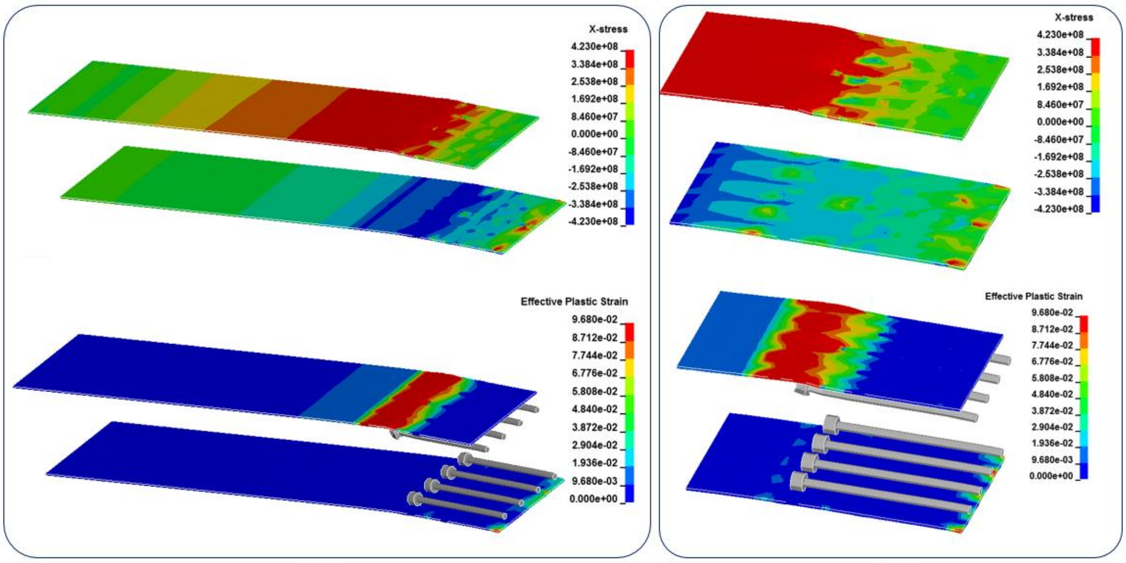

(a) (b)

Figure 59 – Axial stress and Effective plastic strain of faceplates for (a) Specimen E model and (b) Parametric model at D7=70mm

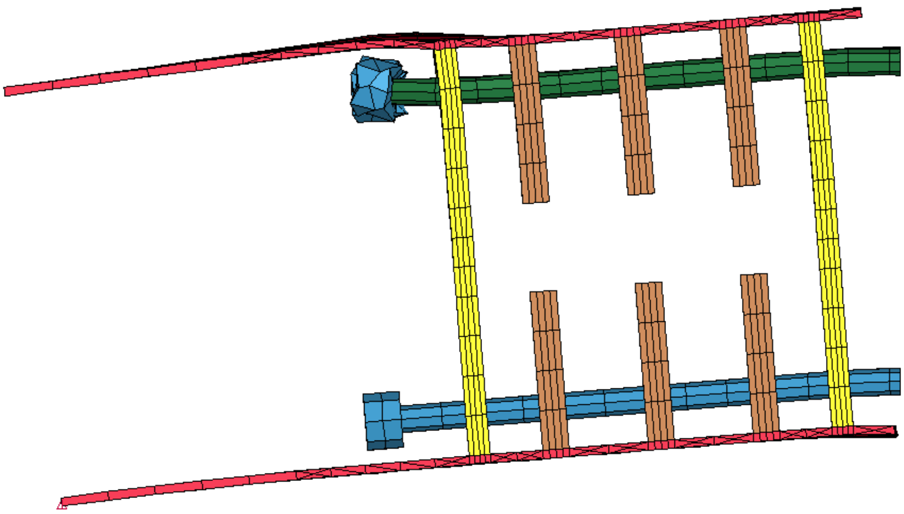

Figure 60 - Deformed steel objects of the parametric model at D7=70 mm

Connection bars

Figure 61 presents the comparison of the axial stress (x-stress) and the actual plastic strain at 70 mm midspan displacement, corresponding to the end of the experimental test, for the connection bars of the two models: Specimen E and the parametric model.

The bars are not placed homogeneously in tension, in fact, 3 out of the 4 bars have a grade of 10.9 and one of 8.8. The bars with grade 8.8 have a yield strength of 640 MPa and an ultimate strength of 800 MPa with an associated ultimate strain of 12.6%; the bars with grade 10.9 have a yield strength of 900 MPa and an ultimate strength of 1000 MPa with an associated ultimate strain of 8.12%. The scale limits in the comparison are defined as the minimum values for stress and strain, respectively 800 MPa as ultimate stress and 8.12% as ultimate strain.

The tensile bars, due to non-uniformity, show different stresses and consequently different strains. In elasticity, all bars behave the same, since they have the same stiffness and geometry, up to 640 MPa when the grade 8.8 steel bar reaches yield strength. After this treasure, the stiffness of this bar changes with the post-elastic of 1.3 GPa, while the others still behave with the normal stiffness of 210 GPa. Because of this softening, the stiffer bars next to it, carry its load. This effect, in stress, is easier to observe in the parametric model, while in strain it is more evident in the Specimen E model. The remaining bars in tension barely yield, reaching a stress of 900 MPa only in the proximity of the heads, which as they bend upwards, as can be seen in Figure 61, locally increase the stress.

The bars in compression, on average, reach a value of 160 MPa far below the yield capacity. This is because there is still concrete in compression that helps.

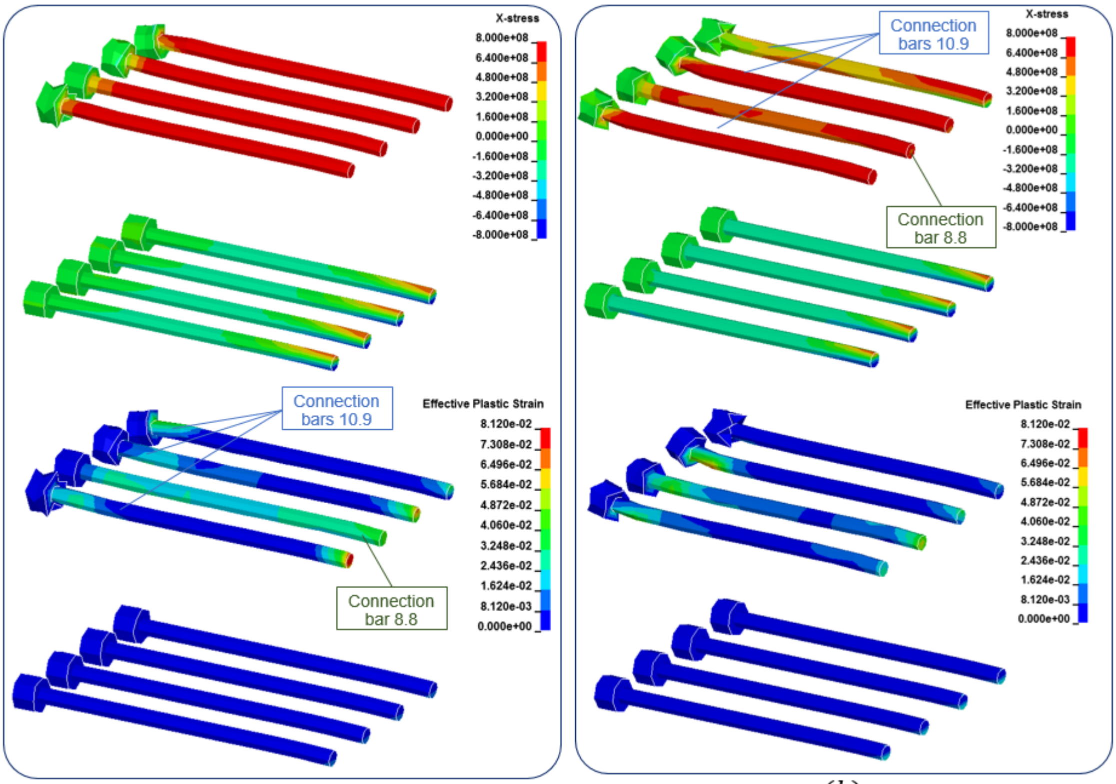

(a) (b)

Figure 61 – Axial stress and Effective plastic strain of connection bars for (a) Specimen E model and (b) Parametric model at D7=70mm

Studs and Tie bars

Figure 62 presents the comparison of the Von Mises stress (v-m) and Effective strain at 70 mm midspan displacement, corresponding to the end of the experimental test, for the studs and tie bars of the two models: Specimen E and the parametric model.

In general, both studs and tie bars do not reach the ultimate capacity but not even the yielding, which is assumed to be 402 MPa for studs and 434 MPa for tie bars. In fact, the deformation comparison refers to the elastic field, contrary to that which was seen so far for the comparison with plates and connection bars.

As far as the studs are concerned, those in tension are much more stressed than those in compression, and a bending principle can be seen in the deformation, with a consequent concentration of the tensile stress in the longitudinal direction of the stud and defined for the first row of studs by the application of load.

The tie bars are longer and smaller in diameter than the studs, which means they are less rigid and therefore allow for greater deformation, in fact, they are much more deformed than the studs, with even local yielding at the connection between the first row of tie bars, from the application of the load, and the faceplate.

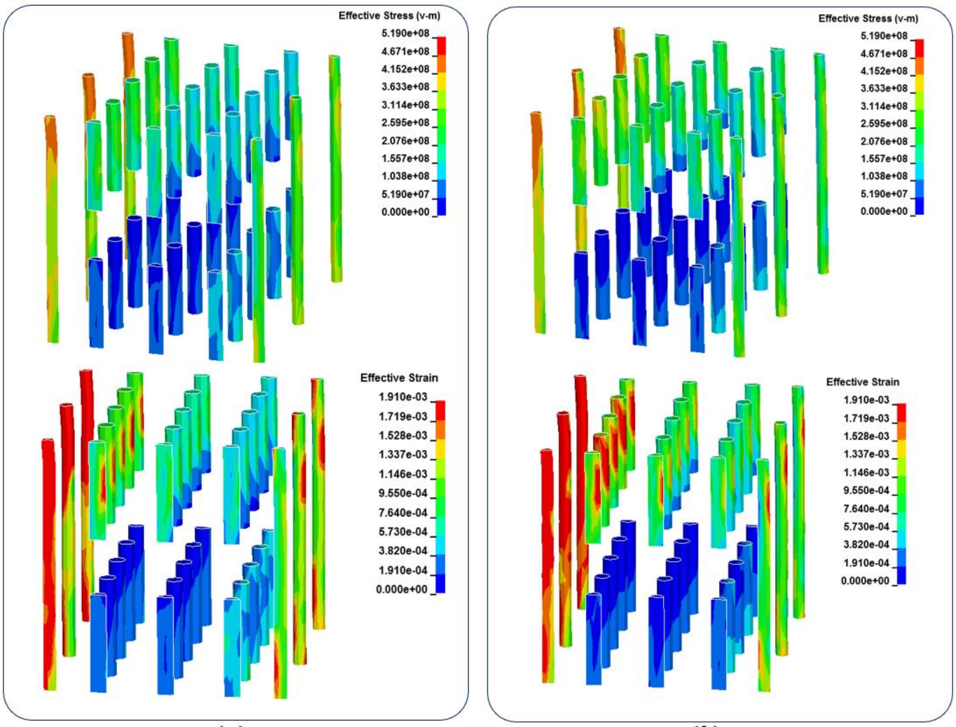

(a) (b)

Figure 62 – Von Mises stress (v-m) and Effective strain of tie bars and studs for (a) Specimen E model and (b) Parametric model at D7=70mm

Concrete

Figure 63 presents the comparison of the two numerical models for the axial stress of concrete at 70 mm of midspan displacement, corresponding to the end of the experimental test. Figure 64 and Figure 65 show the comparison of the two numerical models for the damage variable of concrete at different stages.

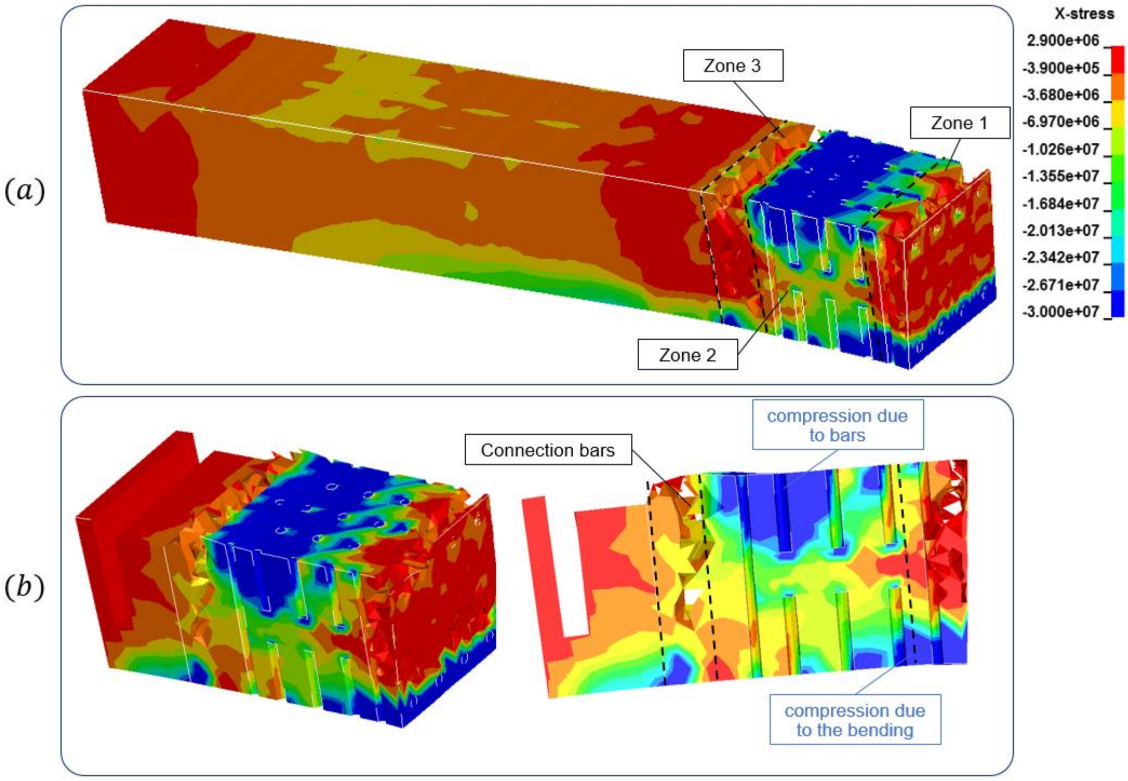

Figure 63 - Axial stress comparison for (a) Specimen E model and (b) Parametric model at D7=70mm

Looking at the axial stress, three different parts with different stress patterns can be recognised:

- *Zone 1 corresponds to the midspan of the beam.*

  The stress pattern is a simple division between concrete in tension, in the upper part of the cross-section (red, see Figure 63), and in compression, in the lower part of the cross-section (blue, see Figure 63).

- *Zone 2, between connection bar heads and zone 1.*

  During bending, a volume of concrete is subjected to compression by the connection bar heads. This volume is greater near the heads and becomes smaller and smaller as it passes from zone 1 to zone 2 until the influence of compression is less than the tension generated by bending at the top of the beam. In this zone, the stress can reach up to 200 MPa without failure due to the confinement effect of the faceplates.

- *Zone 3, after the connection bar heads.*

  Compared to zone 2, however, after the connection bar heads the concrete is in tension because it detaches from the bar heads due to the tensile stresses of bending. As seen in section 3.2.1, confinement does not improve the tensile properties, so a large crack is generated from here.

In addition to the stress analysis, the strain field can also be analysed. In particular, the damage variable varies from 0 (undamaged concrete) to 0.99 (highly damaged concrete).

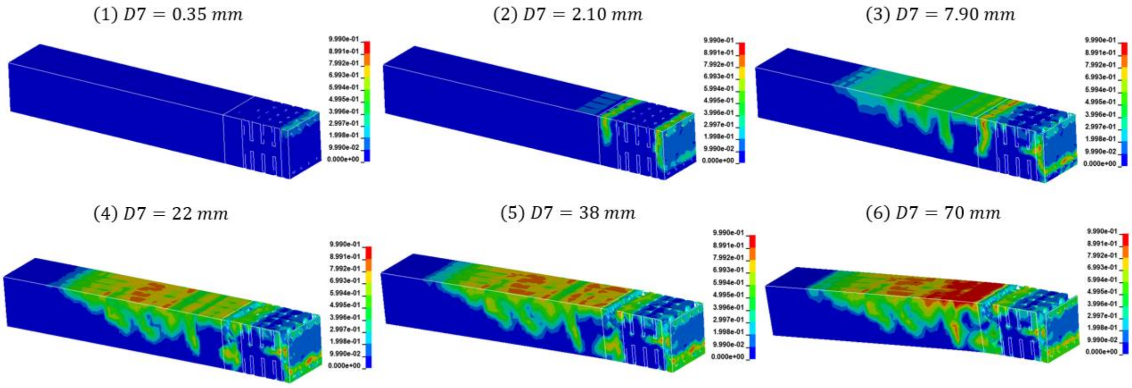

Figure 64 – Damage variable of concrete at different stages for Specimen E model

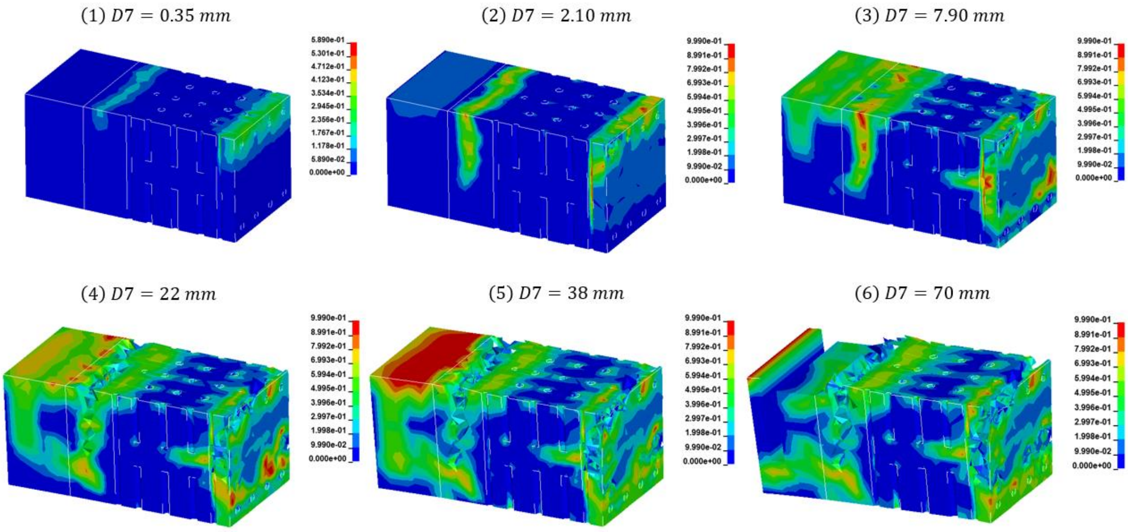

Figure 65 – Damage variable of the concrete at 200 mm of jack displacement for the Parametric model

Looking at the damage variable at each step:

- *Step 1 at 0.35 mm of midspan displacement*

  At this stage, the first crack in the concrete occurs. The upper part of the beam is subjected to bending tension and the lower part is compressed. When the tensile force reaches the concrete's maximum tensile capacity (2.90 MPa), it cracks, and this occurs in zones 1 and 3, which are defined for the stress field. The concrete in between does not crack because it is compressed by the connection bar heads balancing the tension force.

- *Step 2 at 2.10 mm of midspan displacement*

  At this stage, the damaged zone generated in stage 1 improves by enlarging and the cracks deepen.

- *Step 3 at 7.90 mm of midspan displacement*

  At this stage, especially for the Specimen E model, the damages propagate longitudinally along the rest of the beam. Damage on the compression part, in correspondence with the compressed connection bars, begins to be significant.

- *Step 4 at 22 mm and step 5 at 38 mm of midspan displacement*

  These two stages show the intensification of areas already reached by deformation and the erosion of elements that reached 5 % of deformation.

- *Step 6 at 70 mm of midspan displacement:*

  The last stage, corresponding to the end of the experimental test, shows the deformation state of the concrete at the end of the test.

Chapter 5

Parametric analysis

The purpose of this chapter is to present:

- The parametric results for the bending analysis in section 5.1.
- The parametrical results for the axial analysis in section 0.

All 29 combinations presented in section 2.4.1 in Table 7 were carried out for the bending analysis, while for the axial analysis, a reduction of 3 combinations was made for a total of 26 combinations. This reduction is due to the geometry of the numerical model. Being split in half, the overlapping conditions between the studs, referring to combinations 4, 26 and 27, would have eliminated the symmetry condition of the centre section, thus having to define the complete model. It was not considered essential to carry out these combinations based on the results obtained from the bending analysis, where the influence of the overlap between the studs does not lead to great differences in the behaviour of the connection.

For each analysis, the different combinations are presented in graphs in which only one parameter changes at a time to understand the influence of each on the overall behaviour of the connection, and are organised by element as follows:

- Connection bar parameters: diameter (d_b) and ultimate strength ($f_{sy,b}$)
- Faceplates' parameters: thickness (t_p) and ultimate strength ($f_{sy,p}$)
- Concrete parameter: wall thickness (H_c)
- Stud parameters: diameter (d_s) and height (h_s)
- Tie bars and studs spacing parameters: y-spacing (s_{sy}, s_{ty}) and x spacing (s_{sx}, s_{tx})

5.1 Bending parametric analysis

All comparisons are performed with charts comparing the displacement at the midspan of the beam with the bending moment constantly present along the length of the connection.

5.1.1 Connection bars parameters: diameter (d_b) and ultimate strength ($f_{sy,b}$)

Figure 66 presents the bending parametric results of variation in connection bars diameter from M30 to M48 while Figure 67 the bending parametric results of variation in connection bars steel grade between 8.8 and 10.9.

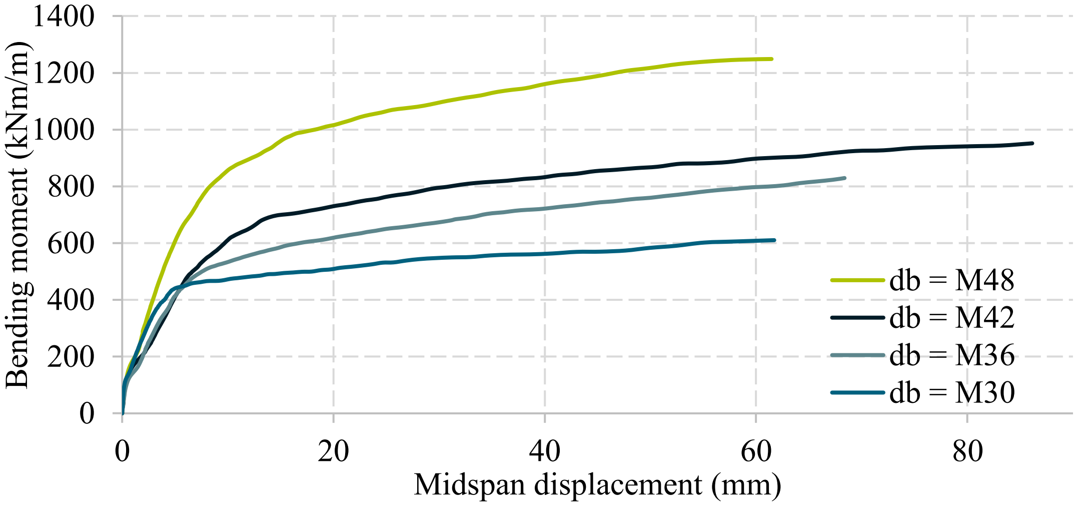

Figure 66 - Bending parametric results of variation in connection bars diameter from M30 to M48 (M48 is the reference case value)

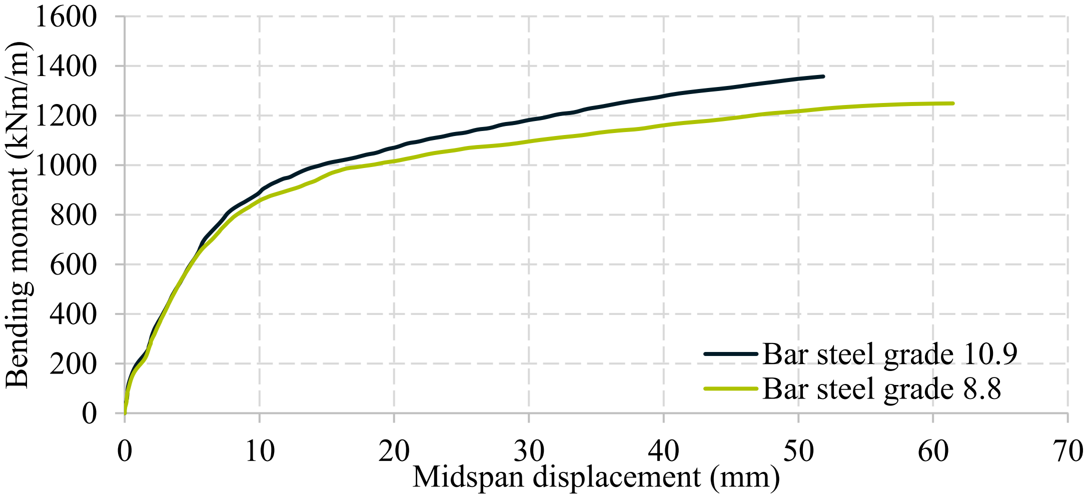

Figure 67 – Bending parametric results of variation in connection bars steel grade between 8.8 and 10.9 (8.8 is the reference case value)

As can be seen from the results, the connection bars' diameter is an important parameter in terms of stiffness and ultimate capacity of the connection: a variation of which generates significant differences in the overall behaviour of the model. In fact, going from 30 to 48 mm results in 2 times increase in ultimate capacity.

This variation is proportional to the area of the connection bars, in particular to the square of the diameters. The area reductions compared to the reference case of 48 mm diameter are 23.4% for the 42 mm model, 43.8% for the 36 mm model and 60.9% for the 30 mm model. Respectively, the reductions in ultimate capacity compared to the reference case are 23.8% for the 42 mm model, 33.7% for the 36 mm model and 51.2% for the 30 mm model. Table 19 summarises the compared values of ultimate capacity reduction and areas, compared to the reference case marked in bold.

Table 19 - Area and ultimate capacity reduction values compared to the reference case marked in bold

Variable connection bar diameter parameter (mm)	Ultimate bending moment (kNm)	Area reductions (%)	Ultimate capacity reductions (%)
M48	**1250**	**-**	**-**
M42	952	23.4%	23.8%
M36	829	43.8%	33.7%
M30	610	60.9%	51.2%

The magnitudes of the reductions are comparable, although more complex interaction behaviours with other materials are responsible for the small gap between the comparison values, and also the bars are not the weakest elements that generate the failure.

In terms of ductility, an optimum can be found for a diameter value of 42 mm, in fact, it is the model that achieved the maximum midspan displacement of 86 mm.

In contrast, the steel grade was found to be a not-so-important parameter in this parametric analysis. This is due to the failure conditions of the model. Basically, the weakest elements of the model turn out to be the studs that create the connection failure, so the connection bars barely yield at the end of the model, as explained in detail in section 6.1.

5.1.2 Faceplates' parameters: thickness (t_p) and ultimate strength ($f_{sy,p}$)

Figure 68 presents the bending parametric results of variation in faceplate thickness from 6 to 14 mm, while Figure 69 the bending parametric results of variation in faceplate steel grade between S235 and S355.

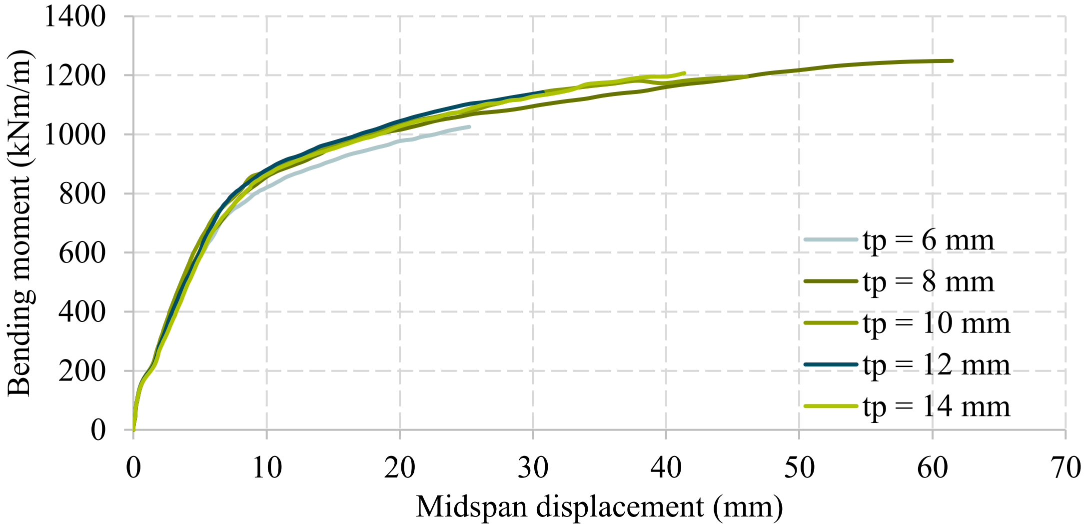

Figure 68 – Bending parametric results of variation in faceplates thickness from 6 to 14 mm (8 mm is the reference case value)

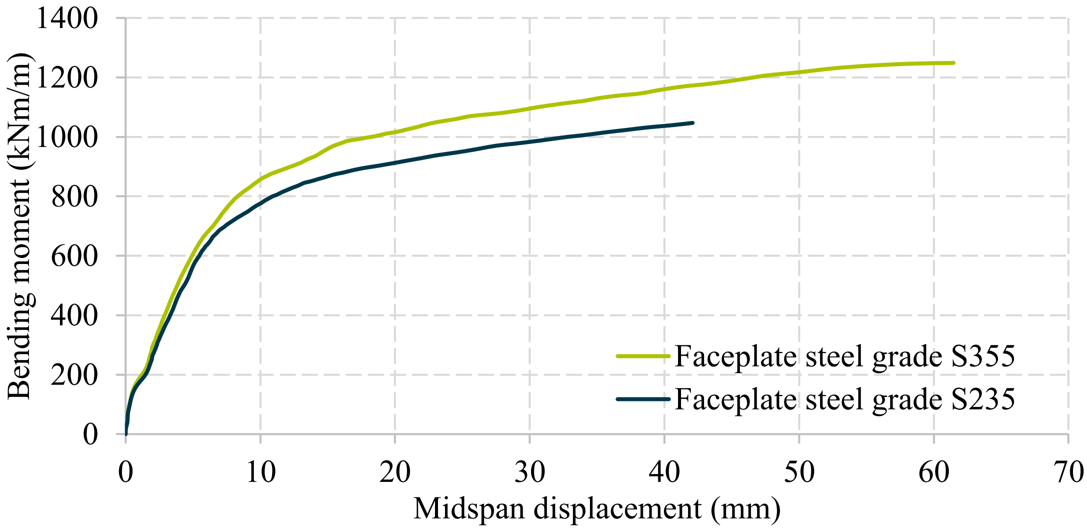

Figure 69 – Bending parametric results of variation in faceplates steel grade between S235 and S355 (S355 is the reference case value)

With regard to the parametric results, it can be concluded that the parametric values referring to the plates do not influence the overall connection behaviour. This is due to the fact that, after the connection bars, the faceplates are the second strongest element in the model and the studs fail before a failure can be triggered in the plates.

5.1.3 Concrete parameter: wall thickness (H_c)

Figure 70 presents the bending parametric results of variation in concrete thickness from 300 to 500 mm.

As for connection bars' diameter, concrete thickness is also an important parameter in terms of stiffness and ultimate capacity. Reducing the thickness results in a significant reduction in stiffness and ultimate capacity.

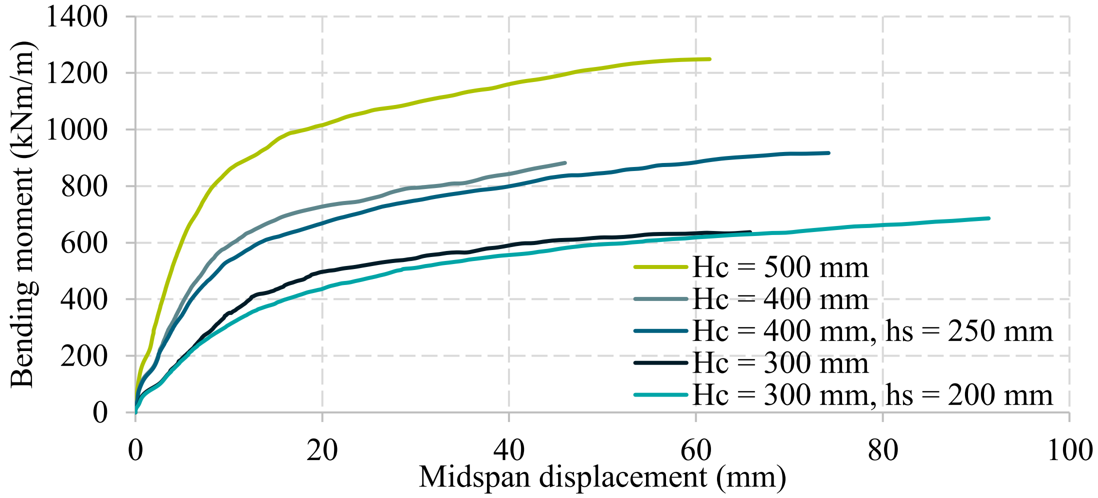

Figure 70 – Bending parametric results of variation in concrete thickness from 300 to 500 mm (500 mm is the reference case value)

As far as the reduction in stiffness is concerned, this is due to the reduction in the inertia of the cross-section. The three models have 120, 75 and 32 GNm of bending stiffness, respectively, for thicknesses of 500, 400 and 300 mm, which means a reduction with respect to the reference case of 37.5% for the 400 mm model and 73.3% for the 300 mm model. Comparing these reductions with the reductions in cubic thickness values with respect to the reference case, a reduction of 48.8% is obtained for the 400 mm model and 78.4% for the 300 mm model. Reductions with comparative magnitudes show that inertia is the cause of the bending stiffness reduction. Table 20 summarises the values of inertia and bending stiffness reductions, compared to the reference case marked in bold.

Table 20 – Inertia and bending stiffness reduction values compared to the reference case marked in bold

Variable concrete thickness parameter (mm)	Bending stiffness (GNm)	Inertia reductions (%)	Bending stiffness reductions (%)
500	**120**	**-**	**-**
400	75	48.8%	37.5%
300	32	78.4%	73.3%

As far as the reduction in ultimate capacity is concerned, the reason lies in the reduction of the lever arm with respect to the cross-sectional area in compression and tension. Figure 71 shows a comparison of the three concrete thicknesses in terms of both damage variable and axial stress, for the same studs' height of 150 mm. The damage pattern is quite similar between the models, with a slightly higher concentration of damage at the midspan cross-section and connection bar heads. In any case, these damage increases are not sufficient to justify a reduction in ultimate capacity compared to the reference case of 500 mm thickness of 29.4%, for the 400 mm model, and 49.6%, for the 300 mm model. Observing the axial stress in the area close to the midspan, where only the connection bars and concrete are located, a clear reduction in the lever arm between the tension (red, see Figure 71) and compression (blue, see Figure 71) can be seen.

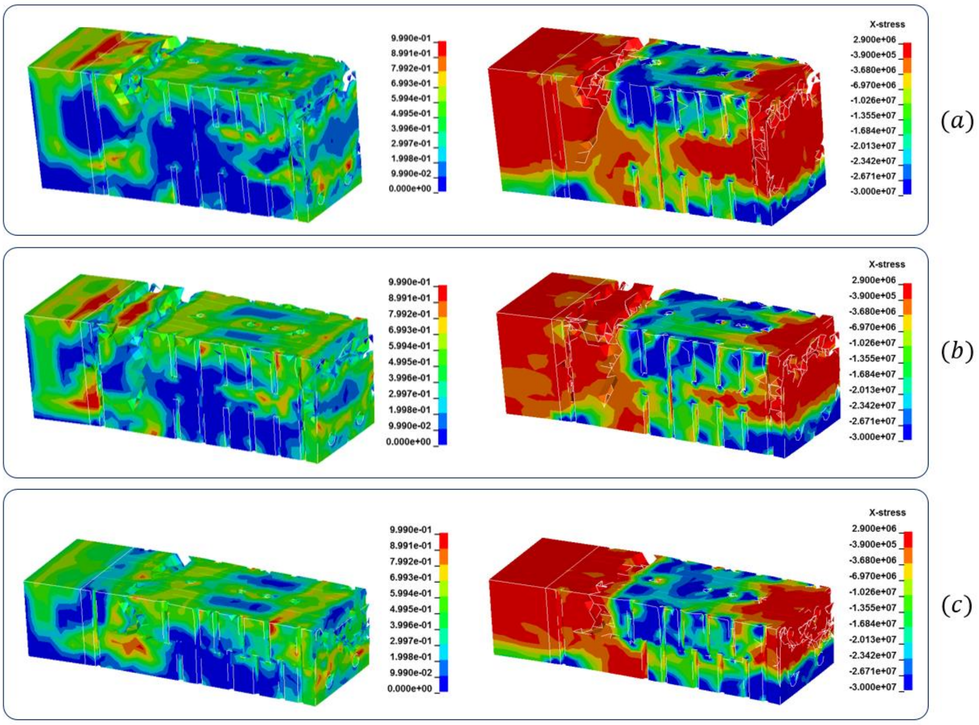

Figure 71 – Comparison of damage variable and axial stress in concrete for the three different cases of thickness combination: (a) 500 mm, (b) 400 and (c) 300 mm at 45 mm of midspan displacement

Under the simplified assumption that the total compressive forces from the compressed bars and the concrete can be applied at the compressed connection bars position, the lever arms with respect to the tension connection bars are 372, 272 and 172 for 500-, 400- and 300-mm thicknesses, respectively. The reductions in lever arms compared to the reference case are 26.9%, for the 400 mm model, and 53.8%, for the 300 mm model. Table 21 summarises the values of the lever arm and ultimate capacity reductions, compared to the reference case highlighted in bold.

Table 21 - lever arm and ultimate capacity reduction values compared to the reference case marked in bold

Variable concrete thickness parameter (mm)	Ultimate bending moment (kNm)	Lever arm (mm)	Ultimate capacity reductions (%)	Lever arm reductions (%)
500	**1250**	**372**	**-**	**-**
400	882	272	29.4%	26.9%
300	630	172	49.6%	53.8%

Again, reductions with comparative magnitudes demonstrate that the lever arm is the reason for the ultimate capacity reduction.

5.1.4 Studs' parameters: diameter (d_s) and height (h_s)

Figure 72 presents the bending parametric results of variation in studs' diameter from 19 to 25 mm, while Figure 74 the bending parametric results of variation in studs' height from 100 to 250 mm.

Variation in studs' diameter

It is surprising and even counterintuitive from these initial results, relating to the diameter of the studs, how increasing the diameter of the studs leads to a reduction in the connection capacity, especially since they represent the weak point of the connection being the first to fail. As already mentioned in the design criteria in section 2.4, the ratio of longitudinal studs' spacing (s_{sx}) to studs' diameter (d_s) is the criterion for the amount of concrete a stud needs to perform properly. Table 22 shows the results of the criteria for the different diameters tested in the parametric analysis with the same longitudinal studs' spacing of 100 mm.

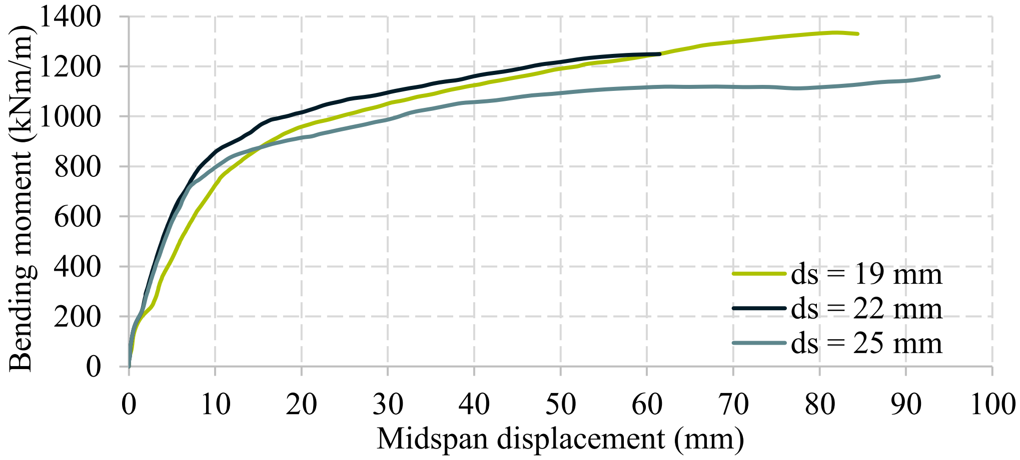

Figure 72 – Bending parametric results of variation in studs' diameter from 19 to 25 mm (22 mm is the reference case value)

Table 22 – Studs design criteria

d_s (mm)	$\frac{s_{sx}}{d_s}$ ≥ 5
19	5.26
22	**4.55**
25	4.00

As can be seen, only the model with a 19 mm stud diameter meets the limit criterion, the other values deviate from the limit value. The consequence is evident in the parametric results. In fact, the model with a diameter of 19 mm works correctly. The model with a diameter of 22 mm, close to the treasure value, initially shows a higher resistance, but then converges to the 19 mm model. Finally, the 25 mm diameter model matches the previous model at first, but since it is the one with the worst design criteria, its ultimate resistance ends up being worse than the 19 and 22 mm diameter models. This analysis concludes that the criterion of the ratio of the longitudinal studs spacing to the diameter is very important in the design of the connection.

Variation in studs' height

In these second results, an optimum in ultimate capacity can be seen at 150 mm studs' height. For smaller values, such as 100 mm, there is a small reduction in capacity after the elastic field, because the concrete begins to be increasingly damaged, especially near the upper faceplate. The consequence is that the shorter studs are completely submerged in the damaged concrete, resulting in lower shear transmission resistance and the disappearance of the anchorage effect, as there is no undamaged concrete left to perform it. On the other hand, excessively increasing the height of the studs does not lead to any improvement. Figure 73 compares the two outermost cases with 100 and 250 mm studs' height, where can be seen the described effects, and the treasure case, coinciding with the reference case value of 150 mm for the same bending moment of 1110 kNm.

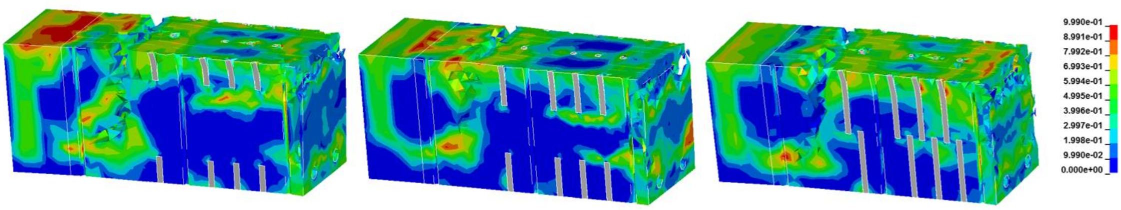

(a) (b) (c)

Figure 73 – Comparison at 1110 kNm bending moment between (a) 100 mm stud height (b) 150 mm stud height (c) 250 mm stud height

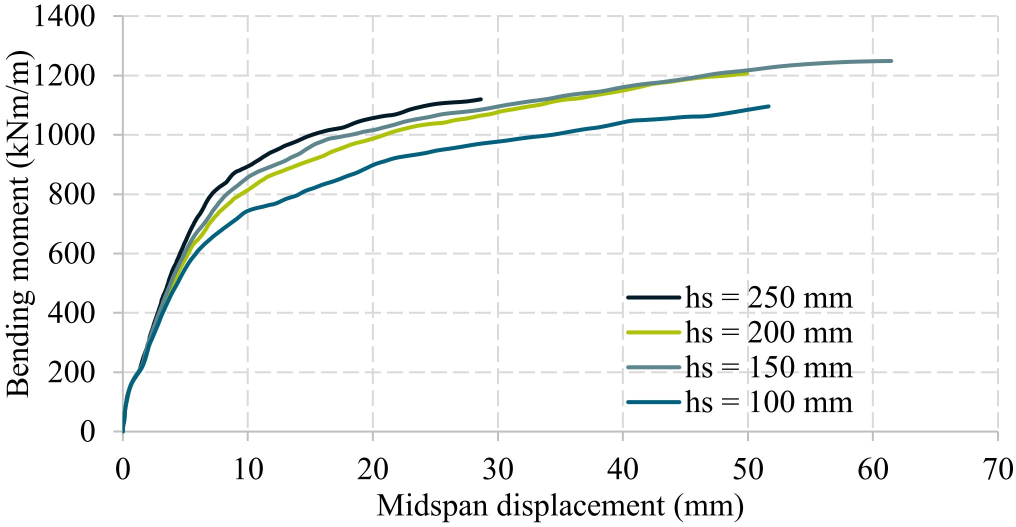

Figure 74 – Bending parametric results of variation in studs' height from 100 to 250 mm (150 mm is the reference case value)

The conclusion is that the studs' height value for the reference case is the optimum to guarantee the best performance for studs under the conditions of the current parametric analysis.

5.1.5 Tie bars and studs spacing parameters: y-spacing (s_{sy},s_{ty}) and x spacing (s_{sx},s_{tx})

The different tie bars and studs' spacing parameters are organised as follows:

- Figure 75 presents the bending parametric results of variation in studs' vertical spacing between 133 and 200 mm for tie bars spacing of 400 mm and M42 connection bars diameter.
- Figure 76 presents the bending parametric results of variation in studs' vertical spacing from 125 to 250 mm for tie bars spacing of 500 mm and connection bars diameter of M48.
- Figure 77 presents the bending parametric results of variation in studs' horizontal spacing from 75 to 150 mm for tie bars spacing of 600 mm and connection bars diameter of M48.
- Figure 78 presents the bending parametric results of variation in studs' horizontal spacing between 100 and 125 mm for tie bars spacing of 500 mm and connection bars diameter of M42.

Each graph has attached a table containing for each combination value respectively the design criteria of the ratio of longitudinal spacing to stud diameter and the stud density intended as the number of studs in a square metre.

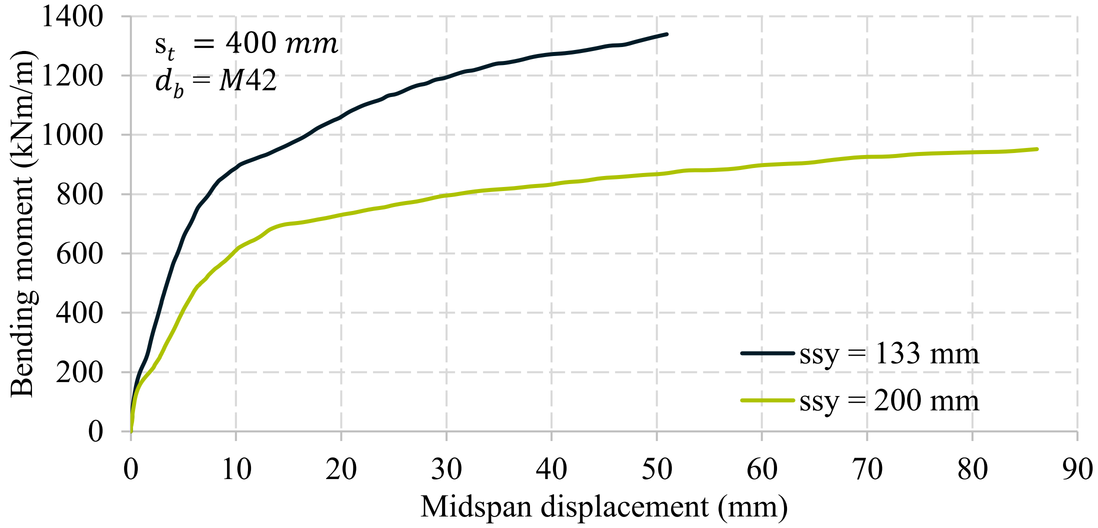

Figure 75 – Bending parametric results of variation in studs' vertical spacing between 133 and 200 mm for tie bars spacing of 400 mm and M42 connection bars diameter (s_{sy}=200mm, s_t=400mm and d_b=M48 are the reference case value)

Table 23 – Studs design criteria for the parametric values of Figure 75

s_{sy} (mm)	s_{sx}/d_s ≥5	Studs' density (-)
133	4.55	37.64
200	4.55	18.75

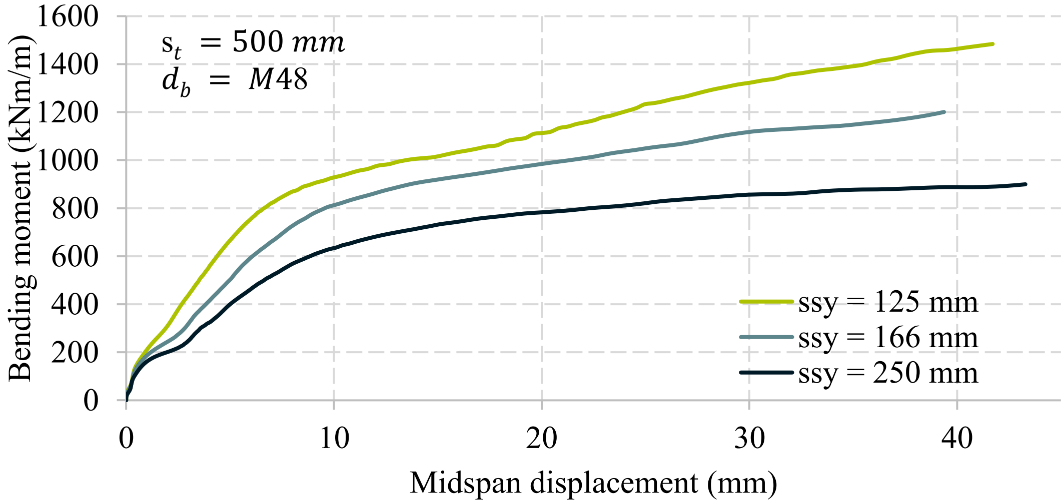

Figure 76 – Bending parametric results of variation in studs' vertical spacing from 125 to 250 mm for tie bars spacing of 500 mm and connection bars diameter of M48 (s_{sy}=200mm, s_t=400mm and d_b=M48 are the reference case value)

Table 24 – Studs design criteria for the parametric values of Figure 76

s_{sy} (mm)	s_{sx}/d_s ≥5	Stud density (-)
125	4.55	48.00
166	4.55	32.19
250	4.55	16.00

Looking at the results of Figure 75 and Figure 76, the conclusion is that increasing the vertical spacing reduces the stud density, which means fewer studs. This results in lower shear strength and therefore lower stress transmission, with a consequent reduction in the ultimate capacity. All the cases presented so far in the spacing comparison do not meet the design criteria, but all have the same value, as the longitudinal spacing does not change, which means that all values have comparable results.

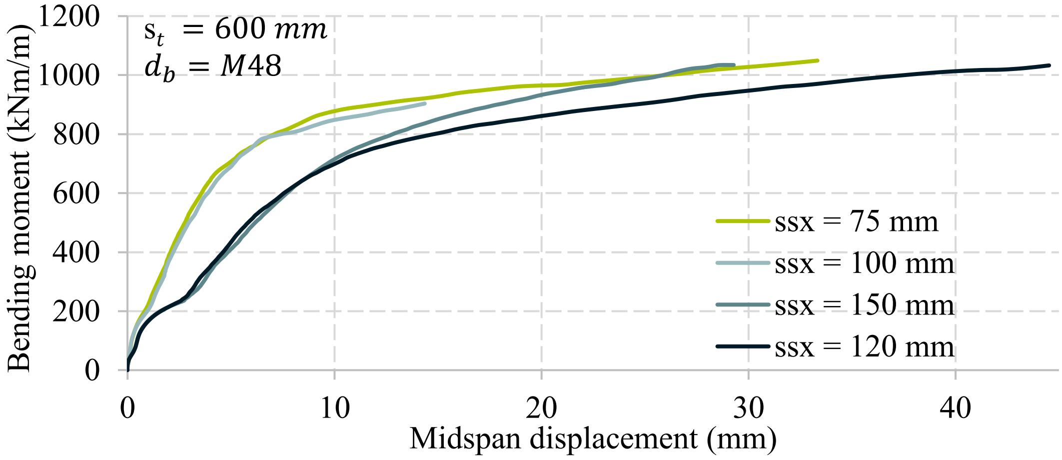

Figure 77 – Bending parametric results of variation in studs' horizontal spacing from 75 to 150 mm for tie bars spacing of 600 mm and connection bars diameter of M48 (s_{sy}=200mm, s_t=400mm and d_b=M48 are the reference case value)

Table 25 – Studs design criteria for the parametric values of Figure 77

s_{sx} (mm)	s_{sx}/d_s ≥5	Stud density (-)
75	3.41	38.89
100	4.55	27.78
120	5.45	22.22
150	6.82	16.67

Once again, the results in

Figure 77 confirms the importance of the design criteria. In fact, out of 4 combinations, there are two pairs, for those who meet and those who do not meet the design criteria respectively, which show completely different behaviour between the two pairs, but comparable values per pair. For each pair, the difference in stud density is not sufficient to appreciate a difference in stiffness or strength, in fact, there is a variation of 5 to 10 studs compared to the previous comparison with a variation in stud density between the combinations of 15 to 20.

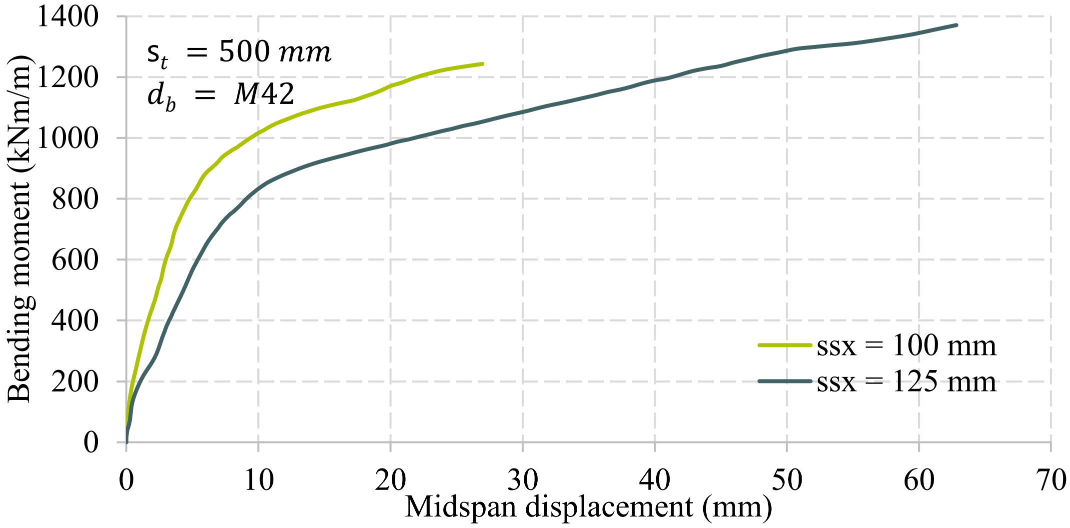

Figure 78 – Bending parametric results of variation in studs' horizontal spacing between 100 and 125 mm for tie bars spacing of 500 mm and connection bars diameter of M42 (s_{sy}=200mm, s_t=400mm and d_b=M48 are the reference case value)

Table 26 – Studs design criteria for the parametric values of Figure 78

s_{sx} (mm)	s_{sx}/d_s ≥5	Stud density (-)
100	4.55	48.00
125	5.68	36.00

It is difficult to draw a conclusion from this last comparison because the values have different design criteria and one of them does not meet the limit. However, overall, they seem to correspond to the previous conclusion by reducing strength and stiffness with increasing spacing and consequently reducing the stud density.

5.1.6 Bending stiffnesses, elastic limit and ultimate capacity

As already explained, the objective of the analysis is to understand the behaviour of the connection by varying certain parameters. The performance of the connection can be summarised in certain mechanical entities that can be calculated in the parametric analysis. In particular, these entities are the bending stiffness, yield limit and ultimate bending moment.

Figure 79 shows the bending moment versus midspan displacement for the reference case of bending, and the mechanical entities responsible for the variations in connection performance. The bending stiffness is proportional to the slopes of this curve since there is a factor $8/l^2$ of difference, and the different bending moments, yield and ultimate limits can be easily represented.

As already seen for the experimental case in section 4.2.1, also in the parametric analysis there are two different slopes in the elastic field. An initial stiffer slope and then, after softening, a second softer slope. These two represent, respectively, the *initial bending stiffness*, corresponding to the actual elastic range of the system, and the *cracked bending stiffness*, where the concrete has reached its elastic limit and cracks, resulting in a softening effect on the behaviour of the connection, although the overall behaviour still appears elastic.

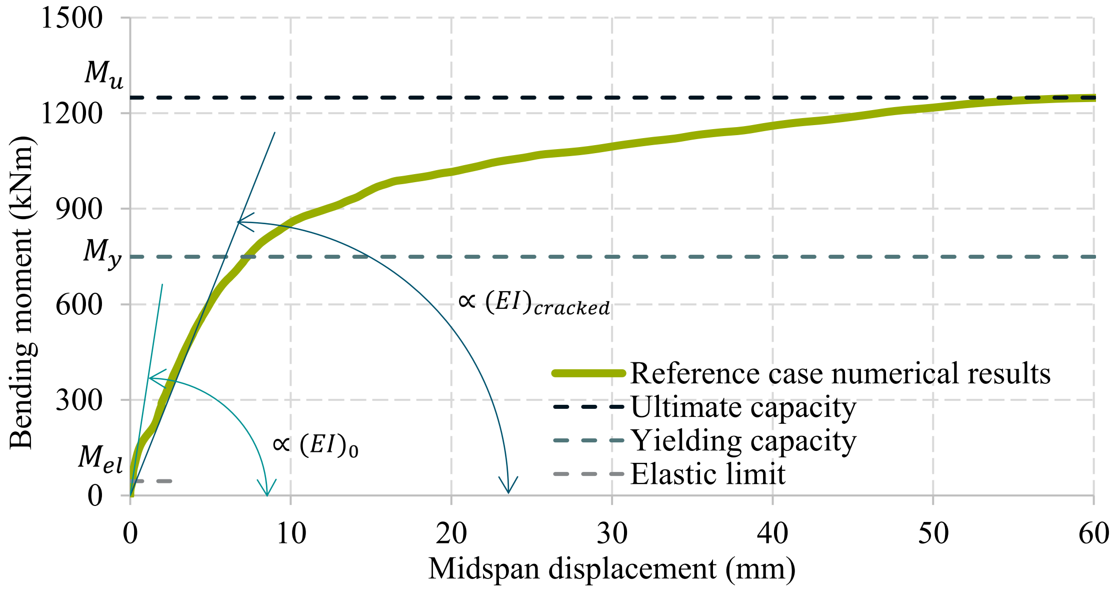

Figure 79 – Definition of mechanical entities for connection performance in the case of bending reference

After these observations, it is necessary to make further distinctions between the mechanical entities. The initial slope can be defined as the *initial bending stiffness* (EI_0) and the second slope is the *cracked bending stiffness* ($EI_{cracked}$). The transition between the two slopes, where softening occurs, is defined by the *elastic limit bending moment* (M_{el}). The *ultimate bending moment* (M_u) corresponds to the maximum value that the curve can reach. As far as the *yield bending moment limit* (M_y) is concerned, it is difficult to define a precise point of variation between the elastic and plastic fields, the yielding can be defined as a 40% reduction from the ultimate bending moment, observing all parametric results.

As a result of the analysis, only the thickness of the wall, the diameter of the connection bars and the density of the studs (as far as the stud spacing is concerned) are responsible for the variation of the bending stiffness and the different limiting bending moments. For these reasons, the next two sections present the bending stiffnesses and the bending moments' evolutions in parametric values for each object of interest mentioned above as responsible for the mechanical connection entities' variation.

Bending stiffnesses

In this section, the initial and cracked bending stiffnesses are shown, and respectively in Figure 80 the evolution of the stiffnesses as the wall thickness varies, in Figure 81 the evolution of the stiffnesses as the diameter of the connection bar varies, and finally, in Figure 82 the evolution of the stiffnesses as the density of the studs varies.

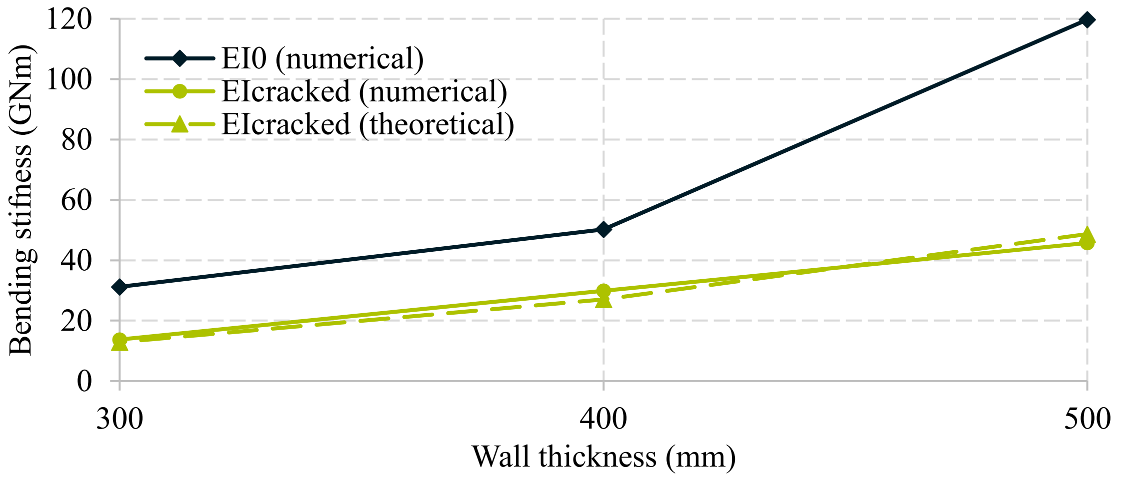

Figure 80 – Initial and cracked bending stiffnesses evolution in wall thickness variation (for M48 connection bars)

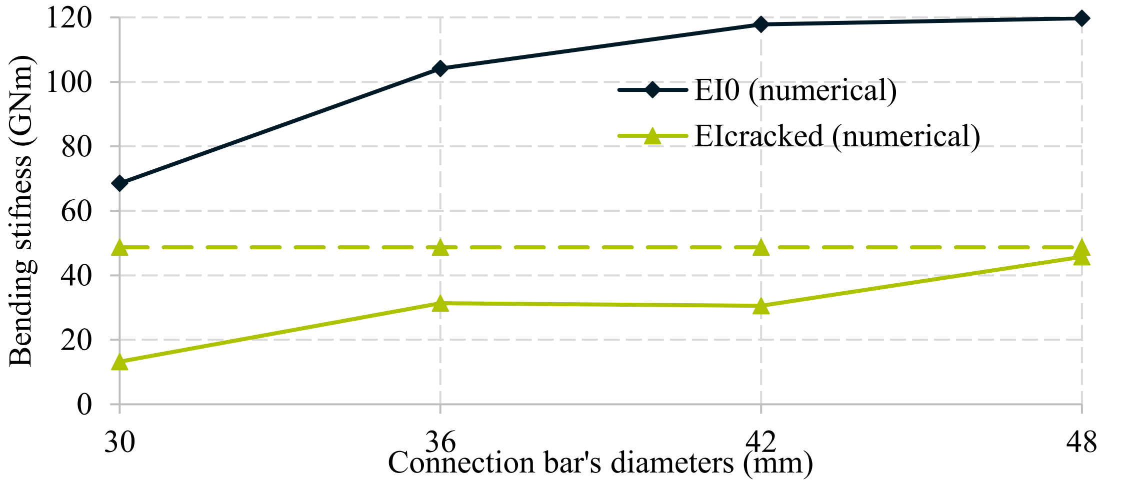

Figure 81 – Initial and cracked bending stiffnesses evolution in connection bar's diameter variation

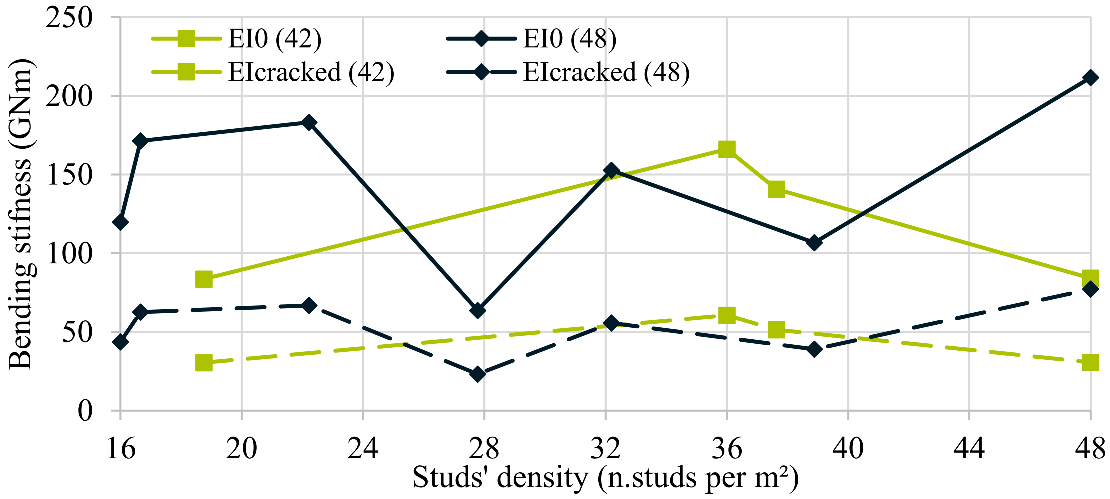

Figure 82 – Initial and cracked bending stiffnesses evolution in studs' density variation

With regard to the wall thickness and connection bar parameters, there is a tendency for the stiffness to increase as the value of the parameter increases. This increase is reasonable because wall thickness increases the inertia of the concrete, while bar diameter increases the inertia of the bars. Since the changes in inertia are greater for the thickness parameter than for the bars' parameter, the changes in stiffness respect this trend and are greater for the former than for the latter. Less obvious is the trend generated by comparing the stud density.

In any case, comparing the initial bending stiffness and the cracked stiffness, it is concluded that the latter is one-third of the former, as the following expression shows:

$$(EI)_{cracked} = \frac{(EI)_0}{3}$$

Based on these observations, an attempt can be made to calculate an analytical value of the stiffness. Firstly, since no pattern is recognised in the density of the studs, their contribution to the bending stiffness calculation is negligible. Leaving only the concrete, plates and connection bars, three different cross-sections can be recognised along the length of the parametric model, as can be seen in Figure 83. The first cross-section has only plates and concrete, the second has plates, concrete and connection bars, and the third has only concrete and bars. The further simplification is to consider only the second cross-section with concrete, plates and connecting bars, as the cross-section along the entire length for the calculation of bending stiffness.

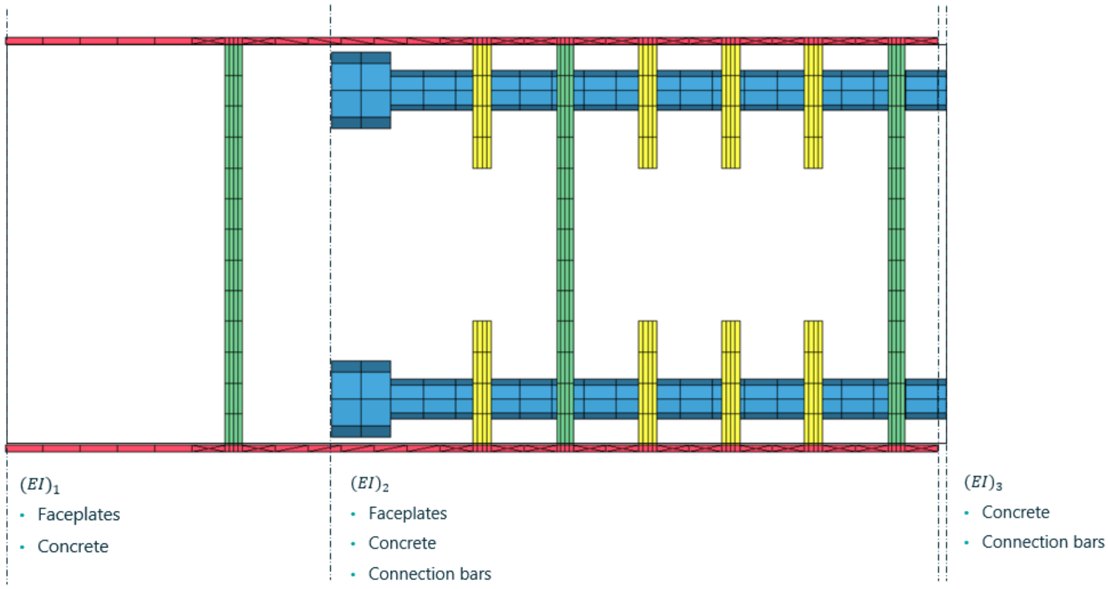

Figure 83 – Different cross-sections along the parametric model's length (bending reference case)

The problem becomes the calculation of inertia in a non-homogenous cross-section of steel and concrete. For this reason, a homogenisation coefficient can be used, transforming the cross-section into a single material, either by increasing the steel elements areas and converting the entire cross-section into concrete or by reducing the area of the concrete and converting the entire cross-section into steel, as demonstrated by the following expression for the concrete area:

$$A_{c,eq} = \frac{A_c}{n}$$

Where, $A_{c,eq}$ is the equivalent concrete cross-section reduced as it was made of steel and n is the homogenisation coefficient equal to the ratio of the young modulus of steel to that of concrete:

$$n = \frac{E_S}{E_c}$$

The inertia of the cross-section can be calculated with the concrete area transformed into steel while maintaining the same thickness and reducing the base (see Figure 86).

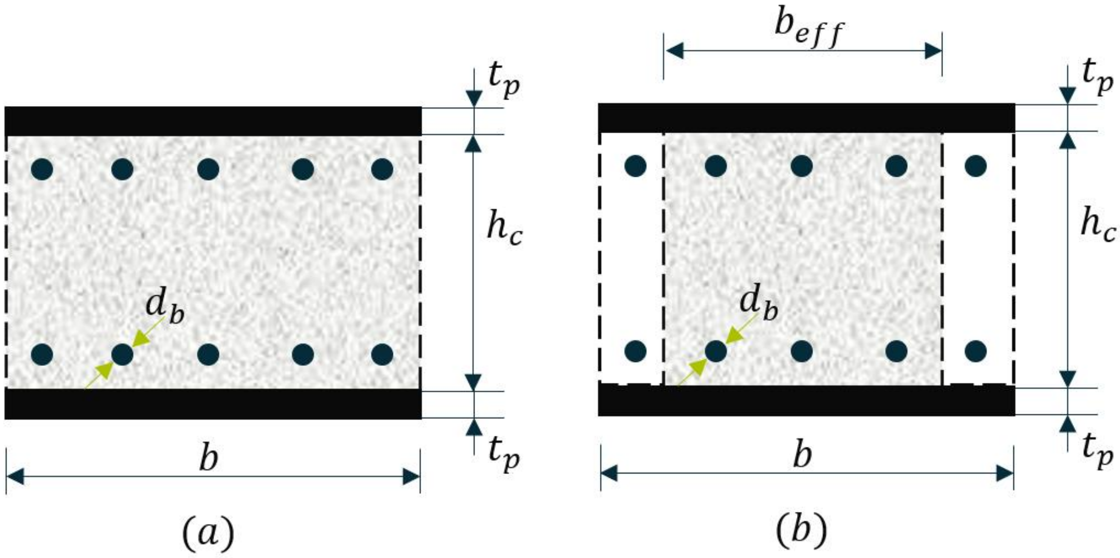

Figure 84 – (a) Cross-section considered for stiffness calculation (b) Homogenised concrete cross-section

With this approach, the theoretical values of the cracked bending stiffness are calculated and shown in Figure 80 and Figure 81. The theoretical values represented are the actual stiffness values divided by 10. A reduction of one order of magnitude is considered to account for the reduction in the cross-sectional area of the cracked concrete, since the effective area of the non-cracked concrete is unknown, to account for the reduced performance due to non-linear effects, and to account for the simplification due to the consideration of only one type of cross-section along the length out of three. Overall, the values provide comparable results and can be described as a good estimation of the cracked bending stiffness. In turn, since the relationship between cracked and initial stiffness is known, an estimate of the initial bending stiffness can also be obtained.

Elastic limit and the ultimate capacity

In this section, the elastic limit, the yielding and ultimate bending moments are shown, respectively in Figure 85 the evolution of the bending moments as the wall thickness varies, in Figure 86 the evolution of the bending moments as the diameter of the connection bar varies, and finally, in Figure 87 the evolution of the bending moments as the density of the studs varies.

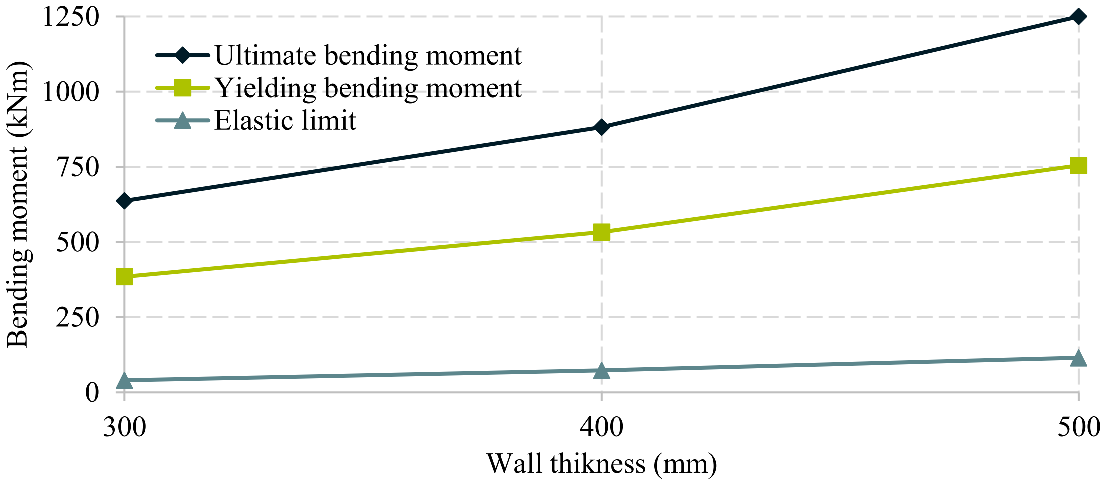

Figure 85 – Ultimate and yielding bending moment evolution in wall thickness variation

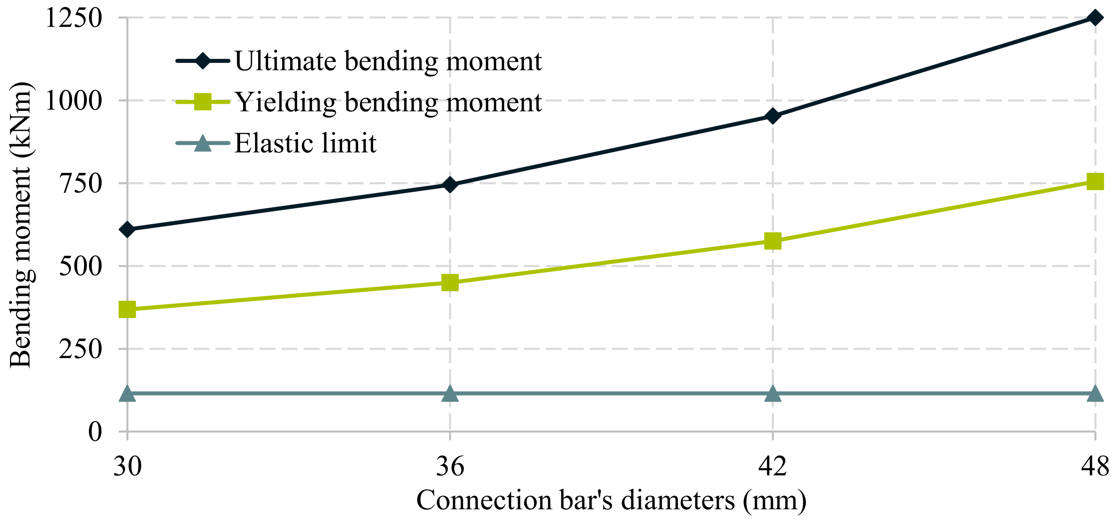

Figure 86 – Ultimate and yielding bending moment evolution in connection bar’s diameter variation

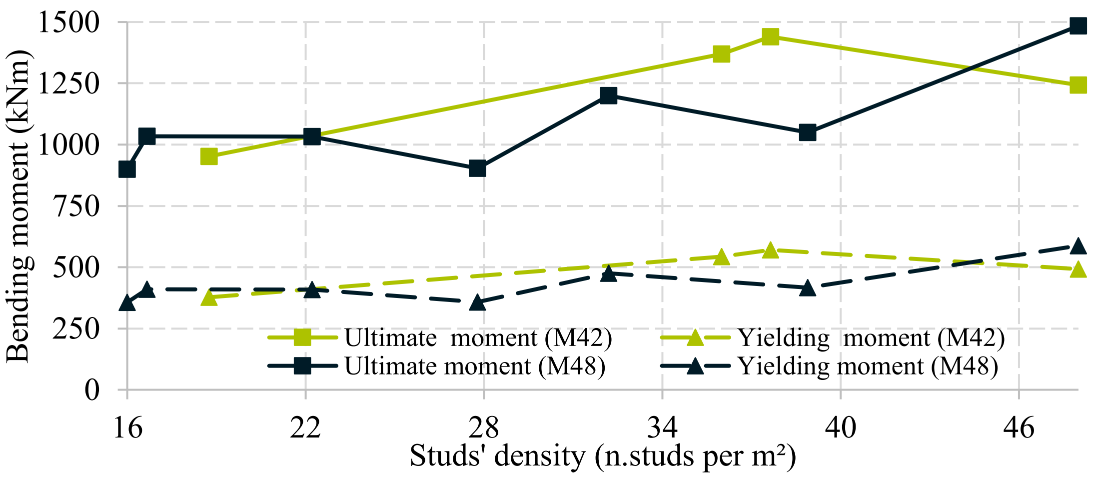

Figure 87 – Ultimate and yielding bending moment evolution in studs’ density variation

With regard to the elastic limit, this is the bending moment calculated according to Navies' equation at the point where the maximum tensile stress is reached in the concrete.

$$\sigma(y) = \frac{M}{I_x} y$$

The Navies' equation is computed at $y = h_c/2$, with the maximum tensile strength (f_{ct}) and with the homogenised inertia as seen in the previous section.

$$M_{el} = \frac{2I_x}{h_c} f_{ct}$$

The ultimate bending moment corresponds to the ultimate values reached in the parametric analysis; the analytical expression is evaluated in Chapter 6 in the analysis of the strength reduction in the connection. The yield bending moment is defined as a 40% reduction from the ultimate moment: $M_y = 0.6M_u$.

5.2 Axial parametric analysis

All comparisons are performed with graphs comparing the horizontal displacement of the faceplates at the load application with the reaction force at the midspan of the beam.

5.2.1 Connection bars parameters: diameter (d_b) and ultimate strength ($f_{sy,b}$)

Figure 88 presents the axial parametric results of variation in connection bars diameter from M30 to M48 while Figure 89 the axial parametric results of variation in connection bars steel grade between 8.8 and 10.9.

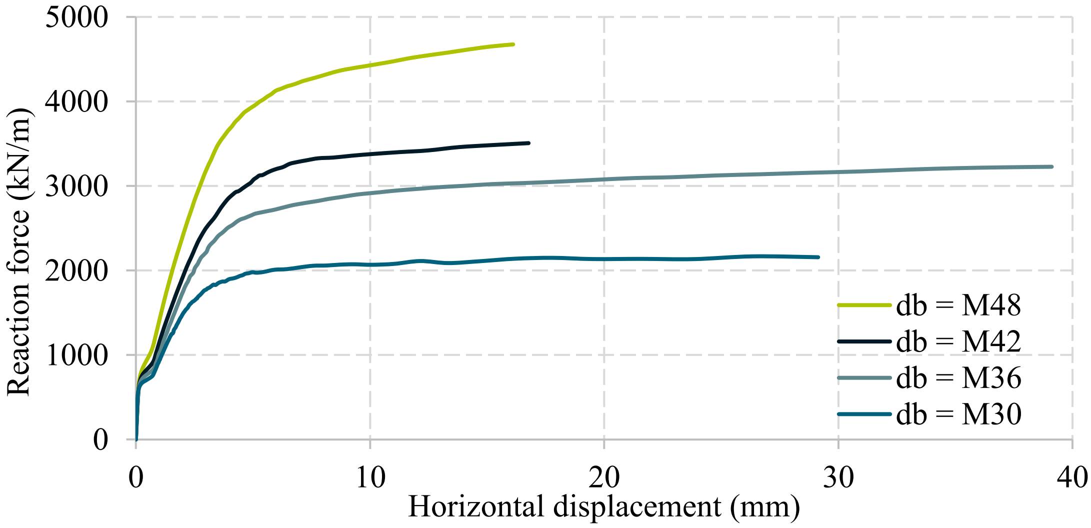

Figure 88 – Axial parametric results of variation in connection bars diameter from M30 to M48 (M48 is the reference case value)

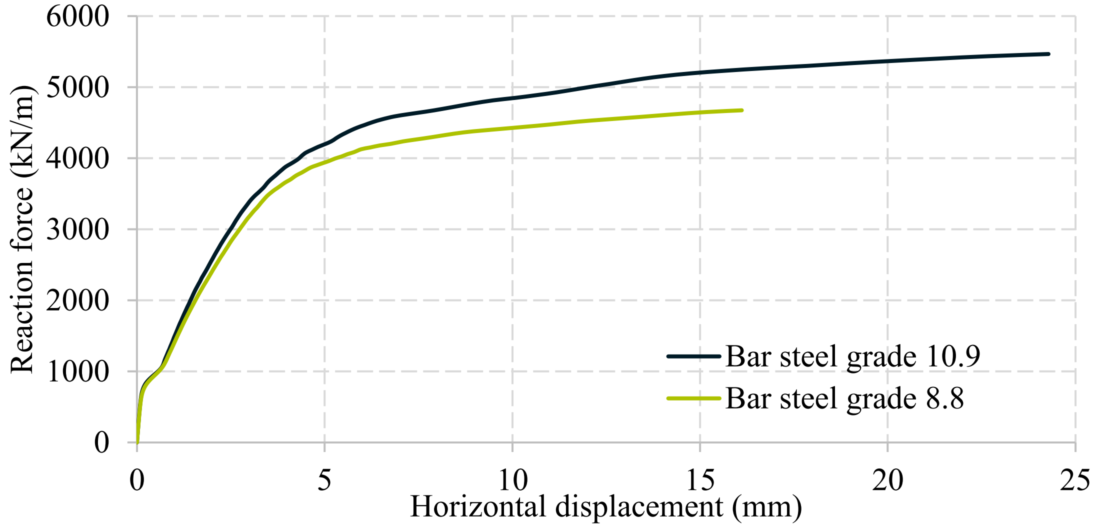

Figure 89 – Axial parametric results of variation in connection bars steel grade between 8.8 and 10.9 (8.8 is the reference case value)

In this first comparison, a behaviour entirely coherent with that observed for the bending analysis, in paragraph 5.1.1, is noted. Once again, the reduction in strength is a function of the connection bar area, in fact, the reduction in ultimate axial capacity with respect to the reference case is 25% for the M42 model, 31% for the M36 model and 53.7% for the M30 model, respectively, almost the same values for the bending ultimate capacity reduction reported in Table 19.

Another similarity is the small difference in the improvement of the strength grade.

The only difference is that in bending, the optimum value for ductility was model M42, whereas now it is model M36.

5.2.2 Faceplates' parameters: thickness (t_p) and ultimate strength ($f_{sy,p}$)

Figure 90 presents the axial parametric results of variation in faceplate thickness from 6 to 14 mm, while Figure 91 the axial parametric results of variation in faceplate thickness between S235 and S355.

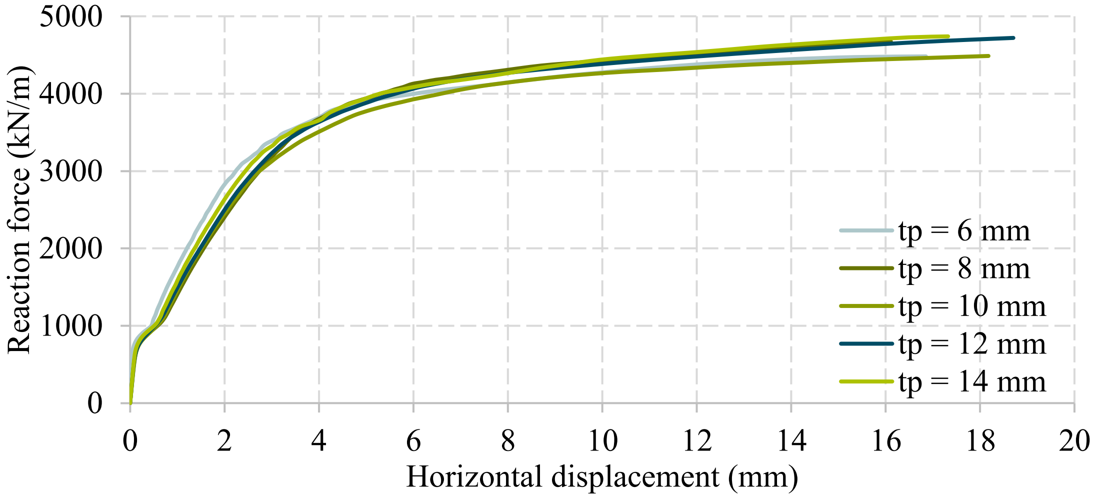

Figure 90 - Axial parametric results of variation in faceplates thickness from 6 to 14 mm (8 mm is the reference case value)

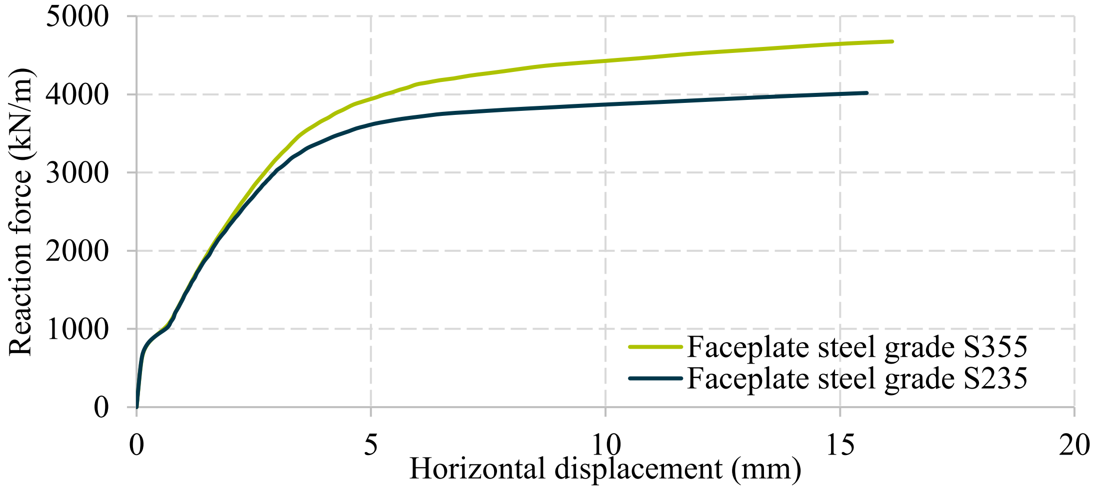

Figure 91 - Axial parametric results of variation in faceplates steel grade between S235 and S355 (S355 is the reference case value)

Once again, the same results of the bending analysis, mentioned in section 5.1.2, can be noted for the axial analysis of the plate parameters. The same conclusion can be extended: since the plates are not the element generating the failure, the influence of the parametric results does not lead to significant changes in the behaviour of the connection.

5.2.3 Concrete parameter: wall thickness (H_c)

Figure 92 presents the bending parametric results of variation in concrete thickness from 300 to 500 mm.

This comparison is the only one with different results from the bending analysis. First, in the bending case reported in section 5.1.3, there is a significant variation in bending stiffness and ultimate bending capacity. In the axial analysis, there is no variation except in the case of the 300 mm thickness. This big difference with the bending case is because, as far as stiffness is concerned, the axial stiffness considers area and not inertia, but once a tension force is applied in the concrete, it soon fails, leaving only the connection bars and plates to provide strength.

The reduction in strength relative to the 300 mm model is due to the high level of damage to the concrete, even in the compressed part near the connection bar heads, which in turn became an impossibility for the transfer of stresses from the plate to the bars. The conclusion is that, at least for this analysis in which the studs represent the failure condition of the connection, the 400 mm thickness can be defined as the minimum to ensure sufficient concrete to transmit the stresses to the connection bars.

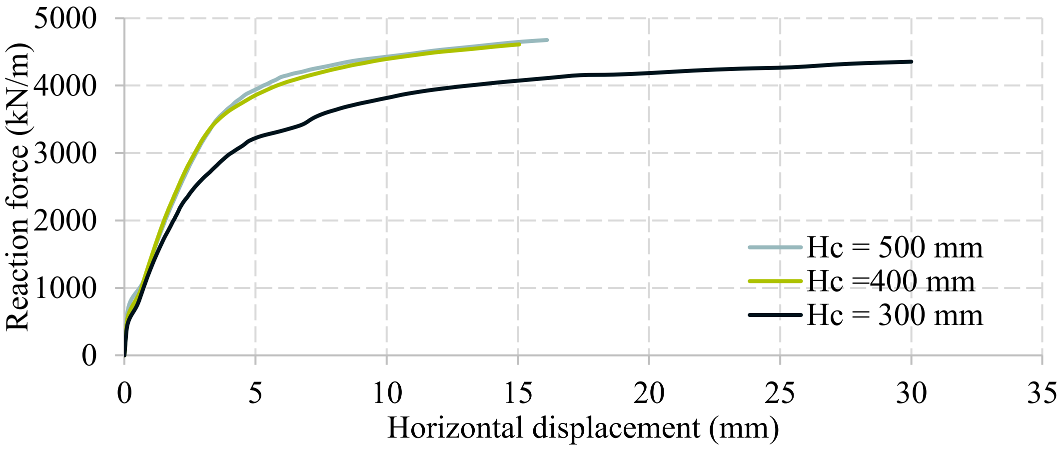

Figure 92 – Axial parametric results of variation in concrete thickness from 300 to 500 mm (500 mm is the reference case value)

5.2.4 Studs' parameters: diameter (d_s) and height (h_s)

Figure 93 presents the axial parametric results of variation in studs' diameter from 19 to 25 mm, while Figure 94 the axial parametric results of variation in studs' height from 100 to 250 mm.

The same behaviour can be seen in the bending analysis of section 5.1.4. The design condition of the ratio of the longitudinal studs' spacing to the diameter is also consistent with the application of the axial load. With regard to the analysis of the diameter variation, for a constant spacing between the studs, increasing it shows an estrangement from the design limit and a consequent reduction in strength. With regard to the height of the studs, once again the optimum can be defined as 150 mm (the reference case value), since lower values lead to a reduction in strength, while higher values do not lead to an improvement in the strength of the connection.

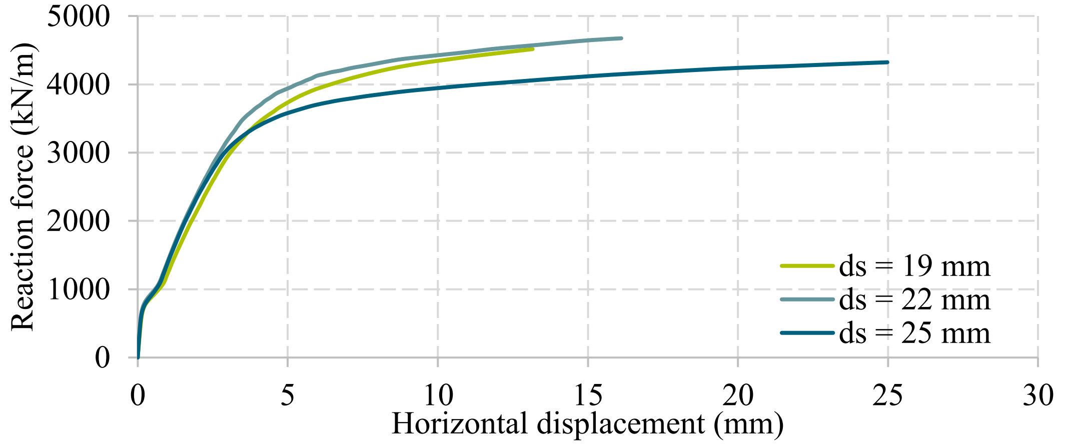

Figure 93 – Axial parametric results of variation in studs’ diameter from 19 to 25 mm (22 mm is the reference case value)

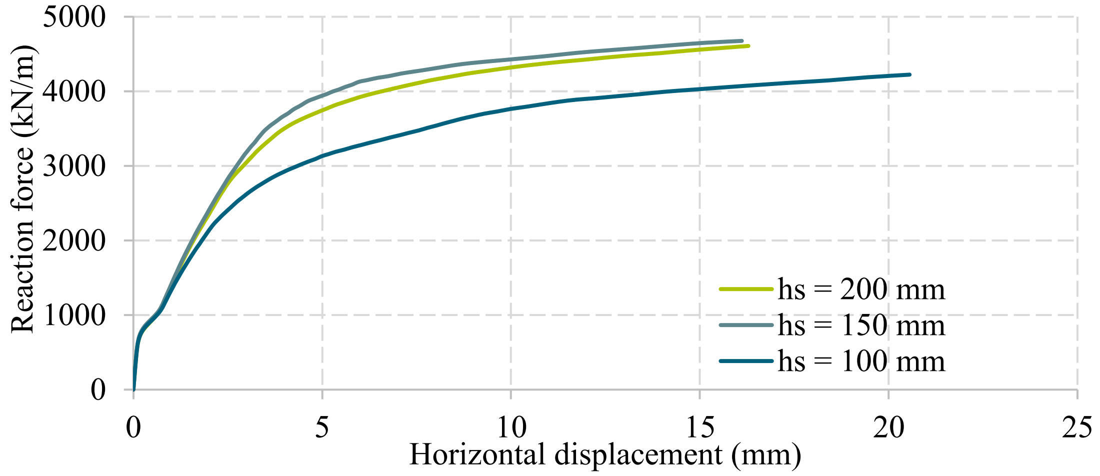

Figure 94 – Axial parametric results of variation in studs’ height from 100 to 200 mm (150 mm is the reference case value)

5.2.5 Tie bars and studs spacing parameters: y-spacing (s_{sy},s_{ty}) and x spacing (s_{sx},s_{tx})

The different tie bar and studs' spacing parameters are organised as follows:

- Figure 95 presents the axial parametric results of variation in studs’ vertical spacing between 133 and 200 mm for tie bars spacing of 400 mm and M42 connection bars diameter.

- Figure 96 presents the axial parametric results of variation in studs' vertical spacing from 125 to 250 mm for tie bars spacing of 500 mm and connection bars diameter of M48.
- Figure 97 presents the axial parametric results of variation in studs' horizontal spacing from 75 to 150 mm for tie bars spacing of 600 mm and connection bars diameter of M48.
- Figure 98 presents the axial parametric results of variation in studs' horizontal spacing between 100 and 125 mm for tie bars spacing of 500 mm and connection bars diameter of M42.

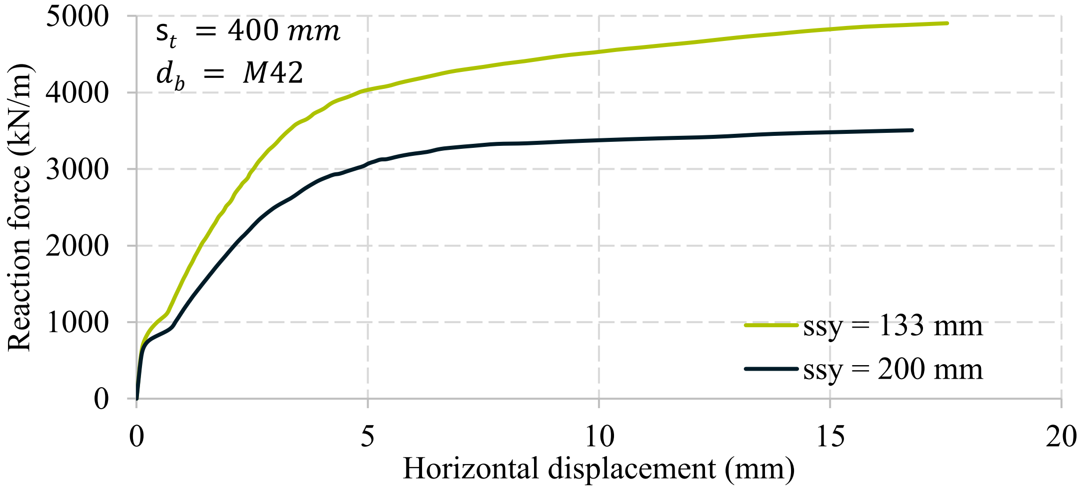

Figure 95 - Axial parametric results of variation in studs' vertical spacing between 133 and 200 mm for tie bars spacing of 400 mm and M42 connection bars diameter (s_{sy}=200mm, s_t=400mm and d_b=M48 are the reference case value)

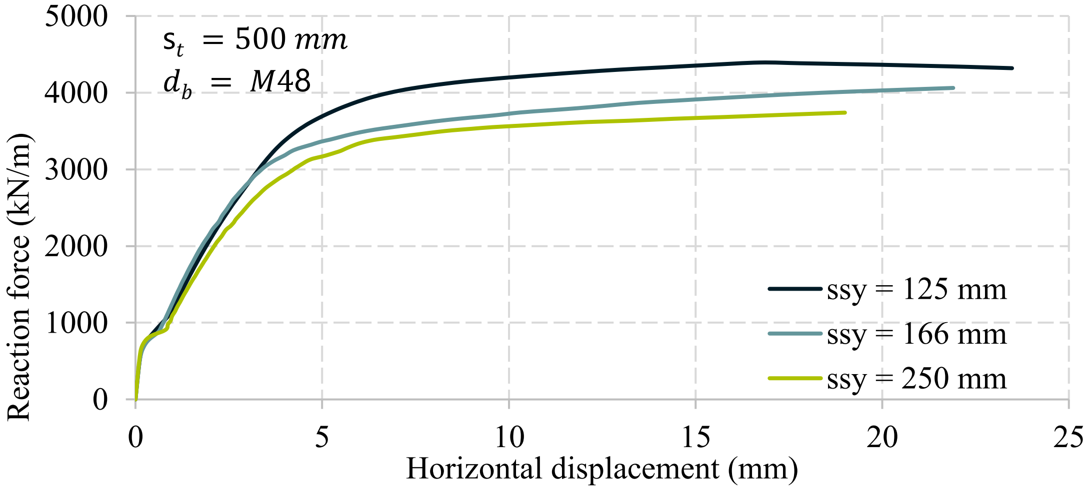

Figure 96 - Axial parametric results of variation in studs' vertical spacing from 125 to 250 mm for tie bars spacing of 500 mm and connection bars diameter of M48 (s_{sy}=200mm, s_t=400mm and d_b=M48 are the reference case value)

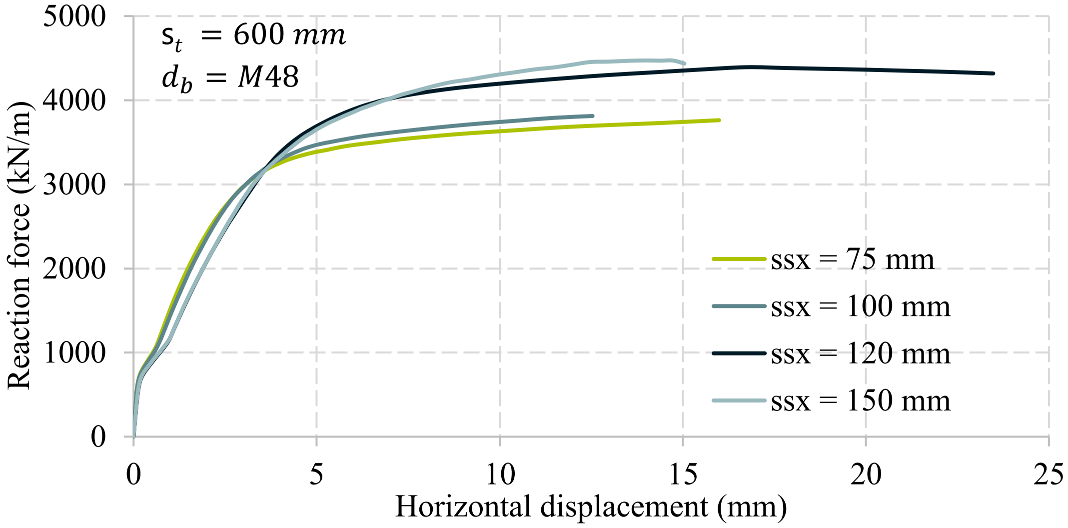

Figure 97 - Axial parametric results of variation in studs' horizontal spacing from 75 to 150 mm for tie bars spacing of 600 mm and connection bars diameter of M48 (s_{sy}=200mm, s_t=400mm and d_b=M48 are the reference case value)

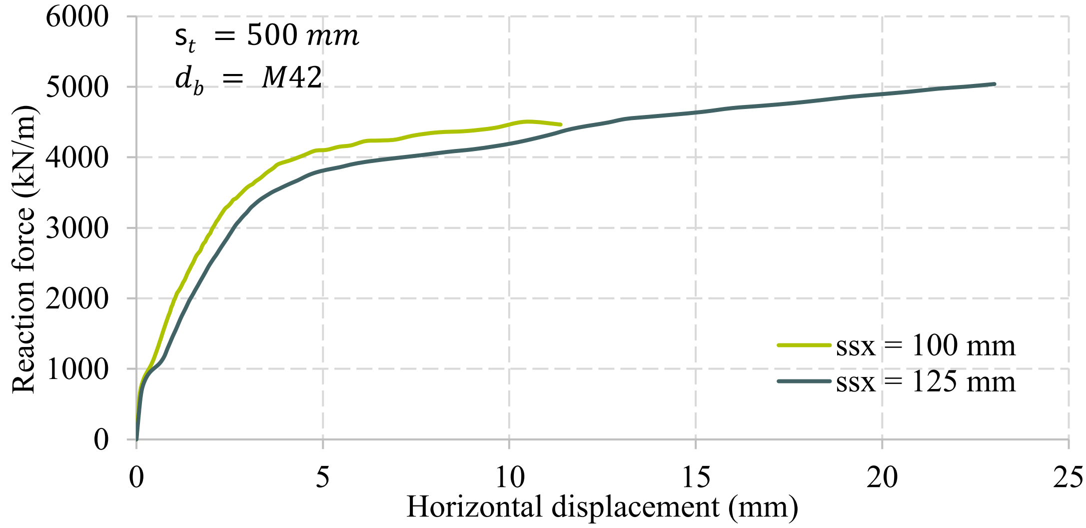

Figure 98 - Axial parametric results of variation in studs' horizontal spacing between 100 and 125 mm for tie bars spacing of 500 mm and connection bars diameter of M42 (s_{sy}=200mm, s_t=400mm and d_b=M48 are the reference case value)

Also, for this last axial analysis, the results completely match the bending results of section 5.1.5. The main conclusion that can be drawn is that increasing the density of the studs leads to an increase in the strength of the connection.

Chapter 6

Connection strength

The objective of this chapter is to:

- understand the failure and yielding modes with section 6.1;
- estimate the reduction in strength of the connection with respect to the SC wall with:
  - the estimation of the SC wall strength in section 6.2;
  - the bending and axial connection strength to compare with the SC wall in 6.3;
- detailed analysis of stud behaviour.

6.1 Consideration of the yielding and failure modes

Figure 99 and Figure 100 show the bending reference case with the evolution at different stages (1 to 5) of the plates and studs' plastic strain. The different stages are at different values of the midspan displacement (D7) from stages 1 to 5 respectively at 4.6, 7.6, 13.1, 35.3 and 61.5 mm, and the last stage corresponds to the failure of the model. In particular, the comparison between stages 1 to 4 is limited in scale to the respective yield strength of the plates and studs, while the last stage, number 5, is limited in scale to their respective ultimate stain values, for a better understanding of the failure conditions.

During the bending, the most damaged concrete is at the midspan of the beam and at the connection bars' heads. Especially in the latter part, the damage is greater, due to the upward movement of the connection bars' heads, as already seen in the connection bars' deformation in Figure 60 of section 4.2. Due to this upward movement, in turn, the concrete is pushed towards the upper faceplate. The studs would like to move with the plate but being anchored in the undamaged concrete, they do not move and tension is generated in the studs.

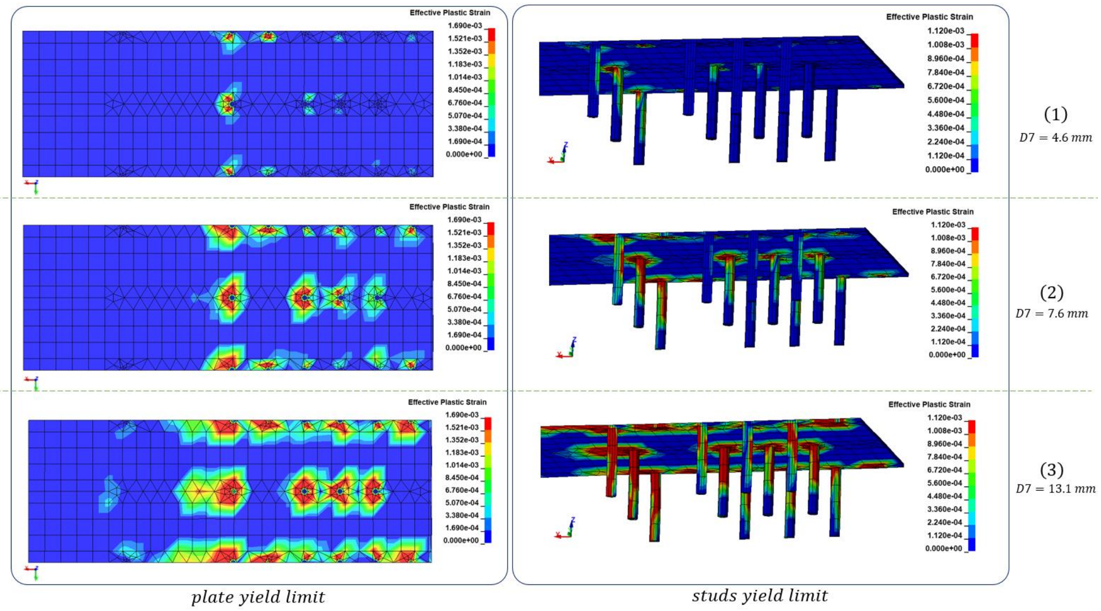

Figure 99 – Comparison at stages 1 to 3 of plate and studs yielding evolution (bending reference case)

In essence, steps 1 to 3 show:

- In plate: deformations around the studs cause the plate to yield before the studs;
- In studs an increase in tension and axial deformation.

The increased tensile force in the studs reduces the pure shear capacity. Due to the reduction in shear strength and the continuous application of the bending moment, the studs begin to bend and the top plate moves horizontally. The beginning of this phenomenon can be seen in stage 4. Failure, represented by stage 5, then occurs in the studs in bending, where the additional stresses resulting from bending, increase the tension in part of the stud cross-section which fails.

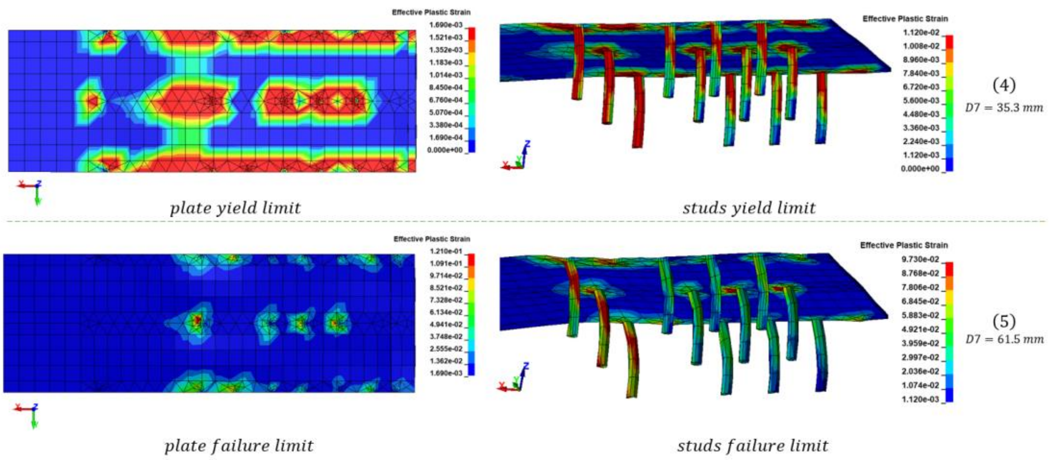

Figure 100 – Comparison at stages (4) plate and studs yielding evolution and (5) plate and studs failure limit (bending reference case)

Figure 101 resumes the two behaviour mechanisms for yielding and failure.

The first is the yielding of the plate around the studs due to the push of the concrete on the plate, while the second is the stud's bending failure. These two conditions are true for all combinations, in both bending and axial analysis, except for combinations 10 and 19.

Combination 10 is the one with 14 mm plate thickness, the difference being that in this case, both, yielding and failure occur in the studs. This is due to the fact that increasing the plate thickness leads to a reduction in stress in the plate and thus yielding occurs first in studs reaching the yielding tension resistance.

Combination 19 is the one with 500 mm tie bars' spacing and 100 and 125 mm as longitudinal and transverse studs' spacing respectively. This combination turned out to be the one with the highest studs' density, 48 per square metre. This condition reduces the concentration of stresses in the studs and the failure occurs in the plate around the studs, where yielding at first occurred, with a consequent detachment of the studs from the plate, generating a punching failure.

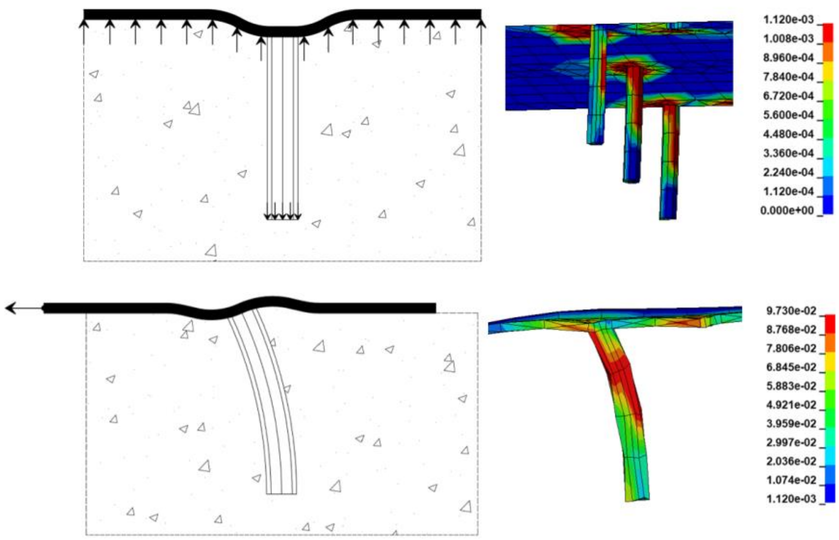

Figure 101 – Yielding and failure modes

6.1.1 Studs' resistance in bending and axial models

The previous section concludes that the studs are the weakest elements in the model which generate the failure of the connection. A further conclusion is that a tensile force creates a reduction in the pure shear strength. The objective of this section then is to understand the amount of the shear strength reduction. The following expression represents the relationship between the shear strength of the studs and the tensile force, a formulation that can be founded in section 5.4.5 of [6]:

$$\left(\frac{F}{P_{Rd}}\right)^{5/3} + \left(\frac{F_{ten}}{P_{Rdt}}\right)^{5/3} \leq 1.0$$

Where:

- F_{ten} is the design tensile force to which the stud is subject;
- P_{Rdt} is the tensile resistance per stud, measured as the ultimate tensile strength for the connection bars in section 2.4.2;
- P_{Rd} is the shear resistance per stud calculated in 2.4.2 for the estimation of the studs' number to transmit the ultimate capacity of the connection bars to the plates;
- F is the actual shear resistance.

Figure 102 shows the reduction in stud shear strength with the increase of the tensile force in the stud. The stud under investigation is the one used in the reference case with a 22 mm as diameter and a steel grade of S235, with a maximum pure shear force of 109 kN and a maximum tensile strength of 98.5 kN. These values can be founded respectively for pure shear, i.e., if the tensile force is zero, or vice versa for pure tension, i.e., if the shear force is zero.

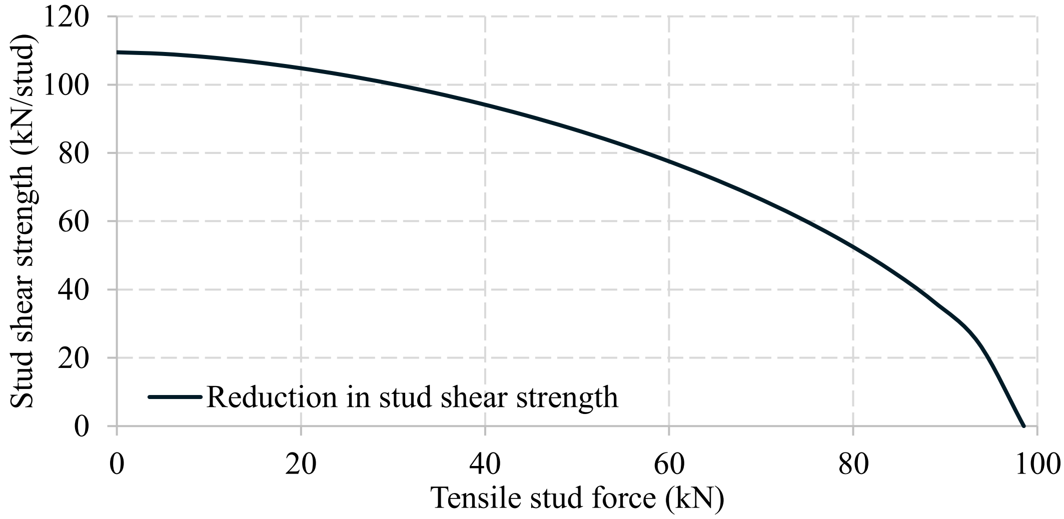

Figure 102 – Reduction in stud shear strength due to the effect of the tensile force

Figure 103 and Figure 104 show the evolution in time of the shear strength of a single stud placed in different rows for the bending and axial reference cases, respectively, compared to the theoretical pure shear strength of 109 kN for both cases.

The actual strength of the studs is much lower, around 40 kN, resulting in a 63% reduction in strength. The second thing to note is that, especially for the bending case (Figure 103), the studs show different tensional states, higher for the first rows that decrease once the edge of the plate is approached. The reason for this is to be found in the distribution of stresses on the plate, as can be seen in Figure 105. In the case of bending, the different rows are subjected to very different stresses, compared to the axial case where the stresses are more uniform. This results in greater deformation differences between the stud rows in bending and less in tension. The maximum tension measured in the studs in both cases is 70 kN.

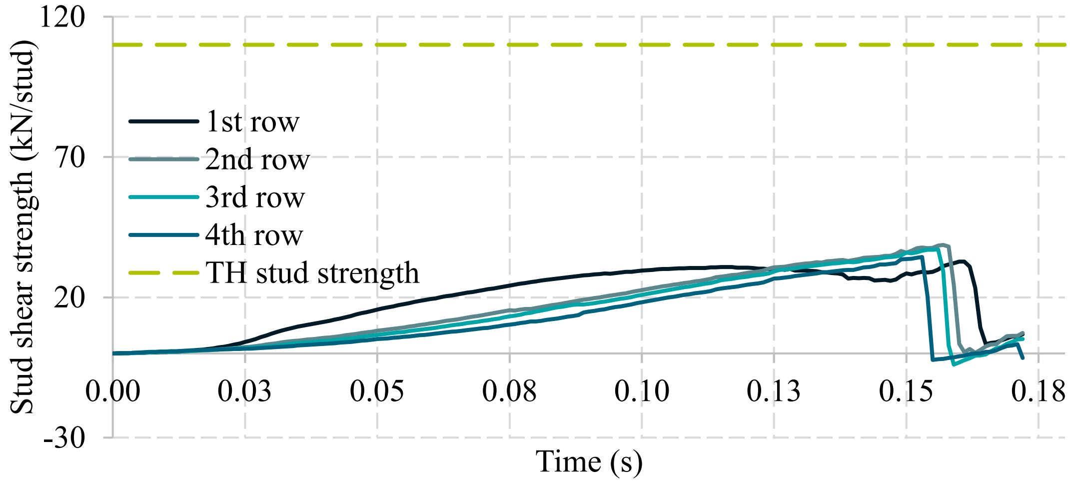

Figure 103 – Shear resistance for a stud placed on different rows of the bending reference case

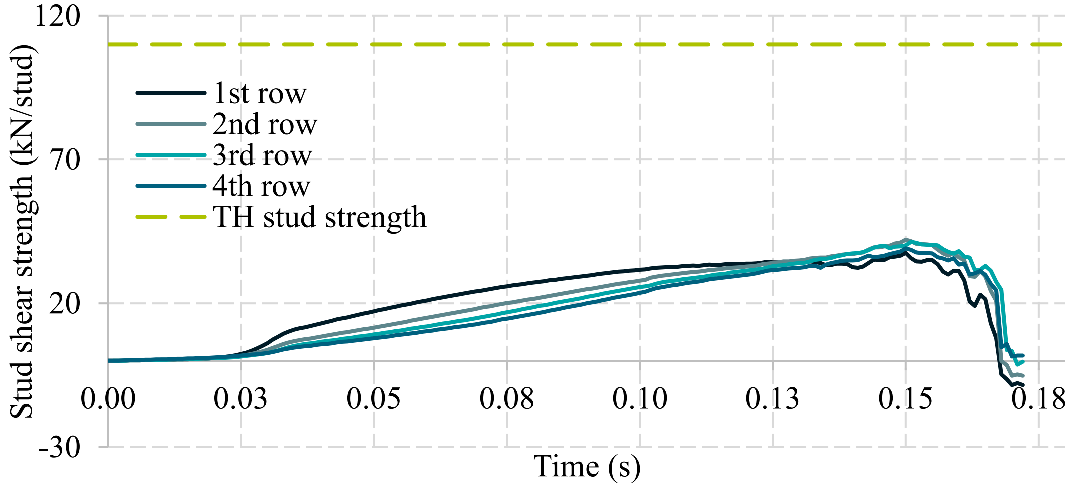

Figure 104 - Shear resistance for a stud placed on different rows of the axial reference case

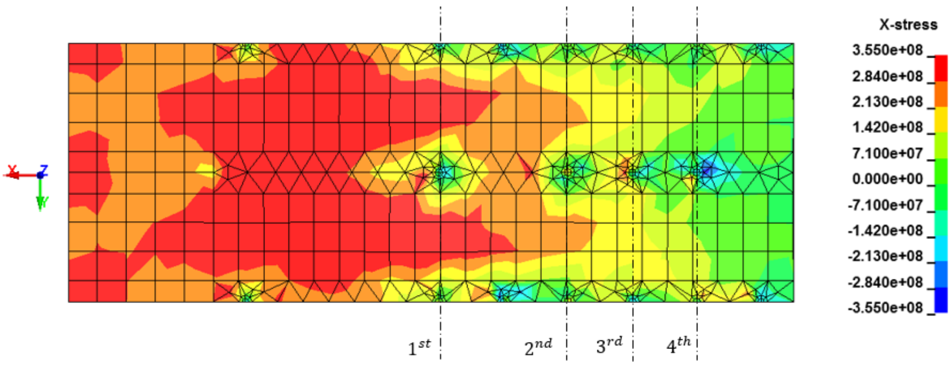

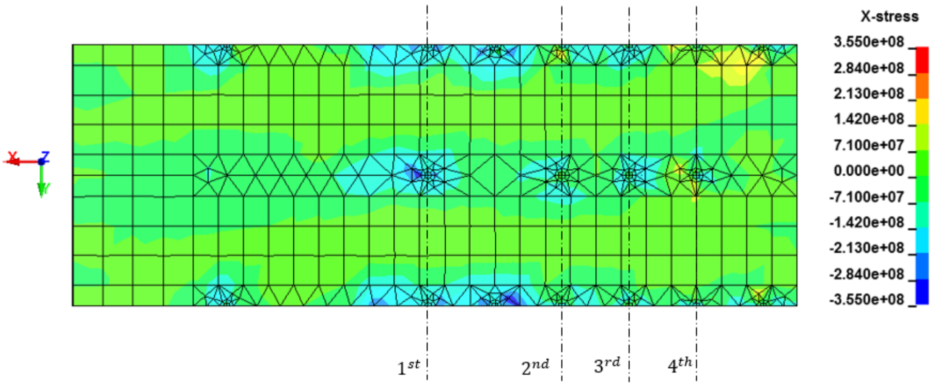

Figure 105 - Axial stresses (x-stress) in the bending and axial reference case limited to the yield stress of 355 MPa at their respective failures

It can be concluded that, since the tensile force is greater than 10 % of the shear strength, this force cannot be neglected in the design of the studs, as shown in [6]. Due to this loss of strength, the number of studs used in the parametric analysis is not sufficient to transmit the ultimate capacity of the connection bars. The models, therefore, will perform less well compared to the theoretical capacity, with strength values reduced by 60% in magnitude. A different methodology must be used when designing the studs.

The problem of taking into account tensile stresses in the studs is indeterminate. In fact, increasing the number of studs to cover the missing strength will result in a reduction of the tensile stress distribution between the studs, since the total tensile force is supported by a greater number of studs. This in turn means a better shear capacity for studs with excess strength and thus the conclusion of having less of them.

6.2 SC wall strength

To estimate the loss of strength in the connection, the strength of the SC wall must first be calculated. In this section, the estimation is performed for bending and axial load application. For the bending resistance, both analytical and numerical solutions are available. For the axial one, since the simplicity of the model is limited to the axial resistance of the plate or the total shear capacity of the studs, only the analytical solution is presented.

6.2.1 Bending SC wall capacity

In this section, numerical and analytical solutions for the bending capacity of the SC wall are presented.

Numerical bending SC wall capacity

To compute the numerical bending resistance of an SC wall, the following variations of the parametric model are performed:

- removal of embedded connection bars;
- removal of the concrete gap at the connection and extension of the horizontal constraint to create midspan symmetry condition on the plates as well;
- use as parametric values those typically used in the SC wall, i.e., 22 mm as the stud diameter, 200 mm as the longitudinal and transverse stud spacing, 20 mm as the tie bar diameter and 400 mm as the tie bar spacing.

Figure 106 shows the load and boundary conditions for the SC-wall model, while Figure 107 shows the comparison of the SC-wall model with the bending reference case.

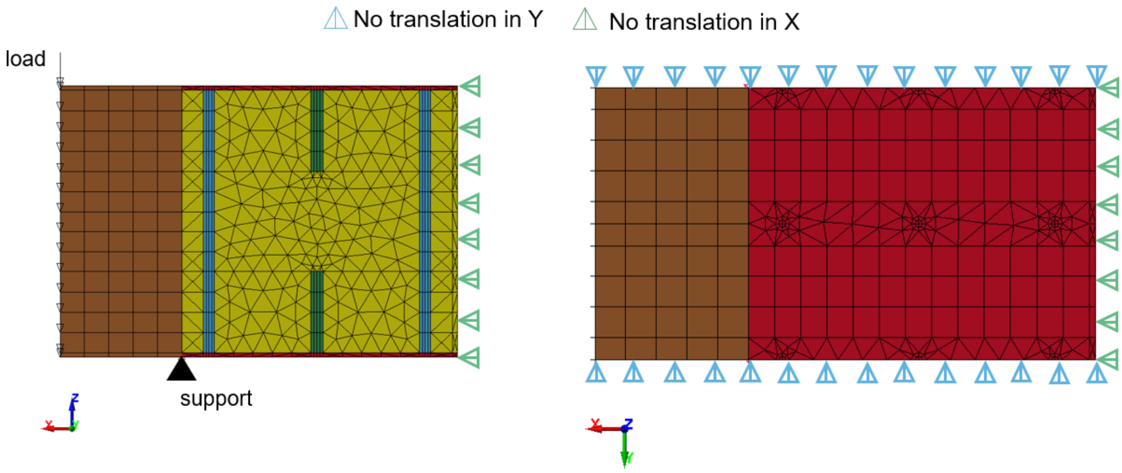

Figure 106 – Load and boundaries conditions for the SC-wall model

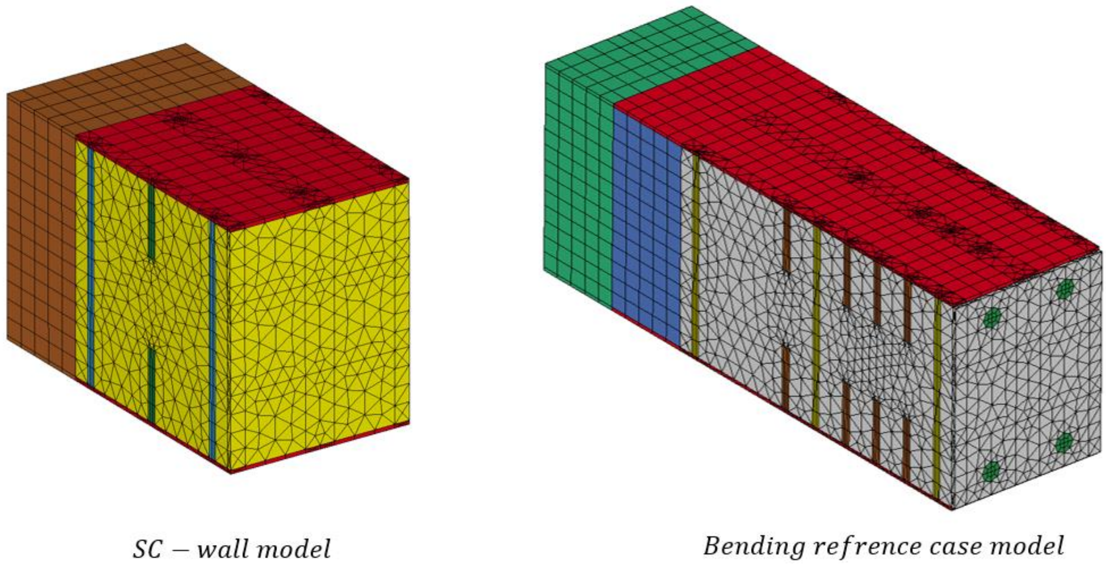

Figure 107 – Comparison between the SC-wall model and the bending reference case model

Figure 108 shows the vertical stress of the concrete and the faceplates at the failure point, which can be seen to reach ultimate stress in the upper tensile faceplate. The lower plate does not even reach yield strength. As for the reinforced concrete RC, a division between the tensile and compressive parts of the concrete can be seen.

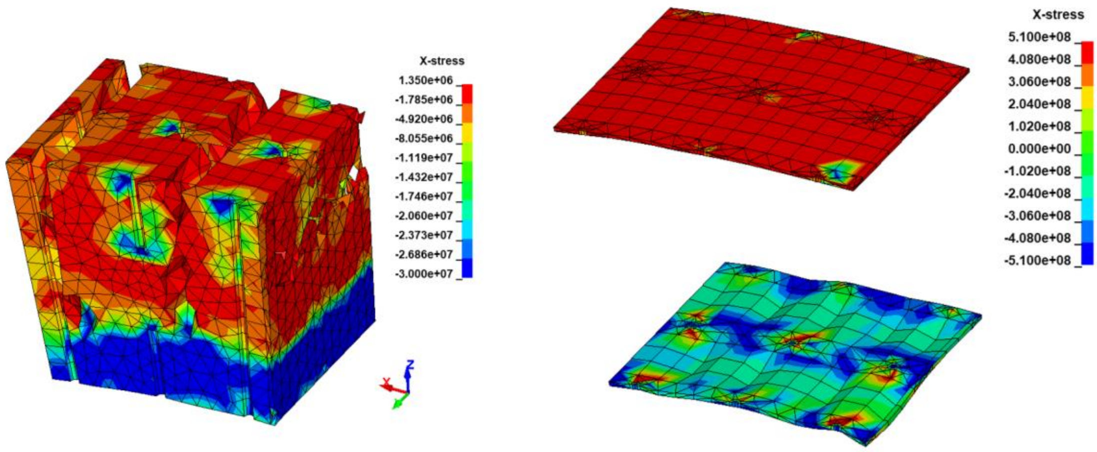

Figure 108 – Axial stress in the concrete and faceplates at the failure

Analytical bending SC wall capacity

Based on the observation of the numerical calculation, an attempt was made to calculate the analytical results for the ultimate bending capacity of the SC wall. The approach used is similar to that of the RC cross-section design, using the following assumptions:

- failure occurs due to the ultimate capacity of the faceplate being reached in tension;
- the compressed faceplate is neglected;

- the position of the neutral axis is found as the equilibrium between the tensile components of the steel and the concrete in compression;
- the base refers to a 1 m width.

The unknowns are two, the position of the neutral axis and the resistant bending moment, and can be found in the two available equilibrium equations. Figure 109 shows the forces at the failure condition of the SC wall according to the mentioned assumption, referred to as the RC design approach.

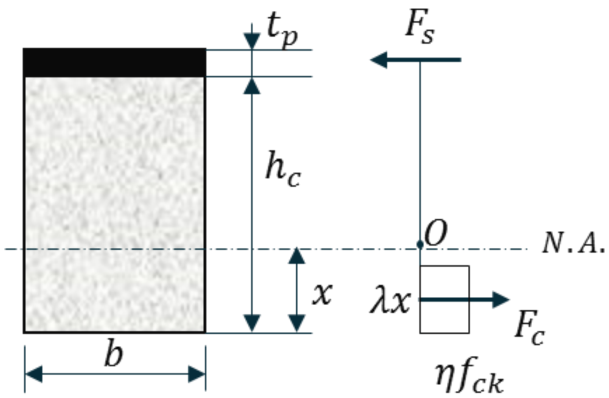

Figure 109 - Forces at the failure condition in the SC wall using the RC hypothesis

Where the different components according to EN 1992-1-1 [14] are:

- $F_s = A_s f_{su,plate}$
- $\begin{cases} \lambda = 0.8 & \eta = 1.0 & f_{ck} \leq 50MPa \\ \lambda = 0.8 - \frac{(f_{ck}-50)}{400} & \eta = 1.0 - \frac{(f_{ck}-50)}{200} & 50 \leq f_{ck} \leq 60MPa \end{cases}$

From the equilibrium equations, the neutral axis and the characteristic ultimate resistance bending moment are:

$$x = \frac{A_s f_{su}}{\lambda f_{ck} b}$$

$$M_{Rk,wall} = A_s f_{su} \left(\frac{t_p}{2} + h_c - \frac{\lambda x}{2}\right)$$

However, the simplification of neglecting the compressed plate was adopted because the compressed stress state is unknown and this increases the unknowns of the problem to 3. Since only two equations are available, this additional unknown makes the problem indeterminate. The assumption of using one of the ultimate or yield capacities of the plate in the compressed stress state is inconsistent since it was noted from the numerical model that both of these conditions are not verified and the stress state is even lower than the yield state. The limitation of this analytical approach is the physical meaning of the

neutral axis. This does not represent the physical division between compressed and tensioned concrete, since for equilibrium the concrete must cover the stresses in the compressed plate, with mechanical properties inferior to those of steel.
Figure 110 compares the numerical and analytical approaches, with the conclusion that the two show comparable values demonstrating the validity of the analytical formulation and the assumptions made. The comparison is made with characteristic values since in the numerical model all the values used are characteristic.

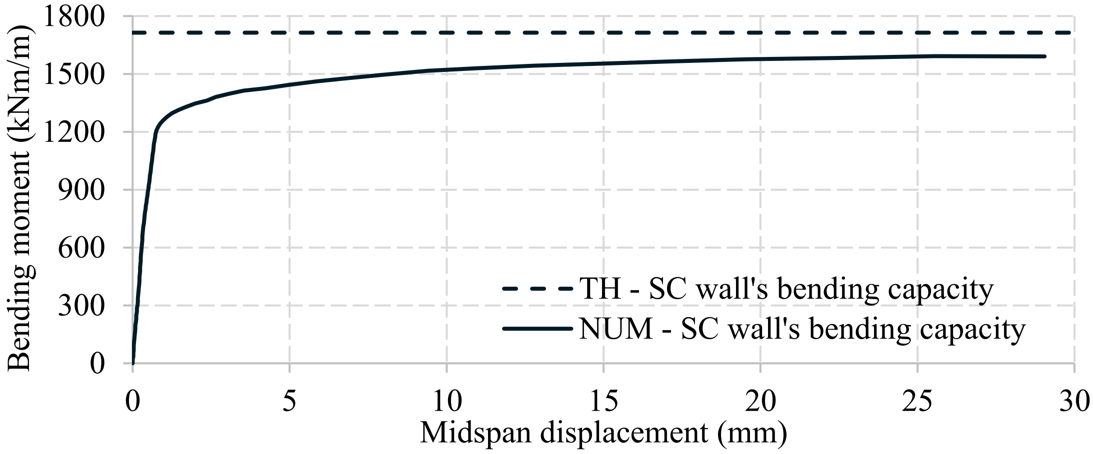

Figure 110 – Comparison between numerical and analytical SC wall's bending capacity

6.2.2 Axial SC wall capacity

The axial strength of the SC wall is the minimum between the axial tensile strength of the faceplates and the total shear strength of the studs, with the hypothesis of neglecting concrete in tension.

$$N_{Rk} = min\{N_{Rk,plate} \quad N_{Rk,studs}\}$$

$$N_{Rk,plate} = 2A_{plate}f_{su,plate}$$

$$N_{Rk,studs} = 2\sum_{i} P_{Rk,i}$$

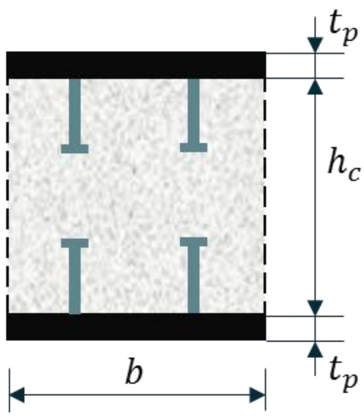

Figure 111 – SC wall with headed studs configuration

For one square metre of SC wall with a plate thickness of 8 mm, stud diameter of 22 mm, tie bar diameter of 20 mm, longitudinal and transverse stud spacing of 200 mm and tie bar spacing of 400 mm. Considering the tie bars as if they were studs, the total number of studs per square metre under these conditions is 25 per plate. Respectively, the tensile strength for the plates is 5680 kN, while the total shear strength of the studs is 5450 kN, which according to the proposed axial strength design, becomes the SC wall axial capacity. In this case, the studs are not subjected to a tensile force, which leads to no reductions in shear strength.

6.3 Bending and axial connection strength

In this section, the connection strengths for bending and axial loading are presented.

6.3.1 Bending connection capacity

In the section are presented:

- the analytical solution for the ultimate bending moment;
- the parametric estimation of the ultimate bending moment for the current parametric analysis;
- the reduction of the strength in the connection with respect to the SC wall;
- additional analysis of alternatives in estimating the number of studs.

Analytical ultimate bending moment

As done for the calculation of the bending capacity of the SC wall in section 6.2.1, the reinforced concrete (RC) assumption can be applied. In particular, the bending resistance of the connection is considered to be limited to the design of the midspan cross-section, where only the concrete and connection bars can be founded. Figure 112 presents the forces under failure conditions in the connection using the RC assumption.

- The failure occurs due to the connection bars reaching their ultimate capacity in tension;
- compressed connection bars are neglected;
- the position of the neutral axis is found as the equilibrium between the tensile components of steel and concrete in compression;
- the base refers to a width of 1 m.

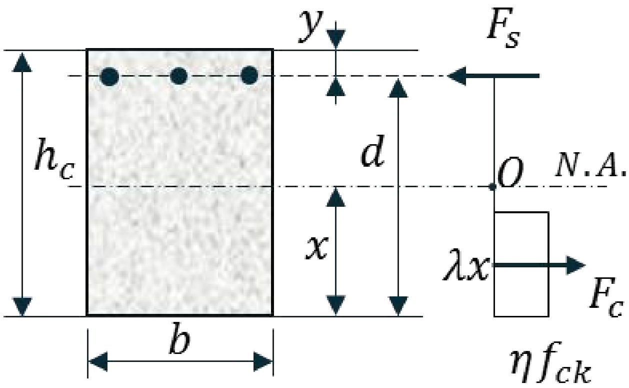

Figure 112 - Forces at the failure condition in the connection using the RC hypothesis

Where the different components according to EN 1992-1-1 [14] are:

- $F_s = A_{bar} f_{su,\mathrm{bar}}$
- $\begin{cases} \lambda = 0.8 & \eta = 1.0 & f_{ck} \le 50MPa \\ \lambda = 0.8 - \frac{(f_{ck}-50)}{400} & \eta = 1.0 - \frac{(f_{ck}-50)}{200} & 50 \le f_{ck} \le 60MPa \end{cases}$

From the equilibrium equations, the neutral axis and the characteristic ultimate resistance bending moment are:

$$x = \frac{A_s f_{su}}{\lambda f_{ck} b}$$

$$M_{Rk,conn} = A_s f_{su}\left(d - \frac{\lambda x}{2}\right)$$

Figure 113 presents the comparison between the analytical and numerical bending capacity of the connection for models M48 and M30. It shows a reduction of 47.9% for model M48 and 47% for model M30. The magnitude of the reduction in strength is comparable to the computed 63% reduction in studs' strength developed in section 6.1.1. It is therefore demonstrated that the studs are primarily responsible for the reduction in resistance in the connection compared to theoretical values.

A possible reason for the gap difference between the expected 63% of strength reduction and the obtained average of 48% is due to the fact that no consideration was given to the confinement of the concrete, which increases its strength and thus improves the performance of the connection with a lower strength reduction. However, an analytical assessment of the confining pressure is complicated to obtain.

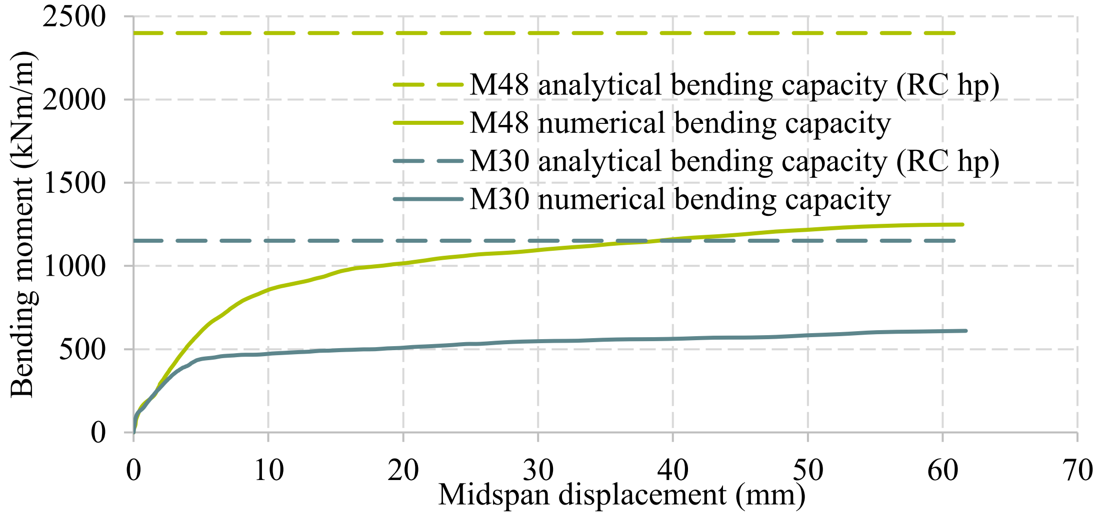

Figure 113 – Analytical and numerical bending capacity of the connection for the M48 and M30 models

Parametric estimation of the ultimate bending moment

The previous analytical expression with the RC hypothesis approach can provide the actual values of the parametric analysis of the ultimate bending capacity knowing the real state of stress at failure in the connection bars. However, this condition depends on many factors that make the problem unsolvable. For this reason, a parametric expression of the ultimate bending moment, as a function of concrete thickness and connection bar diameter, can be provided. The expression is obtained from the iterative linear regression of the available numerical results and is reported below:

$$M_{uk}(d_b, H) = \frac{42}{0.2022 - \sqrt{d_b(H + 0.0928)}}$$

The parametric formulation can be used under the following conditions:

- pure shear design for the studs' number estimation;
- connection bars with steel grade 8.8 only;
- range of validity:
  - Connection bars diameter: $10 \leq d_b(mm) \leq 50$
  - Concrete thickness: $200 \leq H(mm) \leq 600$

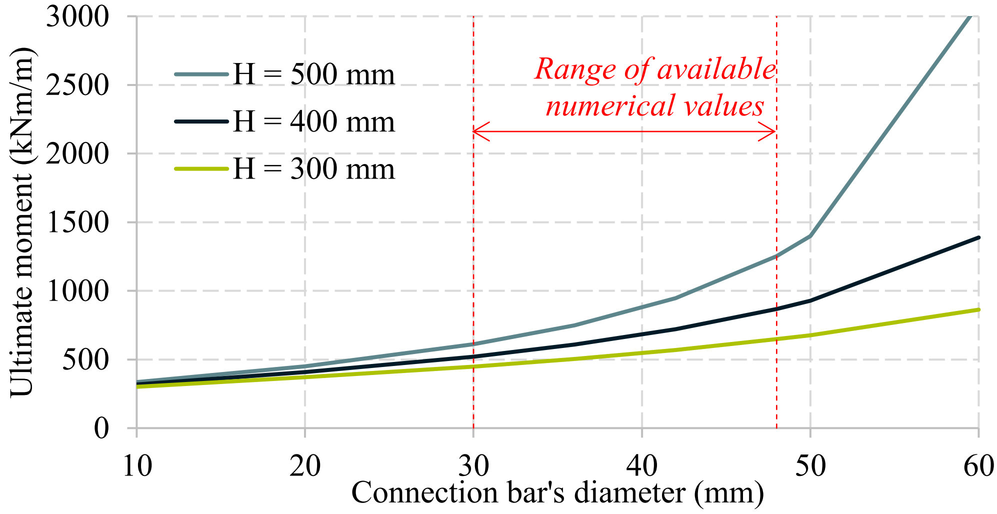

Figure 114 - Ultimate bending moment, obtained from the parametric formula, for different concrete thicknesses (H) at varying connection bar diameters (d_b)

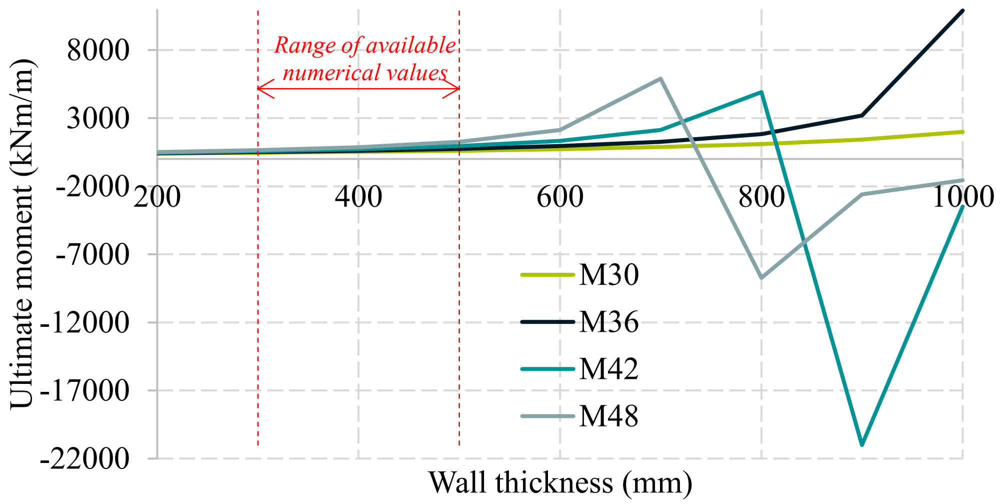

Figure 115 - Ultimate bending moment, obtained from the parametric formula, for different connection bar diameters (d_b) at varying concrete thicknesses (H)

The results of the numerical formulation match perfectly with the available numerical results, as shown in Figure 116.

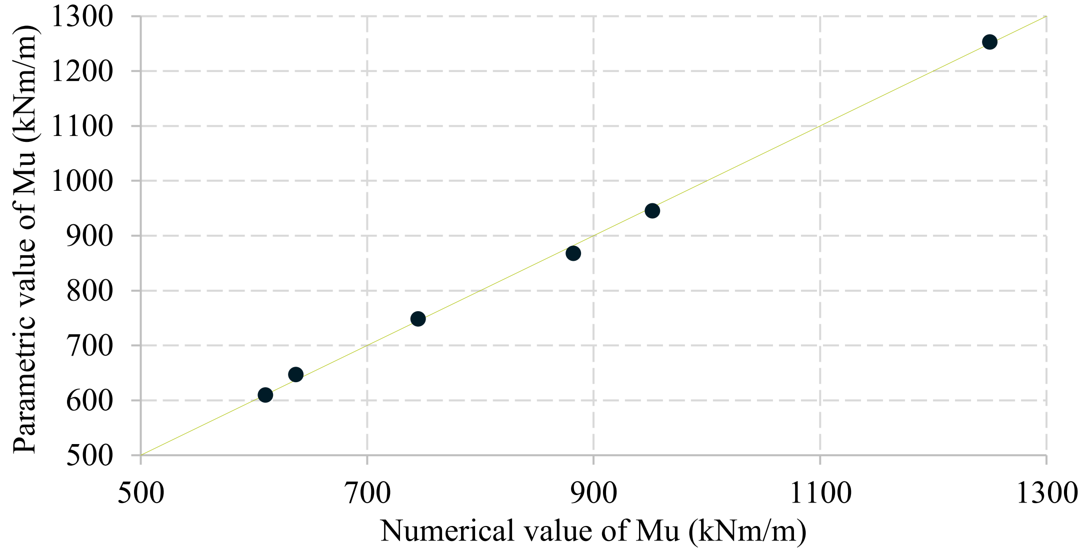

Figure 116 – Numerical and parametric values of the ultimate bending moment

Reduction of bending resistance in the connection

Figure 117 shows the comparison of the ultimate bending moment for the M48 and M30 models with respect to the SC wall model and all respective theoretical values obtained under the RC assumption.

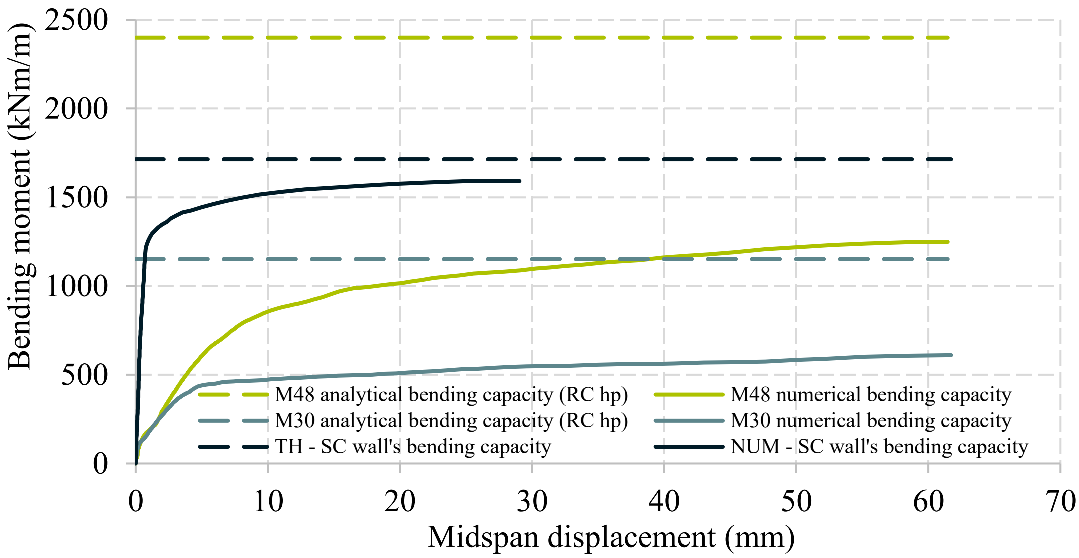

Figure 117 - Reduced bending capacity compared to the SC wall of the M48 and M30 models

As can be seen, numerical models M48 and M30 turned out to be weaker than the SC wall. Respectively, with a reduction compared to the SC wall of 21.4% for the M48 model and 61.7% for the M30 model. The theoretical reduction for the M30 model should have been 27.6%, so more than half of the real strength of the connection is lost. For the M48 model, on the other hand, the theoretical capacity of the connection is even higher than that of the SC wall. This is something physically impossible, even if the bars used can achieve higher results, and if a better stud design is used, then the failure moves from the studs to the plates, which is one of the failure conditions of the SC wall. Therefore, the ultimate capacity of the connection must always be limited to that of the SCS.

Additional bending analysis to improve the stud design

Two further model tests can be developed to improve the stud design and see if different conclusions can be drawn. The two cases refer to:

- Improving the studs' steel grade from S235 to S355;
- Improving the studs' number for stress transmission.

These two additional analyses are presented as follows.

- *Additional bending analysis performed with a higher stud steel grade from S235 to S355.*

  One attempt to improve the design of the studs is to improve the steel grade from S235 to S355. This should improve the tensile strength and consequently also the shear strength, with less reduction in shear capacity. Figure 118 presents the results of this analysis.

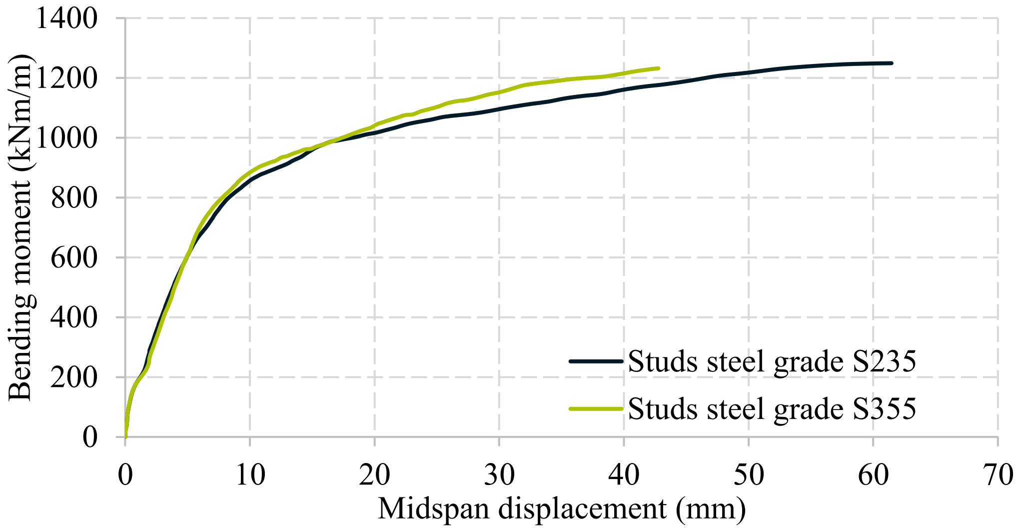

Figure 118 – Bending parametric results of variation in studs steel grade between S235 and S355 (S235 is the reference case value)

As can be seen from the results, nothing changed. This is because by increasing the strength of the studs, the tensile stress absorption also increases proportionally. In fact, the tensile stress increases from 70 kN in the reference case to 83 kN in the studs with improved capacity, leading to almost the same shear capacity of 43 kN per stud.

- *Additional bending analysis with a different studs' estimation number*

The second attempt to improve the design of the studs is to increase their number in the model. The criterion used to estimate the number of studs in the parametric case is to calculate both strengths, the tensile strength of the connection bars and the ultimate shear strength of the studs. By dividing the capacity of the bar by that of the shear stud, the number of studs can be estimated and, based on the spacing of the studs, the length of the connection bars can also be calculated, as explained in section 2.4.2.

The critical aspect of this approach is that studs prove to have a lower capacity due to non-negligible tension. As explained above, if more studs are in the model, the tensions are lower with less shear capacity reduction and better strength. Therefore, it is not easy to understand the number of studs used considering the tensile stress.

For this test, the number of studs is estimated with a maximum shear strength of 50 kN. The total shear strength is considered to be 25% higher than the actual strength shown by the studs in the reference model. In this way, to transmit the total strength of the bars 11 studs per bar are needed, against the 4 for the reference case. Figure 119 shows the results of the test.

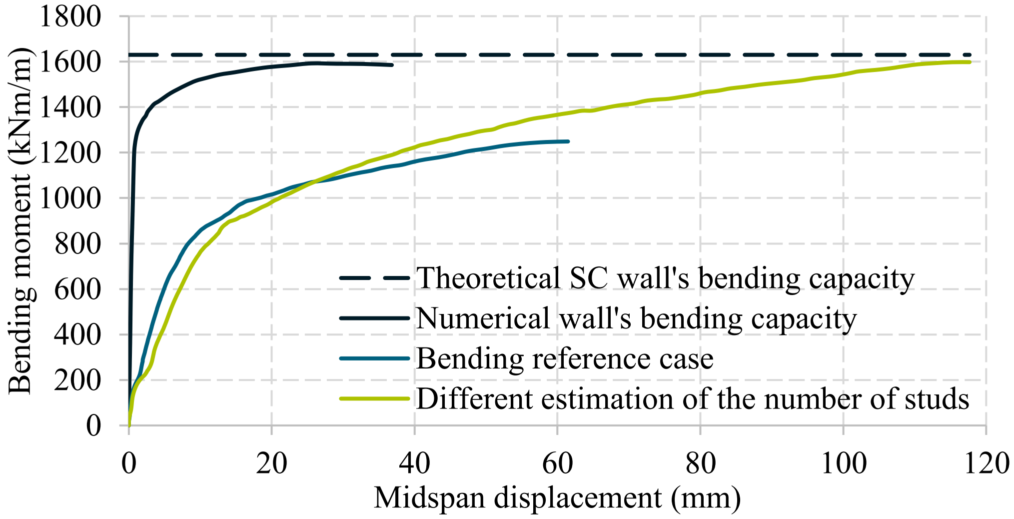

Figure 119 - Bending parametric results for a different estimation of the number of studs' model

As can be seen from the results, the model with a different estimate of the number of studs turned out to have the same strength as the SC wall. This confirms the conclusion made earlier that, although the connection bars can withstand higher stresses, the maximum capacity that can be achieved is equal to that of the SC wall.

In this new model, the tensile force in the studs is reduced to 65 kN instead of 70 kN and the shear force is 40 kN. The behaviour of the connection is completely changed, in fact, as expected, the studs turn out to be less stressed, without yielding. As in the reference case, the connection bars begin to reach ultimate stress locally, but with a high reserve of capacity.

Below is a series of graphical comparisons between the two models, the one with a higher number of studs and the reference case, respectively, at their failure. Figure 120 shows the comparison of concrete between the two models, Figure 121 the comparison of the faceplates and finally Figure 122 the comparison of connection bars and studs.

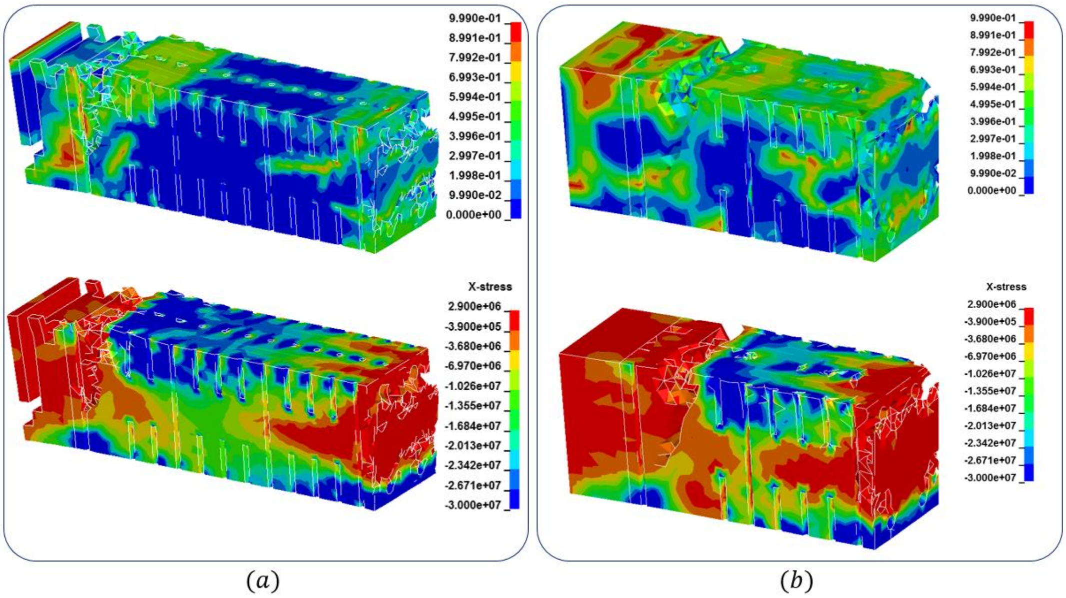

Figure 120 – Comparison of concrete damage variable and axial stress for (a) Large estimation of studs number model (b) Reference bending case (at their respective failures)

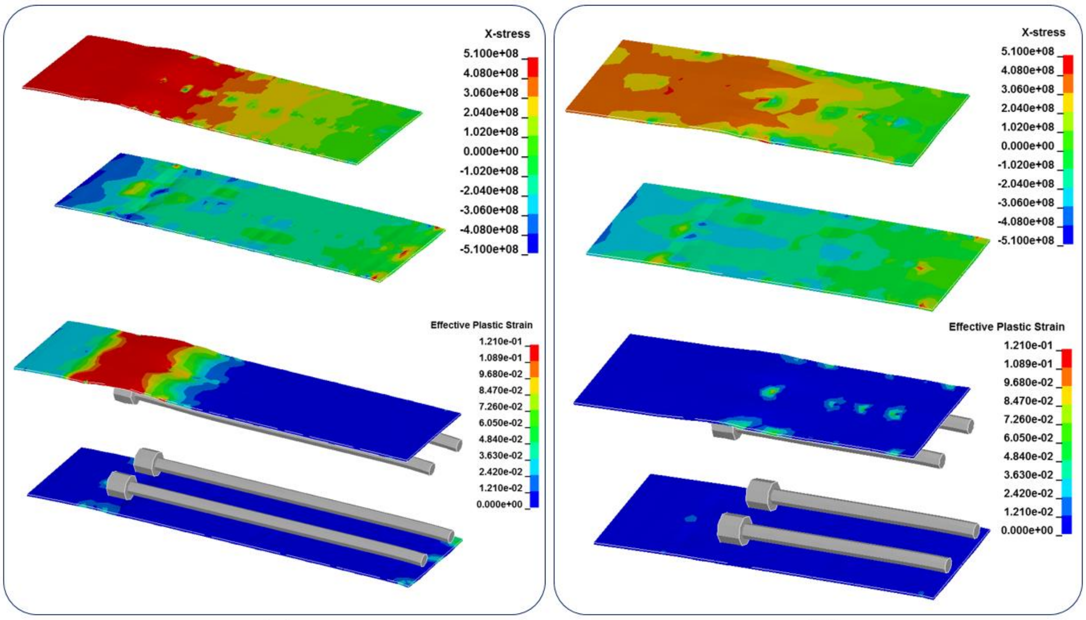

(a) (b)

Figure 121 - Comparison of axial stress and effective plastic strain of faceplates for (a) Large estimation of studs number model (b) Reference bending case (at their respective failures)

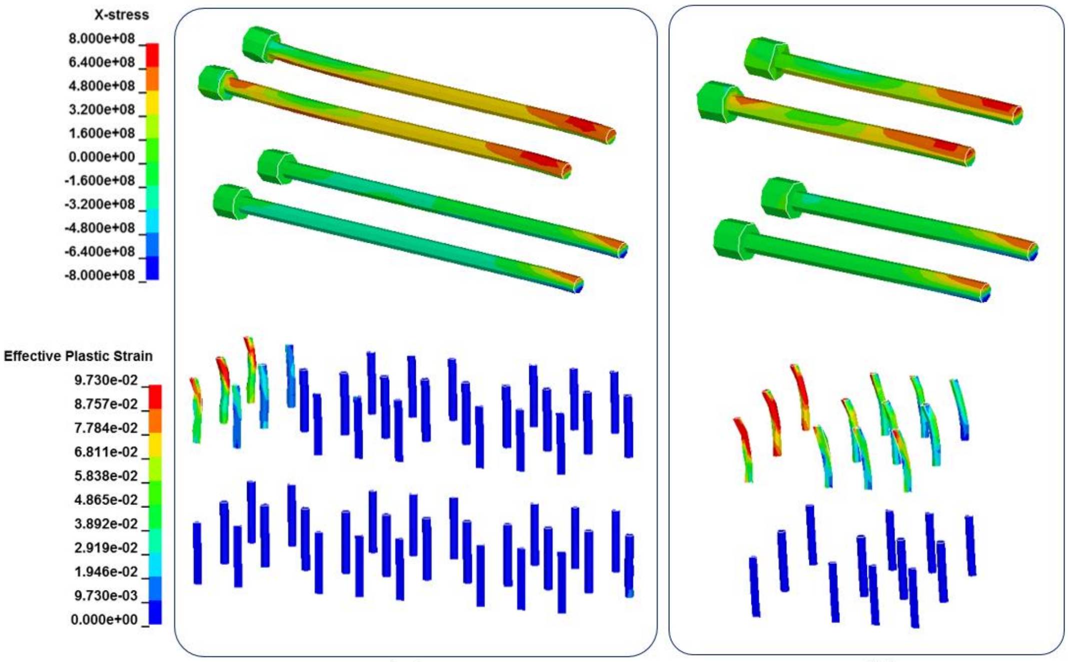

(a) (b)

Figure 122 - Comparison of connection bars' axial stress and studs' effective plastic strain for (a) Large estimation of studs number model (b) Reference bending case (at their respective failures)

6.3.2 Axial connection capacity

In this section are presented:

- The analytical solution for the axial capacity;
- The reduction of the strength in the connection with respect to the SC wall.

Analytical axial connection capacity

The analytical maximum axial capacity is given by reaching the ultimate tensile strength of the connection bars, with the hypothesis of neglecting concrete in tension.

$$N_{Rk,bar} = \sum_i A_{bar,i} f_{su,bar}$$

Figure 123 presents the comparison between the analytical and numerical axial capacity of the connection for models M48 and M30. It shows a reduction of 67.7% for model M48 and 61.9% for model M30. The magnitude of the reduction in strength is comparable to the computed 63% reduction in studs' strength developed in section 6.1.1. With regard to the bending comparison of section 6.3.1, between the analytical and numerical models, values closer to the expected reduction in strength due to the reduced performance of the studs are noted for the axial analysis. The explanation is based on the confinement effect due to the faceplates, which improves the capacity of the concrete and, consequently, the global connection capacity. This explanation can be confirmed with the axial results since for axial loading the confinement is less important because it is not triggered as for bending deformation leading to a closer strength reduction comparison.

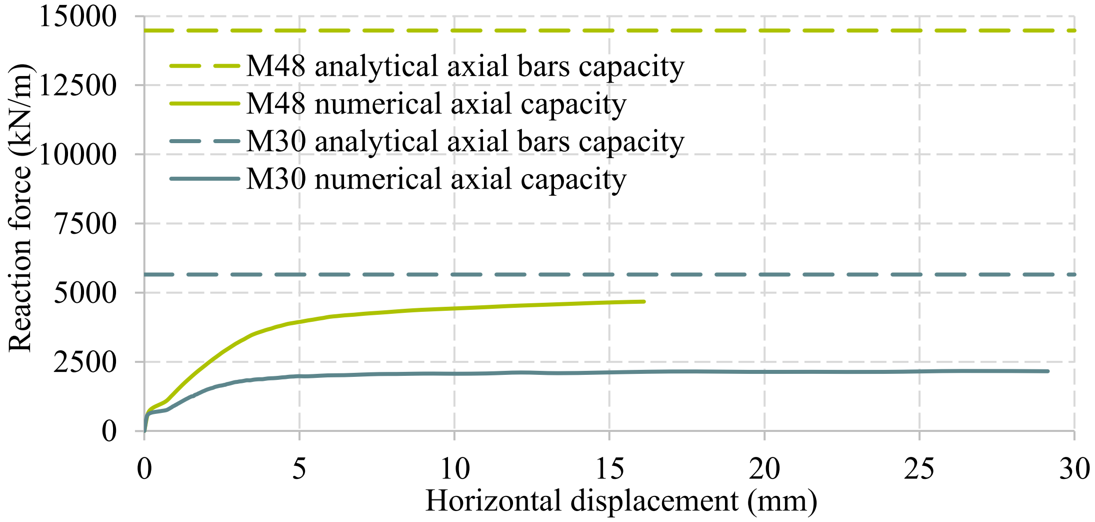

Figure 123 - Analytical and numerical axial capacity of the connection for the M48 and M30 models

Reduction of axial resistance in the connection

Figure 124 shows the comparison of the ultimate axial capacity for the M48 and M30 models with respect to the SC wall model and all respective theoretical values obtained under the RC assumption.

As can be seen, numerical models M48 and M30 turned out to be weaker than the SC wall. Respectively, with a reduction compared to the SC wall of 14.2% for the M48 model and 60.4% for the M30 model. The theoretical capacity for the M30 model should have been almost the same as the SC wall. For the M48 model, on the other hand, the theoretical capacity of the connection is even higher than that of the SC wall. Once again, as in the bending comparison of section 6.3.1, this is something physically impossible, even if the bars used can achieve higher results. Therefore, the ultimate capacity of the connection must always be limited to that of the SCS.

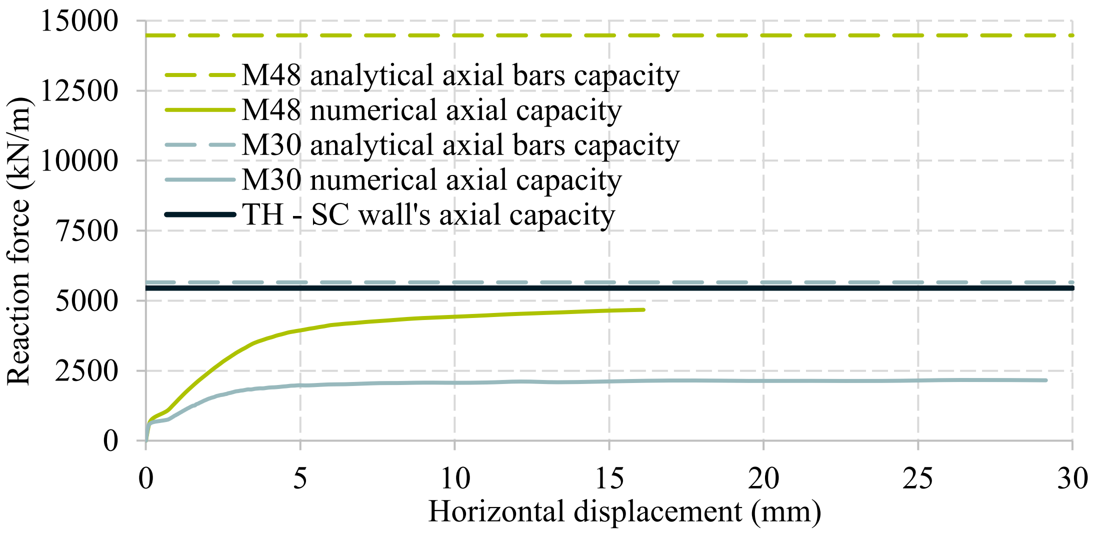

Figure 124 - Reduced axial capacity compared to the SC wall of the M48 and M30 models

6.3.3 Parametric analysis for studs' strength estimation

Studs have proven to be the weakest element that generates connection failure, due to a poor design in the parametric analysis. Since an analytical estimation of the shear capacity is complicated due to the indeterminacy in the estimation of the tension, responsible for the reduction in stud performance, this section presents a parametric stud analysis to isolate the behaviour of the stud for a better understanding, and alternative design for the studs.

Parametric stud analysis

The parametric stud analysis consists of isolating part of the axial parametric model only in the top plate, tie bars and studs included in three longitudinal (s_{sx}) and two transverse (s_{sy}) spacing, as can be seen in Figure 125 and run the combinations related to the studs' parameters. All assumptions regarding boundary conditions, load application, mesh, material properties and contact conditions are the same as the ones present in Chapter 3. The main differences are:

- The addition of the horizontal constraint in the concrete in the x-direction creates a symmetry condition and avoids horizontal movements, in order to concentrate them only on the studs.
- Free edge in the concrete on the side opposite the horizontally constrained side, since the locking of this side for the current analysis was considered superfluous.
- The tie bars in the model, which are required to create the confinement effect of the faceplate, have for simplicity the same steel grade as the studs, corresponding to S235 and not the same faceplate steel grade as for the global parametric model.

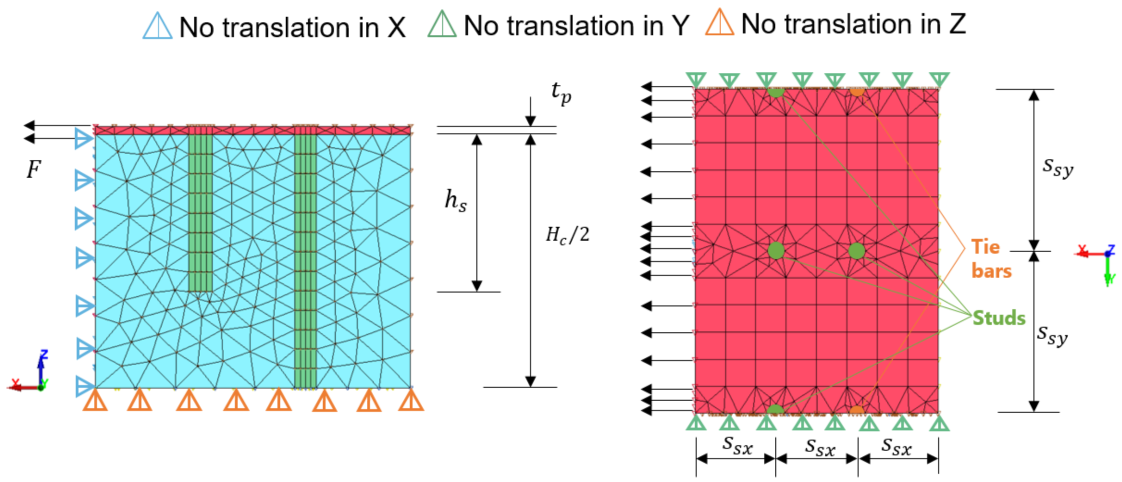

Figure 125 – Stud parametric model

Table 27 shows the parametric combinations performed on this small model. A total of 12 combinations are tested and consist of varying the longitudinal and transverse distance with respect to the recognized reference case in combination number one, marked in bold, and finally varying the diameter and height of the studs.

Table 27 – Combinations for the stud parametric model

Comb N.	s_{sx} (mm)	s_{sy} (mm)	d_s (mm)	h_s (mm)
1	**100**	**200**	**22**	**150**
2	75	200	22	150
3	125	200	22	150
4	150	200	22	150
5	100	125	22	150
6	100	133	22	150
7	100	166	22	150
8	100	250	22	150
9	100	200	19	150
10	100	200	25	150
11	100	200	22	100
12	100	200	22	200

Stud design according to beam theory

An alternative way of designing the studs could be to use beam theory and represent the stud as a double clamp beam subject to a displacement on one side only, as shown in Figure 126. In fact, the displacement generates a bending moment and reaction forces at the nodes.

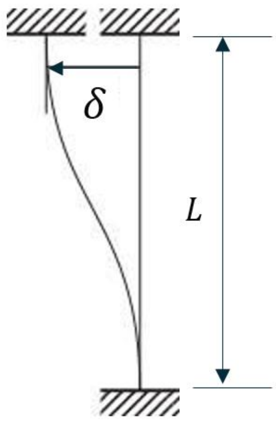

Figure 126 - Stud design according to beam theory

For each combination of Table 27, it is possible to record the value of the displacement at which the system fails in the studs. This displacement can be divided between all elements, tie bars and studs, according to their respective stiffnesses. Below is the formulation of the generic stiffness of this beam system (k), which is a function of the material stiffness, diameter and length of the beam.

$$k = 12\frac{EI}{L^3} = \frac{3}{16}\frac{E}{L^3}\pi D^4$$

Since the tie bars and studs have different lengths and diameters, two different stiffnesses can be written and the reaction force, which represents the bending shear capacity of the tie bars and studs, are respectively:

$$R_{stud} = 12\frac{(EI)_{stud}}{L_{stud}^2}\delta$$

$$R_{tie} = 12\frac{(EI)_{tie}}{L_{tie}^2}\delta$$

These equations are a function of the young modulus and are valid as long as it is constant, however, the displacement observed at the failure is in the plastic field so they change between elastic and plastic values.

It can be simplified by writing the reaction forces as a function of the applied force that generates the displacement. For this purpose, the horizontal equilibrium equations can be written as follows:

$$F = (n_s k_s + n_t k_t)\delta = 12E\left(n_s\frac{I_s}{L_s^2} + n_t\frac{I_t}{L_t^2}\right)\delta$$

Where n_s and n_t are the number of studs and tie bars in the model, respectively. In this equilibrium equation, displacement can be replaced by reversing the previously shown formulae for the reaction forces of studs and tie bars, as follows:

$$\delta = \frac{R_{stud}L_s^2}{12EI_s}$$

$$\delta = \frac{R_{tie}L_t^2}{12EI_t}$$

By substituting the displacement function of the studs or the tie bars parameters, the respective reaction force can be found as a function of applied force and inertia only. This formulation neglects the variation of the young modulus, which can be simplified.

$$R_{stud} = \frac{F}{n_s + n_t\frac{I_t}{I_s}\left(\frac{L_s}{L_t}\right)^2}$$

$$R_{tie} = \frac{F}{n_s\frac{I_s}{I_t}\left(\frac{L_t}{L_s}\right)^2 + n_t}$$

In other words, these formulations use a homogenization coefficient that transforms tie bars as if they were studs when calculating the reaction force of the studs and vice versa for that of the tie bars.

Shear design, beam design and parametric results

In this section, the results of shear design, beam design and parametric results can be compared. The results are shown according to the following subdivisions:

- Combinations 1 to 8 of Table 27 are shown as stud density per square metre, as the spacing is responsible for the variation in stud density (Figure 127);
- Combinations 9 to 12 of Table 27, representing the variation in stud diameter and height, can be shown as the variation of a single parameter such as the stiffness of a double-clamped beam (Figure 128).

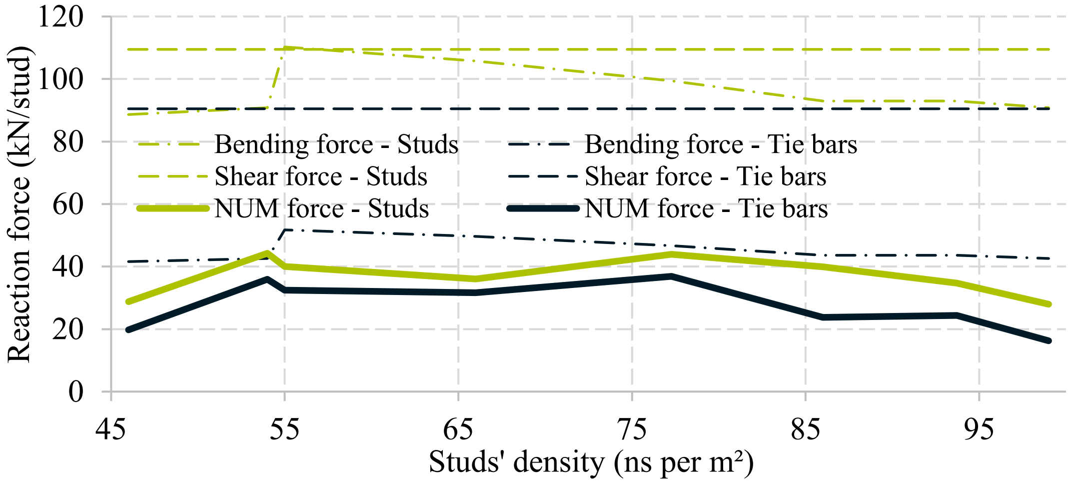

Figure 127 - Shear design, beam design and parametric results comparison by varying stud density

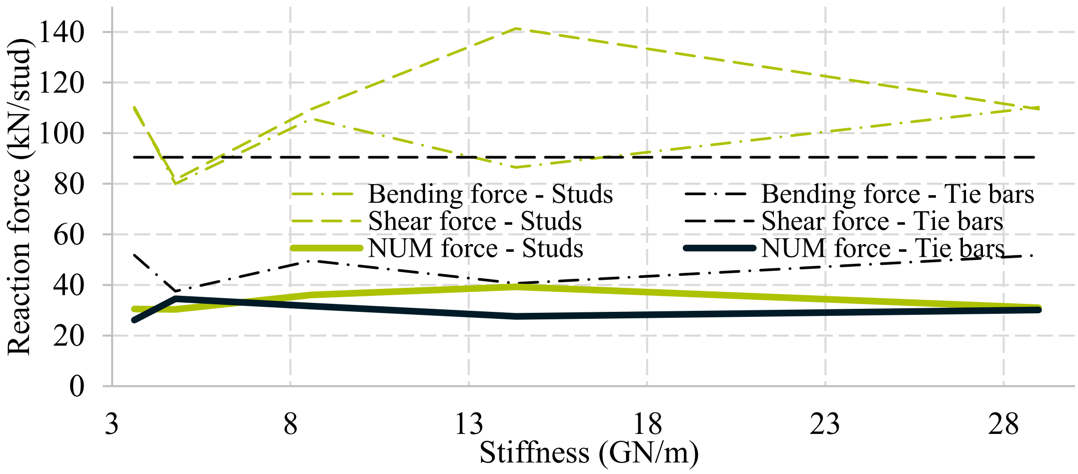

Figure 128 - Shear design, beam design and parametric results comparison by varying the stiffness

As can be seen, for studs, the shear design represents the maximum strength estimate, while the beam design reduces the capacity with respect to shear, with a maximum of 17.4% for the density variation of studs and 38.7% for the stiffness variation. However, this is not a reduction comparable to the numerical values, where the maximum reduction is 74.7% for the density variation and 72.1% for the stiffness variation.

A further observation may be that the average strength in all the different parametric values is 35.6 kN, with maximum and minimum values of 44.2 and 28.0 kN with variations from the mean values of around 20%, considerably negligible. The conclusion is to use a diameter of 19 mm, which meets the design criteria, and considers an average shear strength of 35.6 kN.

As far as the tie bars are concerned, the results of the beam design are close to the parametric ones and then to the parametrical values of the studs. The conclusion of these results leads to the conclusion that tie bars can be considered studs for stress transmission.

Chapter 7

Future projects

Future projects concerning the connection between SC walls by means of embedded connection bars are mainly three:

- Further parametric analyses based on the conclusions of this thesis project led to the definition of a new design criterion for the connection for wall-to-wall connection (section 7.1);
- Further parametric analysis of SCS module connections in other configurations, as planned in the PTAN project [16] (section 7.2).
- Further experimental tests for a better calibration of the numerical model and to improve the external validity of the analysis (section 7.3).

7.1 Proposed SC wall connection design criterion for further parametric analysis

Taking into account all the observations resulting from this analysis, this section describes a proposal for the design criterion of SC wall-to-wall connection with embedded connection bars to be used in a further parametric analysis to be performed by EGIS.

- The ultimate bending capacity of the connection is defined as minimal as that of the SC wall and can be calculated on the base of the faceplate strength and concrete thicknesses, as stated in section 6.2.1.
- No longer evaluate diameter and height as a parameter for studs, but rather consider a stud with the following fixed characteristics:
    - 19 mm in diameter, to meet the design criteria given by the ratio of longitudinal spacing to diameter;

  - 150 mm in height, to use the optimum height value;
  - S235 as steel grade, as a better steel grade does not improve the capacity of the studs;
  - 35.6 kN as the average shear strength of the stud.

- The number of studs to be used is related to the ultimate tensile force that the faceplates can withstand, in order to reach the ultimate capacity of the connection, defined as the capacity of the SC wall.
- Tie bars can be considered studs in the counting of the number of studs, as they have comparable strength.
- Based on the number of studs and spacing, the length of the connection bar can be estimated.
- Based on the connection bar spacing, which defines the number of bars in the connection, the bar diameter can be defined between the standard values of M30, M36, M42 and M48 and the steel grades 8.8 and 10.9 as the value that balances the capacity of the faceplate.

  For instance, for a faceplate of 8 mm thickness and S355 steel grade, with a bar spacing of 200 mm, defining 5 connection bars per metre of connection, the minimum values can be M48 with steel grade 8.8, with a bars' capacity of 5292 kN, or M42 with 10.9 steel, with a bars' capacity of 5040 kN. Where the bar capacity can be calculated as described in section 2.4.2 as the product of the net cross-section area times the ultimate strength.
- In order to reduce the number of studs, ripped bars can be considered. A perfect slip between bars and concrete is considered, improving the bars and thus the transmission of stresses is no longer covered by the studs alone but can be a collaboration between studs and bars with a reduction in the number of studs or at least to be used as structural redundancy in the event of failure of the studs.

7.2 Further parametric analysis of SCS module connections in other configurations

The chapter on the connection between SCS modules in the PTAN document considers different connection configurations as follows [16]:

- SC wall-to-wall connection;

- SC wall-to-slab connection;
- Angle SC wall-to-wall connection.

The first point concerns the topic of the thesis, while the other points are planned in the development of the chapter on the design of SC modules in the PTAN document assigned to EGIS.

7.3 Further experimental tests for SC wall connection

Further tests, in bending and axial, on the SC connections are planned in the SCHEDULE (Steel Concrete High-Efficiency Demonstration eUropean colLaborative Experience) project, which consists of the calculation, entrusted to EGIS, and construction, by EDF, of a DUS (Diesel for Ultimate Safeguard) as a Pilot Building in SCS using embedded connection bars and welding SC connections [8].

The building contains two sets of diesel generators, two fuel tanks, and electrical, ventilation and extraction rooms. In the event of the failure of all other power sources, the two generators supply electricity for up to 72 hours to the buildings containing the equipment needed to remove the heat produced by the nuclear fuel contained in the spent fuel pool.

A total of 56 DUS have been constructed in reinforced concrete at EDF nuclear sites. Therefore, EDF has a rich database on the time and cost of constructing these concrete buildings, and this provides a good basis for comparison with SC construction in order to understand the real convenience of using SC as a replacement for RC [8].
The pilot building is designed and constructed at full scale to provide a realistic basis for comparison with the completed RC buildings. The DUS consists of a rectangular floor plan measuring 24.1x12 m and 14.94 m in height divided into three levels and six rows of SCS modules, as can be seen in Figure 129.

The wall thicknesses generally vary between 300 and 500 mm, with 8 mm plate thickness, with the exception of the Air Plane Crash (APC) barrier in one of the corners, where the thickness reaches 1.30 m, the inner plate is increased up to 12 mm and the outer plate up to 20 mm.

Figure 129 – DUS of the SCHEDULE project completed

To connect the SCS modules, embedded connection bars are used in the first two floors, since tightness is not required, corresponding to the first four rows of SCS modules (see Figure 129). The last two rows, corresponding to the last floor, are realized with welded connections to compare the execution time and strength with respect to the connection performed with embedded connection bars, in order to understand the real convenience of using this connection technique [8]. However, in one of the corners of the top floor, is located the pool with a tightness requirement in which only a welded connection can be performed and the faceplates used are stainless.

For the embedded connections, concerning the bars' diameters, these vary from 27 to 30 mm depending on the required strength of the modules to be connected, with 8.8 or 10.9 as steel grade. The tie bars are both welded and bolted and the welded tie bars have steel grade S355, while the bolted ones have steel grade 8.8. Studs of 19 mm diameter and 150 mm height are used with S235J2+C450 as the steel grade. The faceplates are generally S355 as steel grade, and the concrete is of type C30/37.

Chapter 8

Conclusion

Two parametric analyses with bending and axial loading are carried out to understand the behaviour of the SC wall-to-wall connection with embedded connection bars for a wide range of cases. The analyses consist of 29 and 26 combinations respectively for the application of bending and axial load, for a total of 55 combinations. Each combination in each analysis is defined as a variation of one parameter at a time from the reference case defined by EDF in the PTAN document [16].

The numerical assumptions and simplifications for the development of the parametric models are based on the calibration of the experimental results of the Spacemen E in the four-point beam bending test from WP5 of the SCIENCE project [7].
A first numerical model is developed to reproduce the Spacemen E four-point beam bending test and make numerical choices and assumptions to converge with the experimental results. The model consists of a strip, defined by one longitudinal spacing of the tie bars, and one-half of the beam, for the midspan symmetry conditions of the test. This large model is then simplified by obtaining a second numerical model, which is the parametric bending model, reducing the Spacemen E model to just the connection zone and using a stiffener for load transmission. In this way, a numerical model made up of only parametric values is defined and isolated from the influences of other non-linear effects from the rest of the beam, resulting in a reduction in the size of the model and thus in calculation time. The simplified parametric model is also validated against the experimental results by reproducing the parametric test values.
A further simplification of the parametric bending model is carried out in order to develop the axial parametric numerical model. The main differences lie in the application of the load, which no longer uses the stiffener but consists of the application of tensile stresses in the faceplates, and in the symmetry of the thickness of the beam, which leads to a subsequent reduction in model size and, once again, calculation time.

The numerical parametric models meshes are done with Ansys software [10] and an explicit pseudo-static nonlinear analysis is developed per each combination with LS-DYNA FE software [11].
The material model used for steel is MAT_PLASTIC_KINEMATIC, to develop elastic-plastic behaviour with linear kinematic hardening.
The material model used for concrete is CSCM (Concrete Smooth surface Cap Model) for a better estimation of the non-linear post-elastic phase and damage phenomena. An advantage of this model is the possibility of estimating the increase in strength due to concrete confinement, as the faceplates reproduce this effect.
Finally, an elastic stiffener 100 times stiffer than steel is used to apply the load in the bending analysis, whereas in the axial analysis, since the load consists of stresses applied to the plates without the presence of localised deformations, its use is considered superfluous.
Real unilateral contacts are introduced between the steel elements and the concrete in the connection zone to provide a more realistic contact and a better estimate of the friction between these elements. The merged condition is defined at the head of the studs to simulate the anchorage effect in the concrete.
The modelling approach with the LS-DYNA FE software, compared with the experimental results of the SCIENCE project, shows good general agreement and thus by extension similar behaviour to the physical one.

Both analyses lead to the same conclusions. The weakest element of the connection is the studs, which show a reduction in shear strength of 63% due to non-negligible tensile stress, which causes the connection to fail. The connection shows comparable reductions in strength compared to the SC wall, demonstrating that the cause of the reduction in strength is in the studs. Alternatives to the design of the studs are presented, such as the design of the stud as a double-clamped beam, or the parametric analysis of a reduced model to isolate the behaviour of the studs to define parametric values for the design. The further conclusion from the parametric evaluation of the studs leads to a constant value of the stud capacity averaging 35.6 kN with a 20% margin. The proposed new design criterion states that the evaluation of the number of studs to be used depends on the strength of the maximum capacity condition of the connection, as well as on the design of the connection bars' diameter and the steel grade. Geometrical criteria are no longer to be used when selecting connection bars and, consequently, the number of studs. According to the proposed criterion, the estimation is to be carried out using the average value of reduced shear resistance in the studs, and the optimum values of diameter and height, which were found to be 19 and 150 mm respectively. The connection bars then become a function of the resistance of the faceplate strength, in order to avoid using bars with excessively high resistance margins and then an excessive number of studs. A further conclusion that can be made for studs concerns the density. In fact, it can be seen that an increase in the spacing leads to a reduction in the stud density, which in turn leads to a concentration of stresses in the few available studs, resulting in a reduction in ultimate strength. The design suggestion is to use as high stud density as possible.

The conclusions of the bending analysis are that the ultimate bending moment depends on the area of the connection bars and the lever arm, as expected, defining a ductility optimum at M42 as the diameter of the bars. The bending stiffness depends mainly on the thickness of the concrete since it is the object with the greatest inertia. The plates do not influence the overall behaviour of the connection with their parameters, thickness and steel grade, because they are not the weak point of the connection that generates the failure.

The conclusions of the axial analysis are similar to those of the bending analysis, especially with regard to the overall plate behaviour. Small differences can be seen in the definition of the ultimate tensile force with respect to the ultimate bending moment, which depends only on the connection bars’ cross-section, which is also solely responsible for the variation in axial stiffness, since the concrete cross-section, once in tension, does not contribute to the tensile strength. Recommended concrete thickness values are greater than 400 mm, which is the minimum that guarantees stress transmission to the connection bars.

The main conclusion is that ripped bars can be taken into account to reduce the number of studs. A perfect slip between the bars and the concrete is considered for these analyses. It is important to improve the design of the bars so that the transmission of stresses is no longer covered by the studs alone, but can instead be a collaboration between bars and studs with a reduction in the number of studs and, consequently, the length of the bars.

Appendix 1

Cyclic load application on the reference case

Only for the reference case, a quasistatic cyclic load application is developed, for a better understanding of the connection behaviour. To do that, another support condition is needed to create symmetry in the *plane-yz* and to have the same effect in the positive and negative bending as shown in Figure 130.

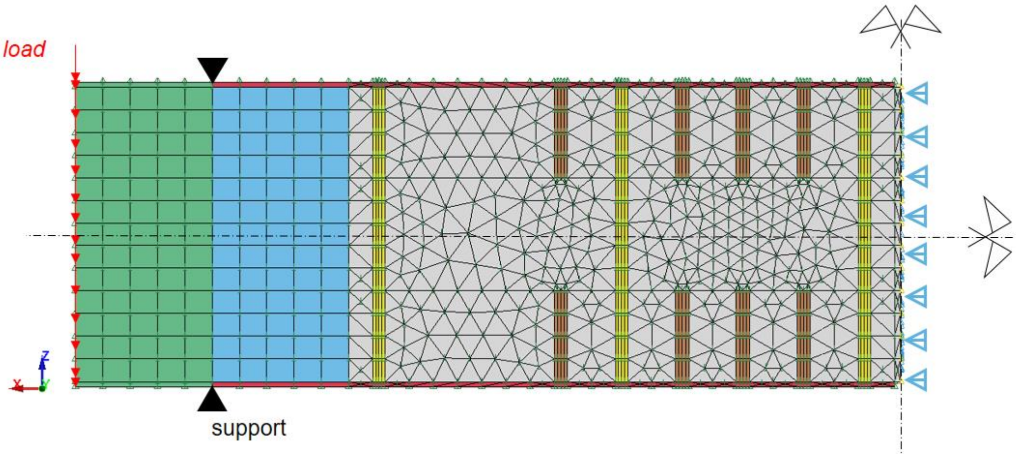

Figure 130 - Double support for plane-yz symmetry

The cycle test consists of three cycles, and each of them reaches the same maximum positive and negative application of the force. Between the three cycles, the maximums (F_1, F_2, F_3) are increasing equally and it corresponds to an increase of one-third of the yielding force measured in the reference case during the monotonic load applications. The last branch of the cyclic test corresponds to the monotonic application of the force up to the maximum force (F_{max}) corresponding to the failure registered for the monotonic test for the reference case. The goal of this test is to understand if under cyclic load there are differences with respect to the monotonic one and if there is a reduction of the capacity.

Figure 131 shows the load application in time for a full load application time of 1.17s, while Figure 132 shows the results of the cyclic load application with respect to the monotonic load application.

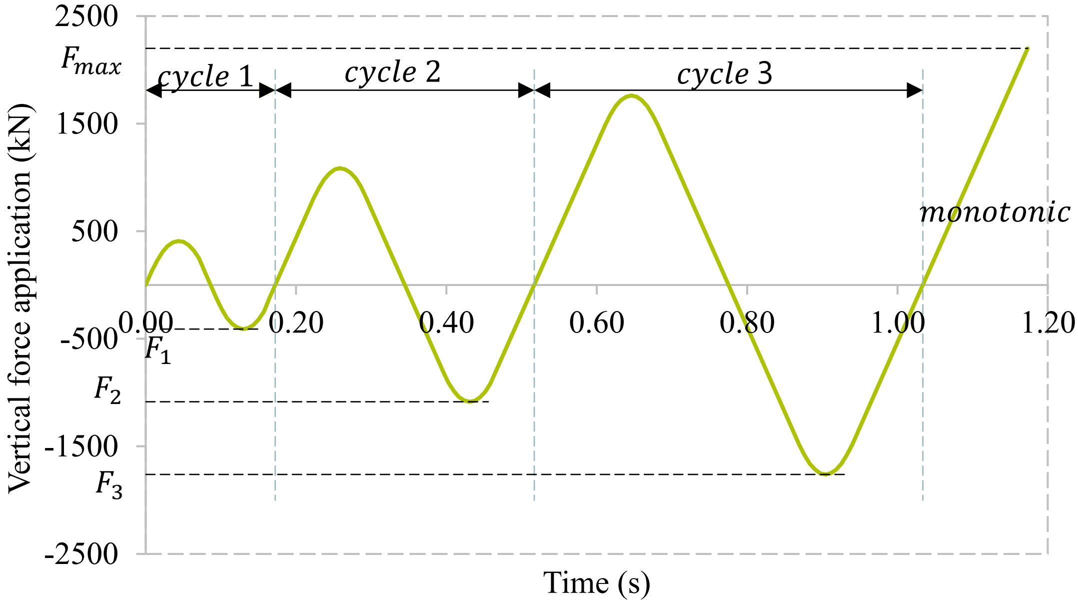

Figure 131 - Quasistatic cyclic load application in time

The conclusion of the cyclic test, as the results in Figure 132 show, is that the application of the cyclic load is contained in the monotonic load curves, positive and negative. The latter, given the symmetry of the cross-section, could be mirrored for a negative moment. The use of the monotonic load is considered sufficient to understand the behaviour of the connection such as stiffnesses and ultimate capacity.

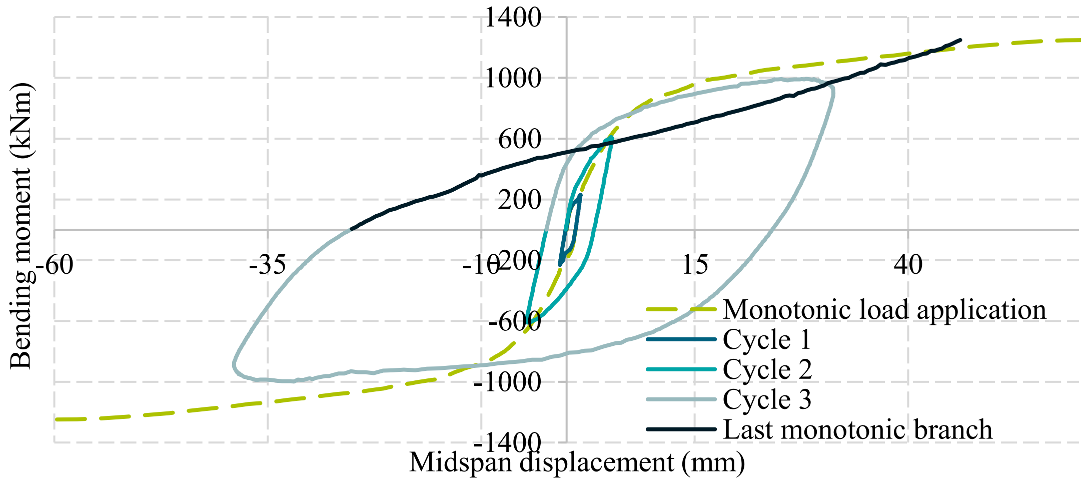

Figure 132 - Cycle load application results

However, a consideration concerns the use of ERODE settings for concrete must be done. In fact, during the monotonic test, concrete elements that reach more than 5% deformation are removed from the model. These elements are mainly located in the tensioned part of the beam and do not add any additional strength, so it is more a matter of visualising cracks and does not affect the final result. In contrast, in the cyclic test, the compression and tension parts change during the test and the elements that were in tension are in turn subjected to compression. If an element has been eroded in tension, it disappears and cannot recover its strength during compression. Therefore, for the cyclic application of the load, the ERODE was deactivated as it influences the results, not in the first two cycles where there are not so many eroded elements, but from the third and so on, as Figure 133 shows

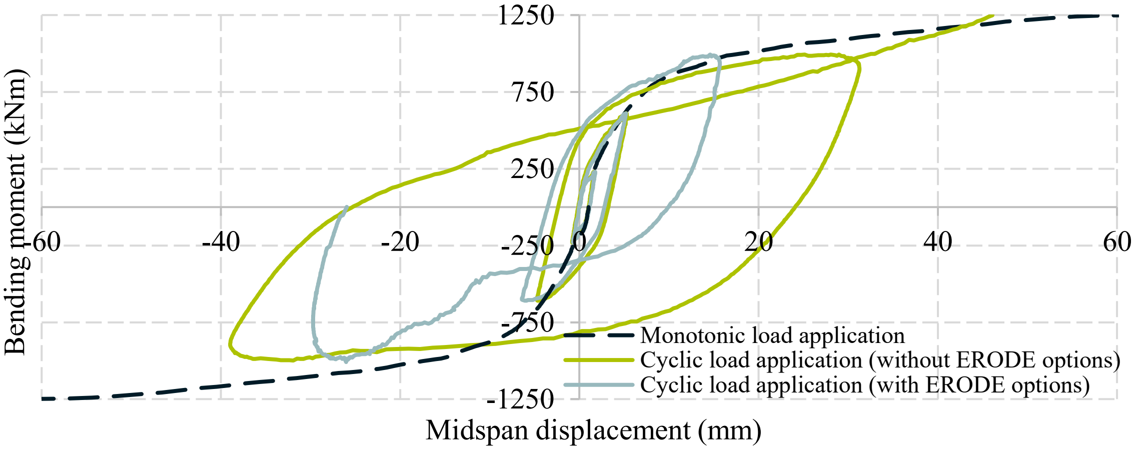

Figure 133 – Effect of using ERODE options in concrete

Figure 134 shows the damage variable for concrete as the model evolves at the maximum and minimum of each cycle. At the minimum, it is easier to see symmetry in the damage pattern with respect to the top and bottom of the section; while at the maximum, it can be seen that there is additional damage at the top of the cross-section compared to the bottom, this is because it is at the beginning of a new cycle.

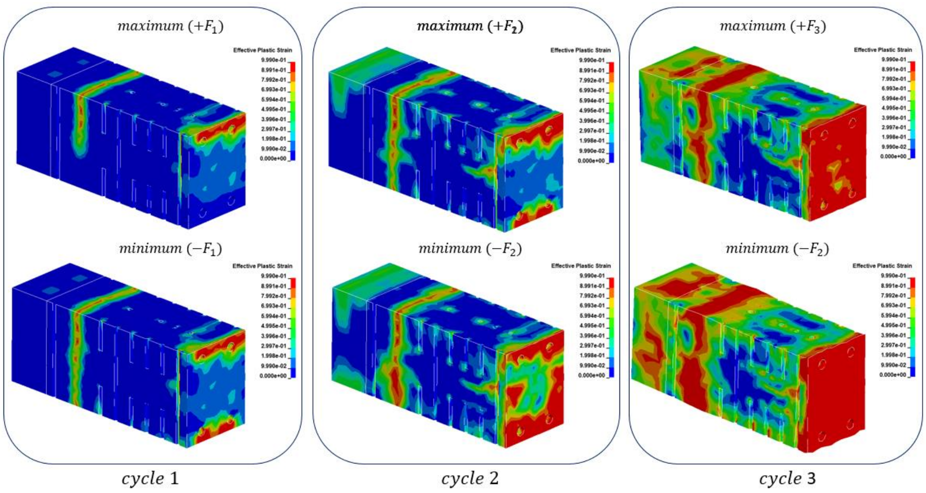

Figure 134 - Damage variable for concrete

Appendix 2

Double elements in the faceplate mesh

This analysis consists of running the parametric model with the experimental values presented in 0with a different quantity of elements in the plate thickness. In particular, the part of the plate in which a single hexahedral element is defined in the thickness of the place (described in detail in 3.1.1) is replaced with two elements, and consequently, a greater quantity of elements will also be present in the remaining part of the plate in which there are tetrahedral elements since it must adapt to the former.

Figure 135 shows the bending moment versus midspan displacement comparison between the two cases with a single or double element in the plate thickness. As can be seen, the two models correspond completely. Some differences can be seen at the beginning of the plastic phase, but then the results converge again. The double-element model in the faceplate mesh was interrupted before the end of the calculation to observe only the trend and see if there were any differences with the single-element model.

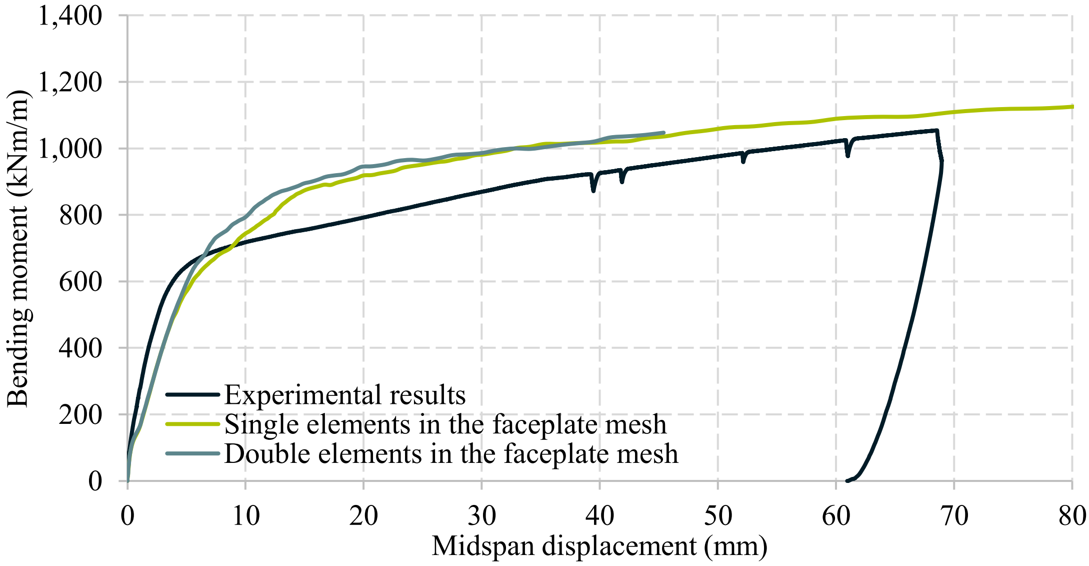

Figure 135 – Different mesh elements in the faceplate thickness

Figure 136 shows an image comparison between the two models with single and double elements in the face thickness at 45 mm midspan displacement. The comparison concerns the plastic deformation of the upper faceplate and the damage variable of the concrete. As far as the concrete is concerned, both cases appear to have the same deformation pattern. A slightly higher strain concentration, approximately 14% more, can be seen in the tetrahedral mesh part of the plate for the double-element model.

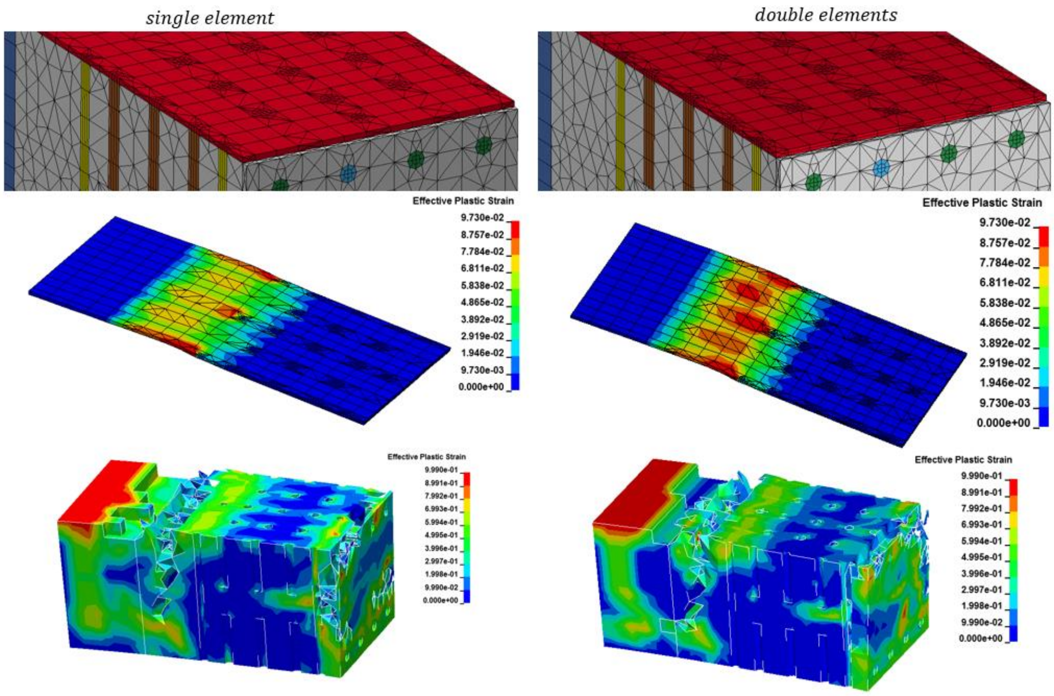

Figure 136 – Single and double elements in the faceplate thickness model comparison

The conclusion leads to the assumption that a single element in the thickness is sufficient for a good representation of the connection. In fact, the model with a larger number of elements in the plate thickness requires 40% more calculation time than the single-element case.

Appendix 3

Activation of the steel-erode option for the bending reference case

Figure 137 shows the reference case with the erode steel option activated. The value of stain erosion depends on the ultimate stress of the respective element. It can be calculated according to the double linear-kinematic with hardening law as the strain at the ultimate stress.

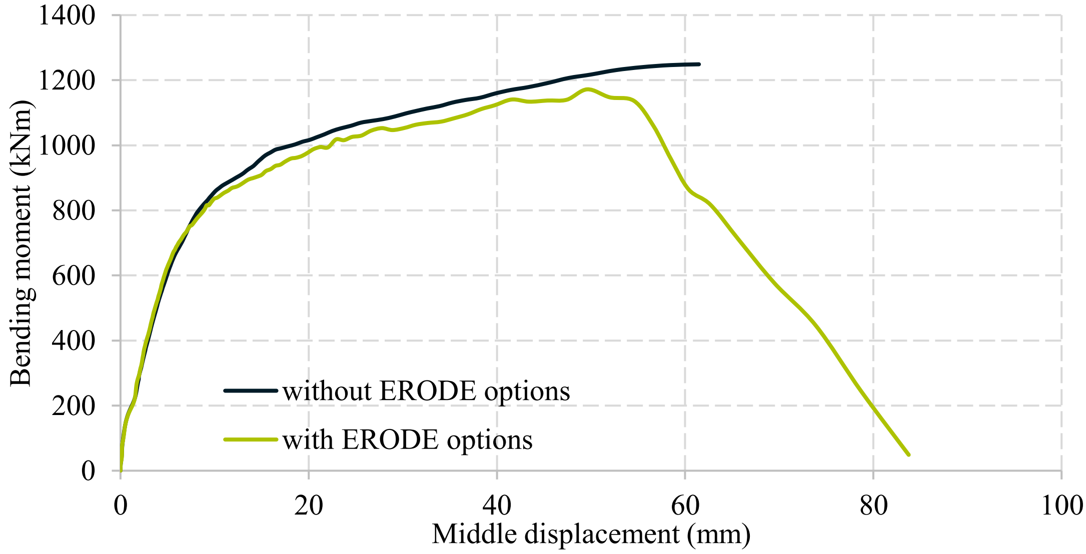

Figure 137 – Reference case using the erode steel option

As can be seen from the test, the failure defined for models without the erode option when the ultimate values are reached in the studs proves to be the overall failure of the model.

Appendix 4

Experimental results on Specimen E materials

The following values in Figure 138 refer to the experimental results of the material used in the Specimen E test [17].

Karlsruhe Institute of Technology (KIT) Materials Testing and Research Institute MPA Karlsruhe	Annex C Page 1 of 20 Pages Test Report No. 14 60 51 0538 from September 16, 2016

SCIENCE WP5: Test 3 – Specimen type E – ambient temperature

C.1

Identification of the test specimen

type of specimen	Specimen type E 8 mm
number of specimen	14-0538/SE

C.2

Material strengths

liner plate, S235JR+N, t = 8 mm	f_y	299 N/mm²	
actual liner plate thickness t = 8,28 mm	f_u	423 N/mm²	
	A_t	31,6 %	
tie bars Ø 20 mm, S355JR+AR	f_y	434 N/mm²	
	f_u	555 N/mm²	
	A_t	27,0 %	
studs Ø 19 mm, L = 150 mm, S235J2 + C450	f_y	450 N/mm²	
(values given on material certificate)	f_u	532 N/mm²	
	A_t	15,7 %	
studs Ø 25 mm, L = 150 mm, S235J2 + C450	f_y	402 N/mm²	
(values given on material certificate)	f_u	519 N/mm²	
	A_t	16,1 %	
		on test date	28 days
concrete C30/37	$f_{c,\,cube}$	42,5 N/mm²	53,1 N/mm²
	$f_{c,\,zyl}$	37,9 N/mm²	45,5 N/mm²
	f_{ct}	2,7 N/mm²	3,0 N/mm²
	$E_{c,s}$	28 000 N/mm²	29 433 N/mm²

C.3

Date, duration and any other relevant test conditions of the test

date of the test	April 20, 2016
duration of the test	10:48 - 13:00 o'clock
temperature of the test	22 °C
loading	2 mm/min simultaneously displacement controlled
distance between supports	1600 mm
lever arm of actuators to supports	1400 mm

C.4

Resistance of the test specimen

bending moment when first concrete crack occurred	~ 83 kNm

Figure 138 - Experimental data on Specimen E materials

References

[1] NDT0143_NT_001 ind. A - PTAN: Technical Status on the Design and Construction of Steel Concrete Structures L2 – Action plan, State of the art and Hypothesis of the parametric studies

[2] R. Kubát, Steel-Concrete-Steel Sandwich Structures In Current Construction, A Short Overview. Ing. Petr Bílý, Ph.D. (2020)

[3] T. Wang, J.B. Yan, Developments of steel-concrete-steel sandwich composite structures with novel EC connectors: Members, J. Constr. Steel Res. 175 (2020) 106335

[4] ANSI/AISC N690-18: Specification for Safety-Related Steel Structures for Nuclear Facilities (2018)

[5] EN 1993-1-8: Eurocode 3: Design of steel structures - Part 1-8: Design of joints (2005)

[6] Aggelopoulos E., Burgan B. Design of Steel-Concrete (SC) composite structures, SCI-P414, The Steel Construction Institute, UK, 2019

[7] SCIENCE: SC for Industrial, Energy and Nuclear Construction Efficiency, RFCS GRANT AGREEMENT NO. RFSR-CT-2013-00017, Final Report, March 2017

[8] BANF186ADT_R001: SCHEDULE - Input Data, Design criteria and Calculation Methodology for the design (2019)

[9] EN 1993-1-1: Eurocode 3: Design of steel structures - Part 1-1: General rules and rules for buildings (2005)

[10] ANSYS v18.2

[11] LS DYNA v7.0

[12] LS-DYNA Manual Volume I R13 Material Models (2021)

[13] LS-DYNA Manual Volume II R13 Material Models (2021)

[14] EN 1992-1-1: Eurocode 2: Design of concrete structures - Part 1-1: General rules for buildings (2004)

[15] D305914007805 “Thermomechanical behaviour of steel concrete and reinforced concrete structures. (WP5, SCIENCE)”, EDF

[16] D305919096962 “TECHNICAL SPECIFICATIONS: PTAN Report + RCC-CW Design and Construction chapters on Steel Concrete Structures” (2020), EDF

[17] ENJD002DLY NT 002 - WP5/D5.4: Report with an interpretation of the test results and conclusion of the behaviour of steel concrete and reinforced concrete structures under thermo-mechanical loading